

Maximizing the use of supplementary cementitious materials (SCMs) in blended cements

Présentée le 23 juillet 2020

à la Faculté des sciences et techniques de l'ingénieur
Laboratoire des matériaux de construction
Programme doctoral en science et génie des matériaux

pour l'obtention du grade de Docteur ès Sciences

par

Yosra BRIKI

Acceptée sur proposition du jury

Prof. D. Damjanovic, président du jury
Prof. K. Scrivener, Dr M. Ben Haha, directeurs de thèse
Dr R. Snellings, rapporteur
Dr J. Skibsted, rapporteur
Dr B. Lothenbach, rapporteuse

Acknowledgements

I wish to express my sincere gratitude to my thesis director, Professor Karen Scrivener. Thank you for giving me this opportunity to be in this wonderful laboratory. Thank you for your support and for your valuable advices. Without your persistent help, the goal of this project would not have been realized. Your attention to details helped to improve the quality of this research.

A very special thank to my co-supervisor Dr. Mohsen Ben Haha. Thank you for giving me this opportunity to fulfil my potential during the PhD. For almost five years (with my master internship), you have been a great support to me. Your comments made me stronger and helped me to improve the findings of this research. The meetings and conversations with you and Karen were vital in inspiring me to think outside the box, from multiple perspectives to form a comprehensive and objective critique.

I would like to thank the members of the jury Dr. Barbara Lothenbach, Prof. Jorgen Skibsted and Dr. Ruben Snellings for letting my private defense be an enjoyable moment. Thank you for the very positive feedback and for the interesting comments to improve the thesis. The president of the jury Prof. Dragan Damjanovic is warmly thanked for organizing the oral exam under these difficult circumstances.

I'm particularly grateful to Dr. Maciej Zajac. Thank you for sharing your knowledge and experience to further improve this research. Thank you also for your kindness and for your advices. I would like also to thank all the scientists in HeidelbergCement: Arnaud Muller, Pawel Durdzinski, Frank Bullerjahn and Gerd Bolte for the scientific discussions. I would like to thank as well the lab (Tanja, Steeve, Inna, Timo..) for helping me in several experiments.

A special thank to François Avet, Paul Bowen and Christophe Labbez for their collaborative effort to improve the quality of the papers.

The LMC team made my four years go very fast. I would like to thank all the LMC members and a special thank to Hui for her nice ideas of travels, Shishi for her kindness and for her delicious food. Alexandru and Monisha thank you for your sweet company in HTC and thank you for the nice plans in Heidelberg. Thanks to the Tunisian team Sarra and Khalil for the nice moments together and for being always here for me. Thanks to Andrea, Maya, Alex, Silas, Diana, Julien, Mahsa, Solene, Remi, Bhagath, Franco, Xeurun, Adrien, Elise, Qiao, Mink, Mariana. I would like also to thank my students for their help: Jean-Baptiste, Emile, Loic and Romain and also summer students: Delphine and Johanne.

A special thank for Maude, Anne-Sandra and Mira for making our life easier with all reservations and bookings. Manue thank you for the cookies and for the nice conversations. LMC lab is not a lab without Lionel, Jean, Antonio and Nathan. I appreciate all of the help that you provide me during these years and a special thank to Lionel for all the interesting discussions that we had and also for your valuable advices.

This thesis is dedicated to my parents. Thank you for your love and support throughout my life. Thanks to my brothers for the unconditional support in these very intense years. Isabelle and Alain were like my parents in Europe to me. Thank you for everything you have done to me until now.

HeidelbergCement is warmly thanked for funding this project.

Abstract

Partial replacement of clinker with supplementary cementitious materials (SCMs) is an effective approach to reduce CO₂ emissions related to cement production. However, there is a maximum substitution level with SCMs beyond which strength decreases. The understanding of the factors controlling the reactivity of SCMs is the main objective of this thesis. This study focused on three main SCMs: limestone, calcined clay and slag.

A decrease of clinker content down to 80% and replacement with fine limestone permits to maintain similar strength to PC up to 7 days. The filler effect of fine limestone enhanced the hydration of C₃S which compensates the dilution of the clinker up to 7 days. The combination of fine limestone (15%) and coarse limestone (5%) showed similar strength to the system containing 20% of fine limestone and also to PC up to 7 days. Strength results were explained by the phase assemblage using gel space ratio.

Metakaolin reaction slows down in LC³ cement paste at late ages. The results indicated that the lack of water-filled capillaries is the most likely mechanism slowing down metakaolin reaction. Internal relative humidity measurements showed that at 28 days pore radius above 13 nm are not saturated with water. Based on Kelvin-Laplace equation, the growth of AFm and C-A-S-H phases were suggested to be limited below a range of pore radius around 3 to 8 nm.

The strength and phase assemblage of LC³ with clinker content from 50% to 30% were studied. The substitution of 70% of clinker by 30% calcined clay and 40% limestone showed strength development passing the criteria for 32.5 N class, using a CEM I 42.5 R for the cement part. In the blend with 30% of clinker, metakaolin reaction did not slow down despite the depletion of portlandite at 7 days. Calcium was most likely consumed from C-A-S-H phases. Strength results of LC³ blends were explained by the combined water fraction approach since gel space ratio requires the quantification of the C-A-S-H composition, which is very challenging for low-clinker systems.

The slow kinetics of slag reaction induced low strength development at early age. The dissolution of slag in NaOH solution with water solid ratio of 100 showed that the addition of calcium significantly slows down the rate of dissolution. In blended cements, slag dissolution might be delayed at early age due to the high concentration of calcium in the pore solution. At late ages, slag reaction in cement paste seems to be limited in capillaries above pore radius of 6 nm due to the lack of water.

The main findings of this research should allow to increase the replacement level of clinker in blended cements.

Keywords: Limestone, LC³, slag, reaction degree, low clinker amount, early and late ages

Résumé

Le remplacement partiel du clinker par des matériaux cimentaires de substitution (MCS) est une approche efficace pour réduire les émissions de CO₂ liées à la production de ciment. Cependant, il existe un taux de substitution maximal avec ces matériaux au-delà duquel la résistance à la compression diminue. Cette étude s'est focalisée sur trois matériaux principaux : le calcaire, l'argile calcinée et le laitier.

La diminution de la teneur en clinker jusqu'à 80 % et le remplacement par du calcaire fin a permis de maintenir une résistance similaire au PC jusqu'à 7 jours. L'effet « filler » du calcaire fin a amélioré l'hydratation du C₃S, ce qui a compensé la dilution du clinker jusqu'à 7 jours. La combinaison de calcaire fin (15%) et de calcaire grossier (5%) permet d'obtenir une résistance similaire avec le système contenant 20% de calcaire fin et aussi avec le PC jusqu'à 7 jours. Les résistances à la compression ont été expliquées par l'assemblage de phase en utilisant le rapport du gel sur l'espace disponible.

La réaction au métakaolin est ralentie dans la pâte de ciment LC³ à âge tardif. Les résultats indiquent que le manque de capillaires remplis d'eau est le mécanisme le plus probable expliquant le ralentissement de la réaction au métakaolin. Les essais d'humidité relative interne ont indiqué qu'à 28 jours, les pores avec un rayon supérieur à 13 nm ne sont pas saturés en eau. D'après l'équation de Kelvin-Laplace, il est également suggéré que la croissance des phases AFm et C-A-S-H soit limitée en-dessous d'une limite de taille de pores comprise entre 3 et 8 nm.

Malgré la substitution de 70 % de clinker par 30 % d'argile calcinée et 40 % de calcaire, le mélange a montré des résistances plus élevées que celles de la classe 32,5 N, le tout en utilisant un CEM I 42.5 R pour la partie ciment. Dans le système avec 30 % de clinker, la réaction du métakaolin n'est pas ralentie malgré l'épuisement de la portlandite à 7 jours. Le calcium est très probablement consommé du C-A-S-H. Les résistances mécaniques des mélanges LC³ ont été expliqués par l'approche de la fraction d'eau combinée.

La cinétique lente de la réaction du laitier a induit une faible résistance à la compression à jeune âge. L'isolement du laitier dans la solution de NaOH avec un rapport eau sur solide de 100 a montré que l'addition de calcium diminue la dissolution du laitier. Dans les ciments composites, la dissolution du laitier pourrait être retardée à jeune âge en raison de la forte concentration de calcium dans la solution de pore. Pour les âges tardifs, la réaction au laitier pourrait être limitée dans les capillaires au-dessus du rayon des pores de 6 nm en raison du manque d'eau.

Les principales conclusions de cette recherche devraient permettre d'augmenter le niveau de remplacement du clinker dans les ciments composites.

Mots-clés : Calcaire, LC³, laitier, degré de réaction, teneur en clinker faible, jeune âge, âge tardif

Contents

Acknowledgements.....	iii
Abstract.....	v
Résumé	vi
List of Figures.....	xi
List of Tables	xiv
Glossary.....	xv
Chapter 1 Introduction	1
1.1 Background	1
1.2 Portland cement.....	3
1.3 Clinker substitution with Supplementary cementitious materials (SCMs).....	4
1.4 Limitation of the use of SCMs	7
1.5 Objective of the thesis	7
Chapter 2 Impact of limestone fineness on cement hydration at early age.....	11
2.1 Introduction	12
2.2 Materials and methods	12
2.2.1 Materials	12
2.2.2 Methods	15
2.3 Results	16
2.3.1 Strength development	16
2.3.2 Heat flow and degree of clinker hydration	16
2.3.3 Chemical effect.....	18
2.3.4 Porosity.....	18
2.3.5 Chloride resistance.....	20
2.3.6 Combination of fine and coarse limestone	21
2.3.7 Correlation between strength and phase assemblage.....	23
2.4 Conclusions	24

Chapter 3	Understanding of the slowing down of metakaolin reaction in limestone calcined clay cement (LC³) at late ages.....	27
3.1	Introduction	28
3.2	Materials and methods	30
3.2.1	Materials	30
3.2.2	Methods	32
3.3	Results	33
3.3.1	Degree of reaction of metakaolin and degree of hydration of clinker	33
3.3.2	Factors slowing down metakaolin reaction and clinker hydration at late ages.....	34
3.4	Conclusions	48
Chapter 4	Strength and phase assemblage of limestone calcined clay cements (LC³) with clinker content from 50% down to 30%	51
4.1	Introduction	52
4.2	Materials and methods	52
4.2.1	Materials	52
4.2.2	Methods	55
4.3	Results	55
4.3.1	Decreasing clinker content with calcined clay amount constant	55
4.3.2	Decreasing clinker content with increasing calcined clay amount.....	59
4.3.3	Correlation between compressive strength and combined water fraction ...	62
4.4	Conclusions	64
Chapter 5	Factors affecting the reactivity of slag at early and late ages.....	67
5.1	Introduction	68
5.2	Materials and methods	69
5.2.1	Materials	69
5.2.2	Methods	70
5.2.2.1	Slag in NaOH solution	70
5.2.2.2	Slag in cement paste.....	71
5.3	Results	72
5.3.1	Factors affecting the rate of slag reaction at early age	73
5.3.2	Factors affecting the rate of slag reaction at late ages	82
5.4	Conclusions	90

Chapter 6	Main findings and conclusions	93
6.1	Conclusions	93
6.1.1	Maximizing the use of limestone in binary cements	93
6.1.2	Factors slowing down metakaolin reaction at late ages.....	93
6.1.3	Effect of decreasing clinker content from 50% down to 30% in LC ³	94
6.1.4	Factors slowing down slag reaction at early and late ages	94
6.2	Perspectives.....	95
6.2.1	Metakaolin reactivity at early age.....	95
6.2.2	Slag reactivity at early age.....	97
6.2.3	Metakaolin and slag reactivity at late ages	97
Appendix.....	99
7.1	Appendix 1: Methods.....	99
7.1.1	Characterization of powders	99
7.1.2	Compressive strength test	99
7.1.3	Cement paste preparation and curing methods.....	99
7.1.4	Methods for cement hydration and microstructure investigations	99
7.1.5	Mass balance approach	102
7.2	Appendix 2: Preliminary study on fly ash cement	104
7.2.1	Chemical composition and mix design.....	104
7.2.2	Compressive strength.....	105
7.3	Appendix 3: Nielsen and Mersmann approach	107
7.3.1	Saturation index using thermodynamic modelling.....	107
7.3.2	Nielsen and Mersmann approach for interfacial energy estimation	107
7.4	Appendix 4: Gel space ratio approach	110
References	112
Curriculum Vitae	122

List of Figures

Figure 1-1. Comparison of embodied energy of construction materials [1]..... 1

Figure 1-2. Evolution of the world average clinker substitution [6].....2

Figure 1-3. Calorimetry curve of modern Portland cement, showing C₃S hydration, ettringite and later AFm formation [7] 3

Figure 1-4. Presence of kaolinite in oxisols (pink), ultisols (yellow) and alfisols (pale green) [23]...5

Figure 2-1. PSD for all powders 14

Figure 2-2. Compressive strength for PC and blended cements 16

Figure 2-3. Heat flow normalized per g of paste a) and clinker b) for PC and blended cements 17

Figure 2-4. Degree of C₃S and C₃A hydration in PC and blended cements 17

Figure 2-5. a) Calcite content in limestone cements b) AFm and ettringite amounts in limestone cements (the points are for PC and quartz blend) 18

Figure 2-6. Porosity evolution at 1 and 28 days of hydration for PC and blended cements..... 19

Figure 2-7. SEM observations for PC and limestone cement at 3 days of hydration 20

Figure 2-8. Chloride content for PC and limestone cement mortars after 6 months of exposure to 3 wt.% NaCl ponding solution 21

Figure 2-9. Compressive strength as a function of fine/coarse limestone powder from 1 up to 90 days 22

Figure 2-10. C-S-H and Hc+Mc amounts for PC and limestone cements at 1, 3 and 28 days 22

Figure 2-11. Correlation between compressive strength and gel space ratio considering the gel as the sum of hydration products..... 23

Figure 3-1. Schematic illustration of homogenous and spherical crystal growth exerting isotropic pressure in large and small pores, note the thickness of the liquid film between the crystal and the pore wall. Adapted from [55]..... 29

Figure 3-2. PSD and BET of all used materials 32

Figure 3-3. Degree of reaction of metakaolin in LC³ cement in a) linear scale and b) logarithmic scale (w/b=0.4)..... 34

Figure 3-4. Degree of hydration of silicate and aluminate phases in PC and LC³ cements 34

Figure 3-5. Portlandite content for PC, LC³ and LC³+5%CH 35

Figure 3-6. Degree of reaction of metakaolin in LC³ and LC³+5%CH 35

Figure 3-7. Degree of reaction of metakaolin and silica fume..... 36

Figure 3-8. Degree of clinker hydration in LC³ and silica fume cement 37

Figure 3-9. Internal relative humidity of PC and LC³ systems 37

Figure 3-10. Degree of reaction of metakaolin (left) and portlandite content (right) in sealed and pore solution cured systems (PSC) 38

Figure 3-11. Solid and interlayer pores (left) capillary and gel pores (right) for sealed and cured LC³ white cement 39

Figure 3-12. Porosity of sealed and pore solution cured LC³ cements 39

Figure 3-13. Degree of reaction of metakaolin for w/b=0.3,0.4,0.5 [12] and 0.6..... 40

Figure 3-14. Relative humidity of PC, LC³ with w/b=0.3 and 0.4..... 41

Figure 3-15. Porosity in LC ³ for w/b=0.3, 0.4 and 0.6	42
Figure 3-16. Phase assemblage of LC ³ for w/b=0.3, 0.4 and 0.6 at 90 days of hydration assuming 2g/cm ³ for C-A-S-H density (bulk density [18,24])	43
Figure 3-17. Saturation index required for Mc growth using interfacial energy of portlandite [65], calcite [64] and Mc with Nielsen's approach [68]	46
Figure 3-18. AFm content in LC ³ for w/b=0.3,0.4 and 0.6	46
Figure 3-19. Saturation index required for C-S-H growth Vs. pore radius (black lines indicate the deviations based on sensitivity analysis)	47
Figure 4-1. PSD and BET of all used materials	54
Figure 4-2. Compressive strength against a) days b) clinker content	55
Figure 4-3. Degree of hydration of silicate and aluminate phases in LC ³ cements	56
Figure 4-4. Amount of reacted clinker in LC ³ cements	56
Figure 4-5. Portlandite content normalized per g of solid for all LC ³ blends	57
Figure 4-6. The reaction degree of metakaolin in calcined clay in all LC ³ blends	58
Figure 4-7. Phase assemblage for LC ³ blends at 28 days of hydration	58
Figure 4-8. AFm and C-A-S-H contents determined by mass balance for LC ³ blends	59
Figure 4-9. Compressive strength for LC ³ _50_30, LC ³ _40_30 and LC ³ _40_40	60
Figure 4-10. Amount of reacted clinker for LC ³ _50_30, LC ³ _40_30 and LC ³ _40_40	60
Figure 4-11. Portlandite consumption for LC ³ _50_30, LC ³ _40_30 and LC ³ _40_40	61
Figure 4-12. The amount of reacted metakaolin in calcined clay for LC ³ _50_30, LC ³ _40_30 and LC ³ _40_40	61
Figure 4-13. Pore structure for LC ³ _50_30, LC ³ _40_30 and LC ³ _40_40	62
Figure 4-14. Compressive strength vs. combined water fraction a) without refinement b) with refinement (The sensitivity analysis is indicated by the dashed lines)	64
Figure 5-1. PSD and BET of clinker, slag and quartz	70
Figure 5-2. Degree of reaction of slag in cement paste a) linear scale and b) logarithmic scale (w/b=0.4)	72
Figure 5-3. The heat release per g of clinker for PC and blended cements (w/b=0.4)	73
Figure 5-4. Compressive strength of PC and blended cement	73
Figure 5-5. Logarithm of the release rate of Al, Si and S in slag-NaOH solution (w/s=100)	74
Figure 5-6. Saturation index of hydrates in slag-NaOH solution	74
Figure 5-7. The amount of C-S-H and hydrotalcite in slag NaOH solution (w/s=100)	75
Figure 5-8. High resolution micrographs of slag in NaOH solution after 30 min and 6 hours	75
Figure 5-9. Degree of reaction of slag in NaOH solution and cement paste	76
Figure 5-10. pH evolution for slag in NaOH solution with and without addition of calcium hydroxide	77
Figure 5-11. Saturation index of C-S-H and in slag-NaOH solution with and without addition of calcium hydroxide	77
Figure 5-12. Logarithmic release rate of sulfur in slag-NaOH solution and in the presence of 0,1, 1 and 10mM of Ca (OH) ₂	78
Figure 5-13. Logarithmic release rate of S vs. calcium addition	79
Figure 5-14. Si concentration and saturation index of C-S-H and in slag-NaOH solution with and without addition of calcium hydroxide	79

Figure 5-15. High resolution micrographs of slag in NaOH solution a) after 30 min and b) 6 hours and with addition of 10mM of calcium hydroxide c) after 30 min and d) 6 hours.....	80
Figure 5-16. Heat cumulative of slag-NaOH solution with and without addition of calcium hydroxide (w/s=10)	81
Figure 5-17. Degree of reaction of slag in NaOH solution with different amount of calcium hydroxide (w/s=100) and slag in cement paste (w/s=0.4).....	82
Figure 5-18. Degree of reaction of slag in cement paste with w/b=0.3, 0.4 and 0.6	83
Figure 5-19. Porosity measurements of slag cement with w/b=0.3, 0.4 and 0.6	84
Figure 5-20. Internal relative humidity for PC and slag cement.....	85
Figure 5-21. Degree of reaction of slag in sealed and pore solution cured conditions a) linear scale and b) logarithmic scale (w/b=0.4)	86
Figure 5-22. Porosity measurements of slag cement in sealed and pore solution conditions at 3 and 90 days of hydration (w/b=0.4).....	86
Figure 5-23. Saturation index required for Ms and Mc growth using interfacial energy estimated by Nielsen's approach [68]	88
Figure 5-24. Hc+Mc and Ms amounts in slag cement w/b=0.3, 0.4 and 0.6	89
Figure 5-25. Saturation index required for C-S-H growth.....	89
Figure 6-1. Compressive strength of PC, slag cement and LC ³ blend.....	95
Figure 6-2. Log release rate of Al and Si in metakaolin in calcined clay (w/s=100)	96
Figure 6-3. Heat cumulative of calcined clay in NaOH solution and degree of reaction of metakaolin in NaOH solution and cement paste.....	96
Figure 6-4. Heat cumulative of slag with and without addition of aluminium nitrate (w/s=100)	97
Figure 7-1. Determination of the composition of C-(A)-S-H from the plot of Al/Ca versus Si/Ca [81]	101
Figure 7-2. MIP results showing derivative and cumulative curves of LC ³ -50 paste samples at 28 days [80].....	102
Figure 7-3. Mix formulations of cement blended with fly ash and limestone	105
Figure 7-4. Strength development of PC, fly ash and fly ash-limestone blends.....	105
Figure 7-5. Correlation between compressive strength and gel space ratio considering the gel as a) sum of hydrates, b) C-A-S-H and c) sum of hydrates and the unreacted limestone and metakaolin	110

List of Tables

Table 2-1. Chemical compositions of all powders.....	13
Table 2-2. Median diameter and specific surface area of all materials.....	14
Table 2-3. Mix proportions of investigated systems (w/b=0.4).....	15
Table 3-1. Chemical composition of clinker, calcined clay, silica fume and quartz	31
Table 3-2. Composition of clinker phases	31
Table 3-3. Mix composition for all investigated blended cement.....	32
Table 3-4. Sensitivity analysis for the determination of the interfacial energy using Mersmann's approach [31]	45
Table 4-1. Chemical compositions of all powders.....	53
Table 4-2. Composition of clinker phases	53
Table 4-3. Mix composition for all investigated blended cement.....	54
Table 5-1. Chemical composition of slag and quartz.....	69
Table 5-2. Mix design for all investigated systems	71
Table 5-3. Solubility product, unit cell volume, density and molecular weight of monosulfoaluminate	87
Table 7-1. Chemical composition of fly ash.....	104
Table 7-2. Element concentrations in LC ³ and slag cement	107

Glossary

Cement notation of oxide compounds:

C: CaO S: SiO₂ A: Al₂O₃ M: MgO F: Fe₂O₃ \$: SO₃ c: CO₂ H: H₂O

Nomenclature

C ₃ S	3CaO·SiO ₂ Tricalcium silicate
C ₂ S	2CaO·SiO ₂ Dicalcium silicate
C ₃ A	3CaO·Al ₂ O ₃ Tricalcium aluminate
C ₄ AF	4CaO·Al ₂ O ₃ ·Fe ₂ O ₃ Ferrite
Cc	CaCO ₃ Calcite
CH	Ca (OH) ₂ Calcium hydroxide or Portlandite
C-(A)-S-H	CaO-SiO ₂ -H ₂ O Calcium silicate (aluminate) hydrate
AFt	C ₃ A·3C\$·H ₃₂ 3CaO·Al ₂ O ₃ ·3CaSO ₄ ·32H ₂ O Ettringite
Ms	C ₃ A·C\$·H ₁₂ 3CaO·Al ₂ O ₃ ·CaSO ₄ ·12H ₂ O Monosulfate
Hc	C ₃ A·Cc _{0.5} ·H ₁₂ 3CaO·Al ₂ O ₃ ·0.5CaCO ₃ ·12H ₂ O Hemicarbonat
Mc	C ₃ A·Cc·H ₁₁ 3CaO·Al ₂ O ₃ ·CaCO ₃ ·11H ₂ O Monocarbonat
Ht	M ₄ AMg ₄ Al ₂ (OH) ₁₄ Hydrotalcite
σ	Edge work
K, K _B	Boltzmann constant
T	Temperature
k _{sp}	Solubility of the crystal
Ω	Unit cell volume
γ_0	Maximum interfacial energy of a crystal at its point of zero charge
R	Gas constant
F	Faraday constant
z	Valence of a (z:z) electrolyte
σ and σ_{\max}	Surface charge of ionic crystals
I	Ionic strength
1/ κ	Debye length
N _{AV}	Avogadro constant
ϵ	Dielectric constant
ϵ_0	Vacuum permittivity
e	Electron charge
ρ	Density
M _w	Molecular weight

C_i	Molar concentration
PC	Portland cement
SCMs	Supplementary Cementitious Materials
w/b	Water to binder ratio
DoR	Degree of reaction
DoH	Degree of hydration
PSD	Particle size distribution
BET	Nitrogen adsorption
XRD	X-ray diffraction
XRF	X-ray fluorescence
SEM	Scanning electron microscopy
TGA	Thermogravimetric analysis
^1H NMR	Proton Nuclear magnetic resonance
MIP	Mercury Intrusion Porosimetry

Chapter 1 Introduction

1.1 Background

Concrete is the most produced man-made material representing about half of everything that is produced in the world. This is due to concrete being a cheap, user-friendly, durable material with high performance. The fact that cement and concrete only account for 5-7% of the anthropogenic CO₂ shows that these materials are ecological compared to other building materials, despite the huge volume produced. Figure 1-1 shows the embodied energy of concrete which is negligible compared to steel or glass for example [1].

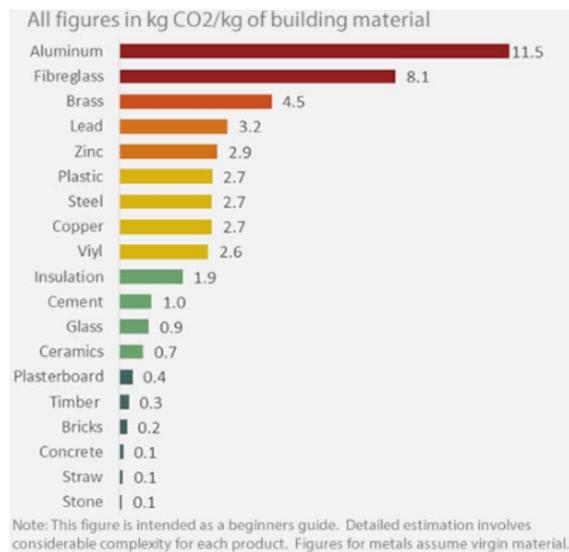


Figure 1-1. Comparison of embodied energy of construction materials [1]

Concrete is a construction material composed of cement (clinker ground with gypsum), fine and coarse aggregates mixed with water which hardens with time. The production of clinker is the most emissive step of cement and concrete production. Clinker production requires the calcination of the raw materials, mainly limestone and clay. These materials are heated at 1450°C. Carbon dioxide is released during the calcination of limestone (CaCO₃) at about 700°C-800°C. The temperature of the kiln allows the reaction of the lime (CaO) with silica, aluminum and iron-containing materials to produce clinker. The calcination of limestone is responsible for about 60% of the CO₂ emissions. The remaining 40% comes from the burning of the fossil fuel to reach the temperature of 1450°C.

Because of the huge quantities of concrete produced, a small reduction of CO₂ emissions achieved per kilogram of cement has a significant impact compared with other industries. The International Energy Agency (IEA) and the The World Business.

Council for Sustainable Development (WBCSD) [2] proposed several mitigation scenarios for CO₂ emissions to limit the global warming to 2°C in 2100. Cement industry has to reduce the CO₂ emissions by 24% by 2050, while the cement consumption keeps increasing [2]. Several approaches have been developed for the reduction of the CO₂ emissions [3–6]:

- Replacement of the fossil fuel proportion for the clinker process by alternative fuels such as used tires, waste oil, plastics, refused-derived fuels and mainly biomass.
- Partial substitution of the raw materials used for making clinker by wastes, and by-products from other industries.
- Optimization of the binder content in concrete with the maximization of the aggregate fractions.
- Recycling of concrete to reduce the amount of construction and demolition waste going to land fill and the amount of resources required for concrete.
- Partial substitution of clinker with supplementary cementitious materials (SCMs). Figure 1-2 shows the evolution of clinker substitutes over the past 25 years. However, the level of decreasing clinker factor is rather constant. This is due to the fact that the supply of the most frequent clinker substitutes mainly blast furnace slags and fly ash of acceptable quality, is relatively modest compared to total cement production [6].

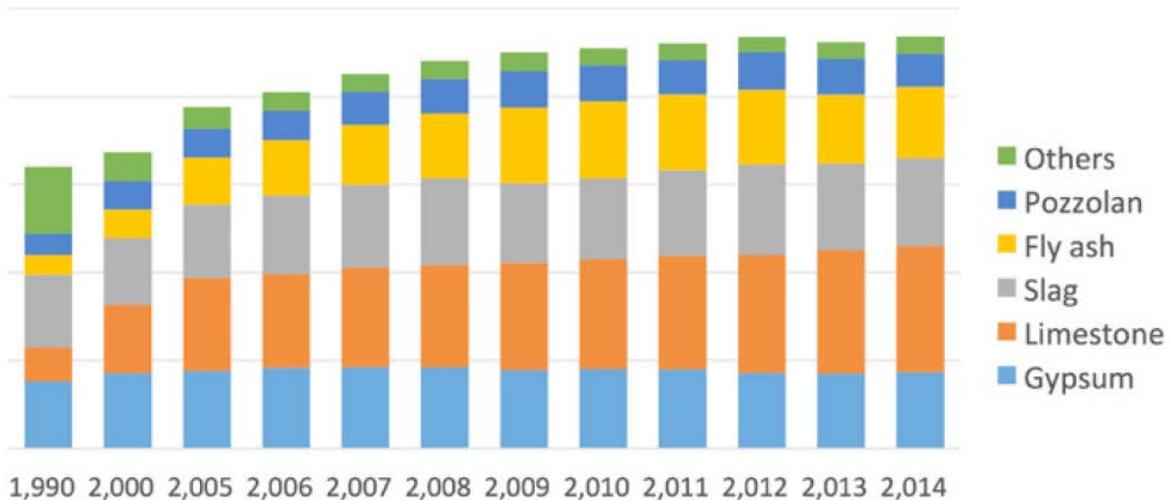


Figure 1-2. Evolution of the world average clinker substitution [6]

1.2 Portland cement

Portland cement clinker contains four principal minerals:

- Alite or tricalcium silicate, Ca_3SiO_5 (in oxide terms $3\text{CaO} \cdot \text{SiO}_2$), abbreviated to C_3S ;
- Belite or dicalcium silicate, Ca_2SiO_4 (in oxide terms $2\text{CaO} \cdot \text{SiO}_2$), abbreviated to C_2S ;
- Tricalcium aluminate, CaAl_2O_6 (in oxide terms $3\text{CaO} \cdot \text{Al}_2\text{O}_3$), abbreviated to C_3A ;
- Tetracalcium aluminoferrite, $\text{Ca}_2\text{AlFeO}_5$ (in oxide terms $4\text{CaO} \cdot \text{Al}_2\text{O}_3 \cdot \text{Fe}_2\text{O}_3$), abbreviated to C_4AF .

The reaction of cement with water is termed "hydration". This involves several chemical reactions which give to the cement its hardening and strength. Most of these reactions are exothermic: the overall heat released can be followed by isothermal calorimetry. A typical calorimetry curve of Portland cement is shown in Figure 1-3.

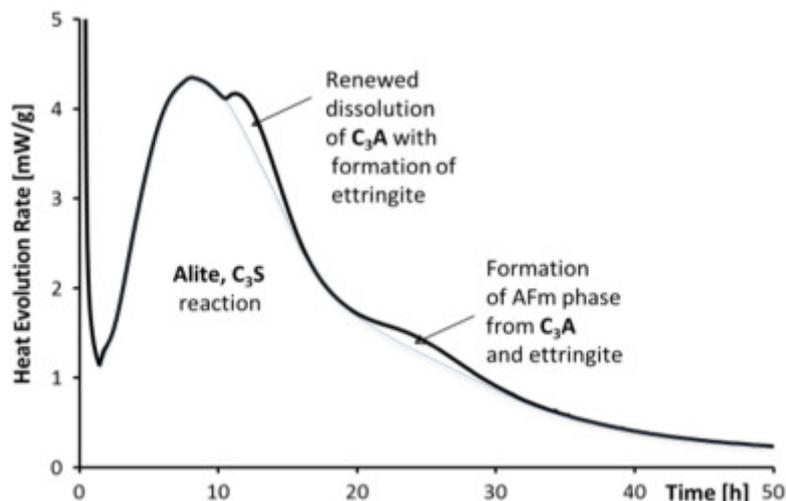


Figure 1-3. Calorimetry curve of modern Portland cement, showing C_3S hydration, ettringite and later AFm formation [7]

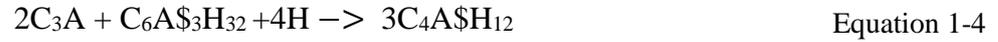
Alite phases (C_3S) in PC react with water to produce crystalline calcium hydroxide (CH) and the nanocrystalline gel calcium-silicate-hydrates (C-S-H) as described in Equation 1-1. The hydration of belite phases (C_2S) occurs in a similar way as alite phases (Equation 1-2) but in a slower rate.



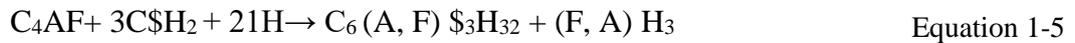
The reaction of C_3A with water is rapid. Calcium sulfates or gypsum delay this reaction (Equation 1-3). C_3A reacts with water, in the presence of gypsum to form a product generally referred to as "ettringite", and also AFt phase (Aluminate Ferrite trisulfate) [8].



After depletion of the sulfate, “monosulfate” is formed as shown in Equation 1-4 which is also termed “AFm” (Aluminate Ferrite monosulfate) [8].

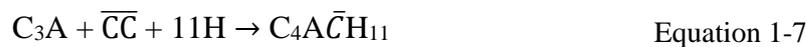
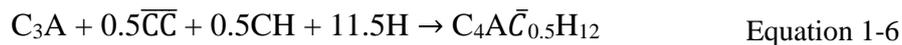


The ferrite phase (C_4AF) reacts in a similar way to the C_3A but more slowly. One important difference is that some of the aluminum in the reaction products is substituted for iron [8]. Additionally, as results of the ferrite phase reactions, iron containing hydrogarnets are formed as described in Equation 1-5:



1.3 Clinker substitution with Supplementary cementitious materials (SCMs)

The most frequently used SCMs for clinker replacement are limestone, slag and fly ash [6,9]. Limestone is a sedimentary rock composed mostly of calcite which is a crystal form of calcium carbonate ($CaCO_3$). Limestone reacts in cementitious systems with the aluminate of the clinker phases. As previously mentioned, after complete consumption of the sulfate source, some of the ettringite reacts with remaining C_3A to form monosulfoaluminate phase (Ms) [10,11]. In presence of limestone, C_3A reacts with calcium carbonate to form hemi-(Hc) and monocarboaluminate phases (Mc) [10–16] (Equation 1-6 and Equation 1-7). As a consequence, ettringite phase is retained [11,13].



About 2-5% of limestone reacts during hydration of Portland cements [10,12]. The limiting factor for limestone reaction is the aluminate from C_3A and C_4AF . The amounts of Hc and Mc are related to the initial aluminate content of clinker [13] and the initial aluminate to sulfate ratio of the system [16].

Slag is a by-product from the steel industry. Different types of products are obtained depending on the method used to cool the molten slag. These products include air-cooled blast furnace slag (AC-BFS), expanded or foamed slag, pelletized slag, and granulated blast furnace slag [17]. Ground-granulated blast-furnace slag (GGBFS) is obtained when slag is cooled and solidified by rapid water quenching to form a glassy material [18]. GGBFS shows hydraulic cementing properties after

grinding. The composition of GGBFS can range from 30-50% for CaO, 28-38% for SiO₂, 8-24% for Al₂O₃, and 1-18% for MgO [19]. This composition is closer to Portland cement than the other SCMs. In blended cements, slag exhibits both hydraulic and pozzolanic behaviour, i.e. slag also consumes portlandite. The reaction of slag cement leads to the formation of C-(A)-S-H with a lower calcium to silicon ratio compared to Portland cement, a hydrotalcite-like phase, ettringite and AFm phases including strätlingite C₂ASH₈ [19].

Fly ash is the combustion residue of coal-burning electric power plants, which flies up with the flue gas stream and is removed by mechanical separators, electrostatic precipitators, or bag filters [20]. The composition of fly ash is highly heterogeneous [21]. Fly ash is mainly composed of SiO₂, but it can contain also significant quantities of Al₂O₃ and CaO [19]. Fly ash reacts as pozzolanic material.

Slag and fly ash have been cost-effective substitutes for Portland cement for several decades [5]. However, these SCMs are not widely available and they are almost fully used in cement [9]. The limited availability of fly ash and slag means that their contribution to decrease the carbon footprint of cement will not exceed 10% of the CO₂ reduction targets [4]. In recent years, clays and especially kaolinitic clays, have receiving increasing attention and this is due to their wide availability, especially in equatorial to subtropical parts of the world. Figure 1-3 shows the wide availability of kaolinitic clays, present mainly in oxisols, ultisols and alfisols (in pink, yellow and pale green on the map). Interestingly, kaolinitic clays are widely present in regions where the demand for cement is increasing significantly [22].

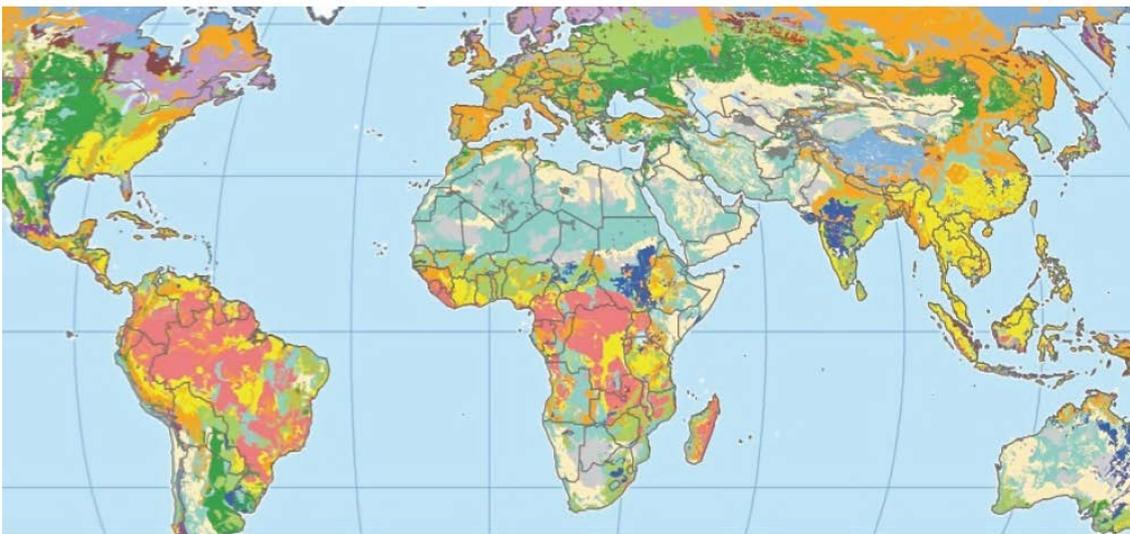
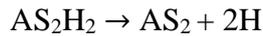
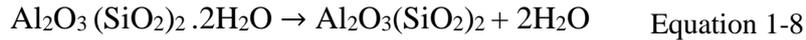


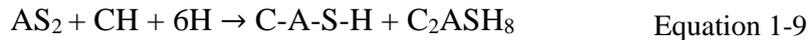
Figure 1-4. Presence of kaolinite in oxisols (pink), ultisols (yellow) and alfisols (pale green) [23]

Kaolinitic clays are the most suitable type of clays because they are the most reactive. This higher reactivity is explained by their structure. Kaolinite is different from other types of clays such as illite or smectite by its layer structure which is 1:1 type [23,24]. The basic structural unit of kaolinite consists of one tetrahedral (Si–O) sheet and one octahedral (Al–O) layer and its stoichiometric formula is $\text{Al}_2\text{Si}_2\text{O}_5(\text{OH})_4$ [25]. Without calcination, kaolinite clays are not reactive. The pozzolanic activity of kaolinite clays can be obtained by thermal activation between 600°C and 900°C [26]. Kaolinite transforms into an amorphous metastable phase called metakaolin, according to Equation 1-8 [24].



The reactivity of metakaolin has been linked to the structural disorder during the dehydroxylation process [24,27]. A change of the coordination number of Al from octahedral Al^{VI} to Al^{IV} and especially Al^{V} has been reported [27]. This Al^{V} is not observed for the other types of calcined clays.

Metakaolin reacts as a pozzolanic material to form mainly C-A-S-H, with sometimes strätlingite after portlandite depletion [28–30]. This reaction is summarized in Equation 1-9



The combination of calcined clay with limestone in Limestone Calcined Clay Cements (LC^3) allows higher clinker substitution level while maintaining good mechanical properties. In LC^3_{50} , the clinker content is reduced down to 50%, and similar strength to plain cement can be obtained from 7 days onwards, even using calcined kaolinitic clays with only 40% of kaolinite [31]. This is explained by the pozzolanic reaction of metakaolin, the reaction of calcite with the aluminate from the clinker and from the reaction of metakaolin with calcite. Metakaolin provides extra aluminates which increase the formation of carboaluminate hydrates, according to Equation 1-10



In addition to the chemical effect, the SCMs affects the hydration of blended cement in a physical way [19]. This effect is usually referred to as the filler effect. The main mechanisms contributing to the filler effect are:

- SCMs and particularly limestone, enhance cement hydration by providing nucleation sites for C-S-H [32]. Additionally, the presence of fine SCMs increases the shearing rate during mixing because of the decrease of the distance between particles [32,33]. The nucleation sites and the increase of the shearing rate lead to the enhancement of the heterogenous nucleation of C-S-H.

- The replacement of clinker with SCMs increases the water to clinker ratio while maintaining the same water to solid ratio. This dilution effect means that extra space is provided for clinker hydration [19].

1.4 Limitation of the use of SCMs

Partial replacement of clinker with SCMs is an effective approach to reduce the environmental impact of cement and concrete. However, blending cement with SCMs presents some limitations:

- The replacement of clinker by limestone is limited above 10-15% in blended cements. Beyond this limit, strength decreases compared with plain cement due to the decrease of clinker factor.

- The combination of calcined clay and limestone in LC³ blend permits to decrease clinker factor down to 50%. Compressive strength of LC³ is similar to PC from 7 days onwards. However, metakaolin and clinker do not achieve full reaction even over long-term period.

- The replacement of clinker by slag shows similar or better durability properties to plain cement. However, the reaction of slag is generally slower and lower than that the hydration of clinker phases. The slow kinetics of slag leads to low early age strength development.

1.5 Objective of the thesis

The goal of this project is to understand the factors controlling the reactivity of SCMs in blended cement. The insights gained in this study permits to find ways to maximize the replacement level of SCMs in blended cements. The thesis refers to the key steps for understanding of the factors limiting or enhancing the reactivity of SCMs. All the chapters are adapted from papers being submitted to the Cement and Concrete Research journal. The thesis is organized in the order detailed hereafter:

Cement blended with fly ash was not fully investigated in this project since the preliminary results showed poor strength development compared to Portland cement. The initial findings for fly ash cement are detailed in the appendix 2.

Chapter 2 investigates the influence of limestone fineness on strength and cement hydration for 20% of clinker substitution. The combination of two limestone fineness was studied in terms of strength development and phase assemblage.

Chapter 3 presents a fundamental approach to understand the mechanisms slowing down metakaolin reaction in LC³ cement paste at late ages.

Chapter 4 investigates the performance of LC³ formulations with clinker content down to 30%. The phase assemblage is characterized to better understand strength development.

Chapter 5 investigates the factors limiting the reaction of slag in cement paste at early and late age.

Chapter 6 summarizes the conclusions of the studies and gives the suggestions for further work.

Chapter 2 Impact of limestone fineness on cement hydration at early age

Disclaimer: This chapter is adapted from the preprint version of the following article being submitted to Cement and Concrete Research journal – with permissions of all co-authors:

Y.Briki ^a, M.Zajac ^b, M.Ben Haha ^b, and K.Scrivener ^a “Impact of limestone fineness on cement hydration at early age”

^aLaboratory of Construction Materials, EPFL, 1015 Lausanne, Switzerland

^bHeidelberg Technology Center GmbH, Rohrbacher Str.95, 69181 Leimen, Germany

My contribution: Methodology, experiments, analysing, writing

Abstract

This study compares the influence of two limestone fineness on strength development and cement hydration. The replacement of clinker by 20% of fine limestone ($d_{v,50}=2 \mu\text{m}$ and $\text{SSA}=4,21 \text{ m}^2/\text{g}$) permits to obtain similar strength development to PC up to 7 days. The beneficial impact of fine limestone is explained by the filler effect of limestone, i.e. the extra nucleation sites for C-S-H and the dilution effect. The influence of coarse limestone ($d_{v,50}=130 \mu\text{m}$ and $\text{SSA}=0,46 \text{ m}^2/\text{g}$) on cement hydration is mainly observed at late ages due to dilution effect. The combination of fine and coarse limestone was also studied. Similar strength was obtained for 20% fine limestone and 15% fine limestone mixed with 5% coarse limestone. This is explained by similar phase assemblage. Additionally, the results showed that despite the similarity of specific surface area, limestone is more effective than quartz for the enhancement of cement hydration.

Keywords: fineness, filler effect, dilution effect

2.1 Introduction

Ground limestone is a widely available material and it has been used for several decades in cement as partial clinker substitute. Limestone contributes to the hydration of cementitious system in two manners: chemically and physically [10,13,16,19,34–37]. Limestone reacts in cementitious systems with the aluminate to produce hemi- and monocarboaluminate phases [12,16,36]. As a consequence, the formation of ettringite is retained [10].

In addition to the chemical effect, limestone acts as filler in cementitious systems [19]. As such, limestone enhances cement hydration by providing nucleation sites for C-S-H [32]. Moreover, the presence of limestone particles increases the shearing rate during mixing because of the decrease of the distance between particles [32,33]. The nucleation sites and the increase of the shearing rate lead to the enhancement of the heterogenous nucleation of C-S-H. Berodier and Scrivener [32] showed that limestone is more effective in increasing the nucleation of C-S-H compared to quartz. It has been proposed that this is due to the solubility of limestone which gives higher calcium near the surface [35]. However, the addition of limestone increases the water to clinker ratio [19]. This dilution effect means that more space is available for clinker hydration.

In terms of strength development, the chemical and physical effects of limestone permit to compensate the decrease of the clinker content up to 15% replacement [38]. Above this limit, the properties of blended cement with limestone tend to decrease due to the decrease of the clinker content [10,16].

This research looks at the impact of limestone fineness at the higher level of 20% substitution. The influence of the fineness of limestone on cement hydration was investigated. The combination of two limestone fineness was studied. Phase assemblage and strength development were investigated.

2.2 Materials and methods

2.2.1 Materials

Clinker was provided from HeidelbergCement. Soluble anhydrite was from Saint-Gobain, it is produced by heating natural gypsum at 200°C, which makes it highly soluble and much more reactive than natural anhydrite [39]. Two limestone powders with different particle sizes were used in this study referred as fine limestone (FL) and coarse limestone (CL). The content of calcium carbonate was above 98% as measured by thermogravimetric analysis (TGA). Fine quartz (FQ) is from Sibelco company. The chemical composition of the materials determined by X-ray fluorescence (XRF) analysis are shown in Table 2-1.

	Clinker	Limestone	Quartz
CaO	64.41	54.21	<0.01
SiO ₂	20.62	0.96	99.62
Al ₂ O ₃	5.71	0.25	<0.01
Fe ₂ O ₃	3.7	0.22	0.016
MgO	1.63	0.89	<0.01
Na ₂ O	0.18	-	<0.01
K ₂ O	1.27	-	<0.01
SO ₃	0.97	-	<0.01
TiO ₂	0.3	-	<0.01
P ₂ O ₅	0.12	-	<0.01
LOI	0.8	42.6	0.1

Table 2-1. Chemical compositions of all powders

Particle size distribution of the powders determined using the laser diffraction technique with a Malvern Mastersizer is plotted in Figure 2-1. Table 2-2 summarizes the median diameter ($d_{v,50}$) and the specific surface area (SSA) determined by nitrogen adsorption. In order to distinguish between the contribution of fine and coarse limestone in combined fraction systems, the coarse limestone was sieved to remove all fine particles. The particles were dispersed using sodium metaphosphate following the recommendations in the book “A practical guide to Microstructural Analysis of Cementitious Materials” [40]. Afterwards, limestone particles were wet sieved. The PSD was checked to make sure that all fine particles were removed as shown in Figure 2-1.

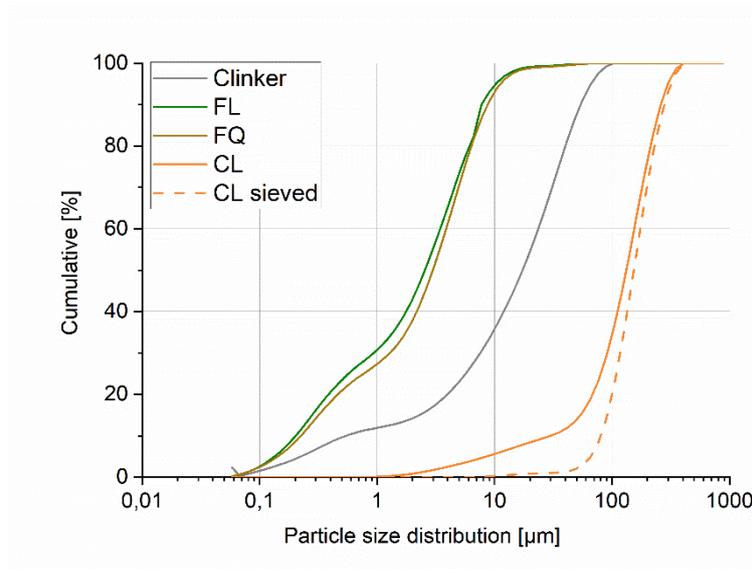


Figure 2-1. PSD for all powders

	Clinker	FL	CL	FQ
$d_{50}(\mu\text{m})$	15	2	130	2
$\text{SSA}(\text{m}^2/\text{g})$	0.85	4.21	0.46	4.07

Table 2-2. Median diameter and specific surface area of all materials

Table 2-3 shows the different blended cements investigated in this study. Beside the reference cement PC, systems blended with fine and coarse limestone were compared. The replacement of fine limestone with fine quartz with similar fineness (Table 2-2) was investigated to understand better the filler effect of both powders. The combination of fine and coarse fractions of limestone was also investigated in this study. The pastes were blended with a water to binder ratio 0.4. Regarding the sulfate adjustment, a content of 4.5% of soluble anhydrite (2,64% of SO_3) was added to clinker in Portland cement. Recently, Zunino and Scrivener [41] showed that fine fillers increase the hydration of alite in the main heat evolution peak, so that more sulfate is adsorbed by C-S-H during this peak. Therefore, the sulfate depletion peak occurs earlier when fillers are incorporated into the cement. Thus, higher amount of anhydrite (5%) corresponding to 2,94% of SO_3 was added to limestone blended cements.

	Clinker	FL	CL	FQ	Anhydrite
PC	95.5	0	0	0	4.5
20FL	76	19	0	0	5
15FL_5CL	76	14.25	4.75	0	5
10FL_10CL	76	9.5	9.5	0	5
5FL_15CL	76	4.75	14.25	0	5
20CL	76	0	19	0	5
20FQ	76	0	0	19	5

Table 2-3. Mix proportions of investigated systems (w/b=0.4)

2.2.2 Methods

Compressive strength of PC and blended cements was tested following the European standard EN 196-1.

The cement paste was mixed for 2 min at 1600 rpm and the exothermic reaction was followed by calorimetry (TAM Air, TA Instruments).

Cement pastes were placed in plastic cylinder bottles (2 cm of diameter, 5 cm height) and sealed with parafilm. For each testing age, four slices of the sample with 2mm thickness were cut with a diamond saw using deionized water as a lubricant. One fresh slice was used for X-Ray Diffraction (XRD) measurements for the characterization of crystalline phases formed during hydration.

The hydration was stopped with isopropanol for the remained slices as it is recommended as the least damaging solvent for the microstructure [42]. The following experiments were carried out:

For porosity characterization, mercury intrusion porosimetry (MIP) was used with a contact angle of 120°. SEM was used for qualitative microstructure investigations. The phase assemblage of all studied systems was estimated by the mass balance approach [21,31]. The methods employed in this study are detailed in Appendix 1: Methods.

For ponding tests, mortar mixtures were cast in cylindrical (11cm diameter - 30 cm height) moulds. After 24 h of curing in sealed conditions, specimen was demolded and stored in a fog room (RH>95%). After 28 days of curing, the mortar cylinders were cut into two halves. The epoxy was applied on all surfaces except the saw cut face and submerged in 3wt. % NaCl solution. Chloride profiles were obtained in accordance with ASTM-C1152 procedure after 6 months of exposure.

2.3 Results

2.3.1 Strength development

Figure 2-2 shows the strength development for PC and blended cements. Up to 7 days, fine limestone cement shows strength similar to PC. Replacing fine limestone powder with fine quartz powder, gave slightly lower compressive strengths, throughout the testing period, with the largest differences at 2, 3 and 7 days. Coarse limestone cement shows the lowest strength development for all ages.

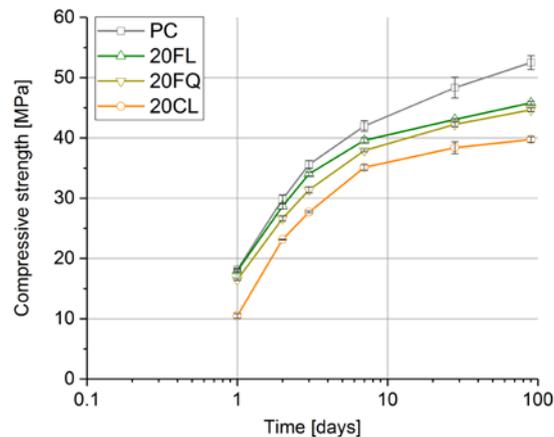


Figure 2-2. Compressive strength for PC and blended cements

2.3.2 Heat flow and degree of clinker hydration

Figure 2-3 shows the heat flow normalized per g of paste a) and per g of clinker b) for PC and limestone/quartz cements. The induction period seems to be not affected with the addition of fillers. At the end of the induction period, the heat increases more sharply and steeply for both fine additions, slightly more for the limestone than the quartz. The non-normalized heat flow showed that the increase of C_3S hydration is higher for limestone and similar for quartz – i.e. the enhancement effect of fillers, compensates the dilution effect due to the decrease of clinker amount. This is not the case for coarse limestone showing lower heat release per g of paste compared to PC.

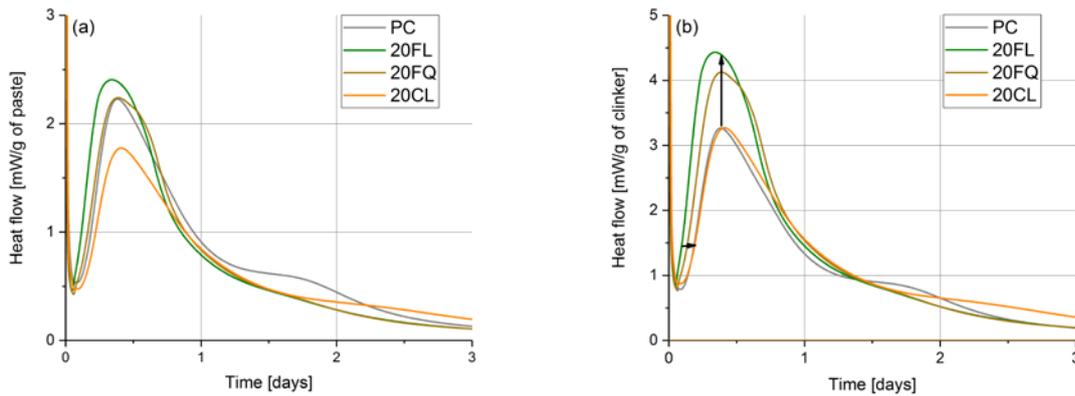


Figure 2-3. Heat flow normalized per g of paste a) and clinker b) for PC and blended cements

The degree of hydration of C_3S and C_3A measured by XRD-Rietveld analysis is shown in Figure 2-4. Fine limestone and quartz enhanced C_3S hydration for all ages. The enhancement effect is higher with fine limestone as previously for the heat flow (Figure 2-3). At 1 day, coarse limestone shows similar degree of hydration of C_3S compared to PC. Afterwards, the hydration is increased with the same slope as PC. C_3A hydration is enhanced in the presence of fine limestone particles but seems to be delayed in coarse limestone cement up to 7 days. This could be explained by the additional sulfate to the system in comparison to Portland cement and lower alite hydration (less adsorption of sulfate on C-S-H). After 7 days there is little further hydration of C_3S and C_3A in any of the systems.

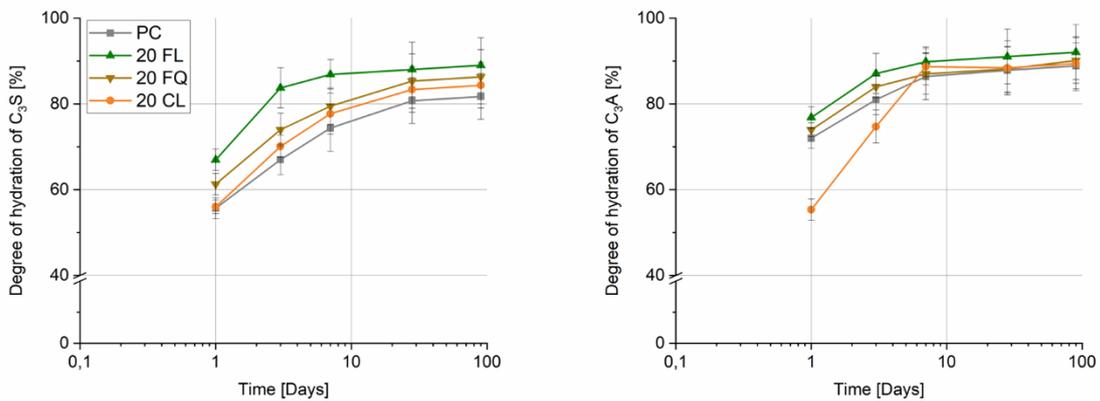


Figure 2-4. Degree of C_3S and C_3A hydration in PC and blended cements

2.3.3 Chemical effect

Figure 2-5 shows the calcite content a) and the amount of ettringite and AFm contents b) in limestone blended cements. Ettringite and AFm amounts in PC and quartz cements are indicated as points. Up to 7 days, higher amount of ettringite and AFm phases are obtained with fine limestone addition. This is in line with the higher hydration of C_3A (Figure 2-4) along with higher calcite reaction. Ettringite and AFm contents are comparable between PC, coarse limestone and quartz cements up to 7 days. The low amount of ettringite in coarse limestone is explained by the delayed hydration of C_3A as mentioned earlier. The presence of AFm even in PC and quartz cements is explained by the presence of calcite in clinker as shown by XRF (Table 2-1). AFm amount does not fully correspond to the amount of calcite reacted at late ages. This is due to the small error measurement related to calcite quantification induced by the preferred orientation of calcite.

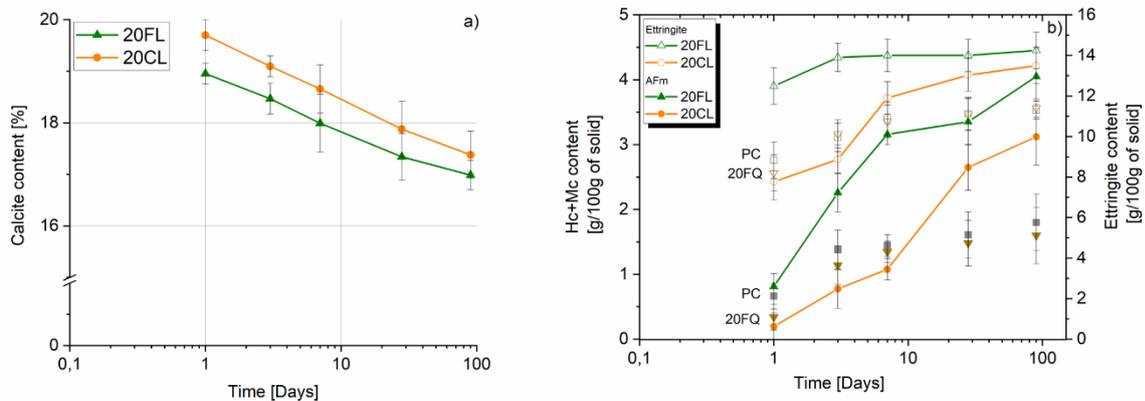


Figure 2-5. a) Calcite content in limestone cements b) AFm and ettringite amounts in limestone cements (the points are for PC and quartz blend)

2.3.4 Porosity

The impact of the incorporation of limestone and quartz on porosity after 1 and 28 days of hydration was investigated and plotted in Figure 2-6. At 1 day, cement blended with fine limestone and fine quartz show similar critical entry pore radius to PC (30 nm) but higher total porosity. On the other hand, coarse limestone shows higher total porosity and higher critical entry radius. At 28 days, the substituted systems have slightly higher porosity than the PC system. A similar critical entry radii (11 nm) is obtained for all systems, with that of the coarse limestone system still slightly higher.

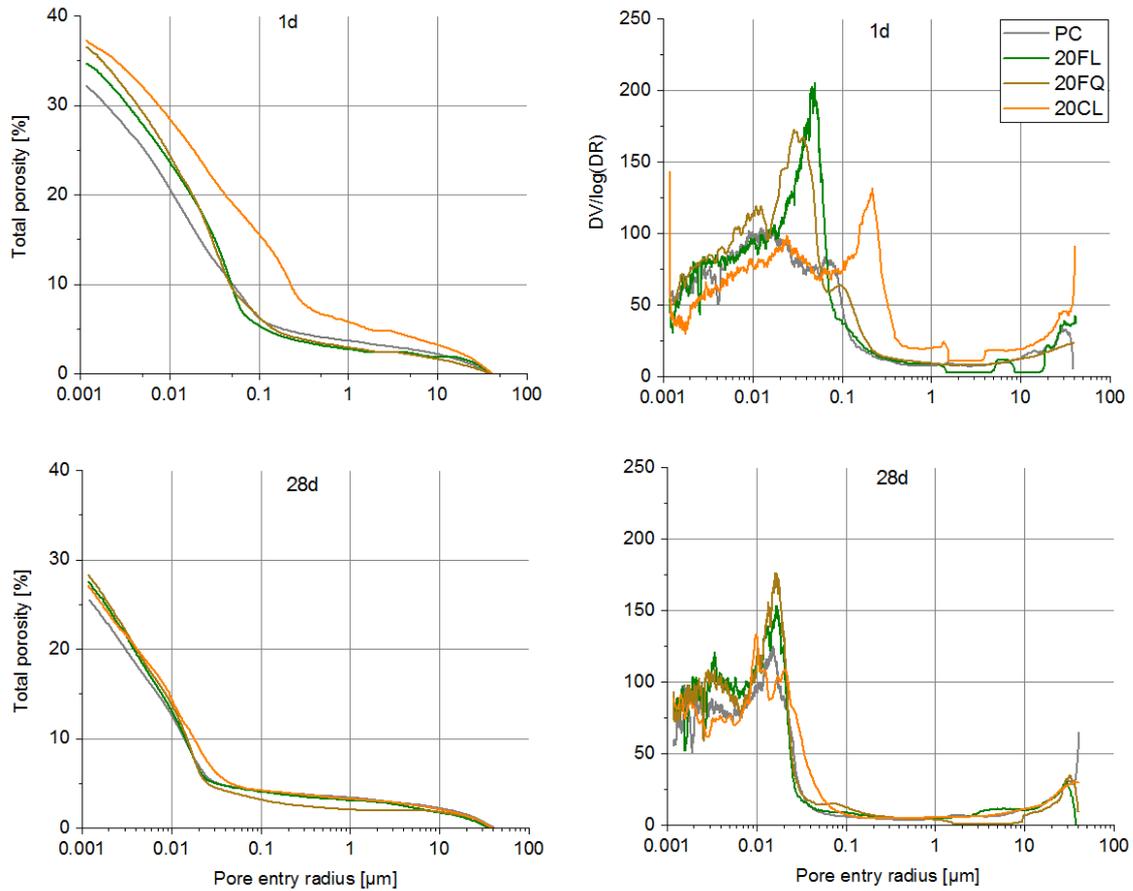


Figure 2-6. Porosity evolution at 1 and 28 days of hydration for PC and blended cements

Microstructural observations at 3 days for PC and limestone cements are shown in Figure 2-7. PC shows denser microstructure compared to the limestone cements. Fine limestone particles are well dispersed between the anhydrous clinker particles, while larger voids are apparent in the coarse limestone cement.

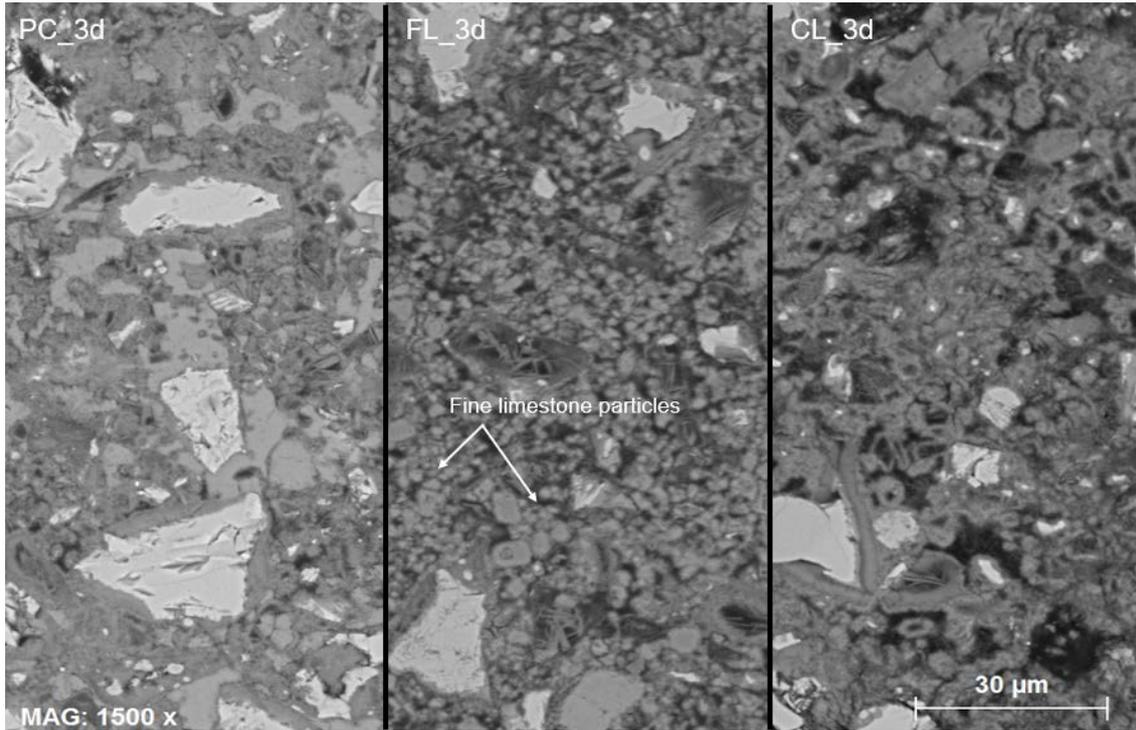


Figure 2-7. SEM observations for PC and limestone cement at 3 days of hydration

2.3.5 Chloride resistance

The chloride penetration profile in mortar samples after 6 months of exposure to 3 wt.% NaCl solution is given in Figure 2-8. The highest chloride content is observed with coarse limestone cement at the surface of the sample but also in depth. Slightly less chloride penetration is seen with fine limestone cement. Both limestone cements showed similar pore structure at 28 days (Figure 2-6) explaining the similarity in terms of chloride resistance after 6 months of exposure to NaCl solution. PC mortar shows the lowest chloride penetration.

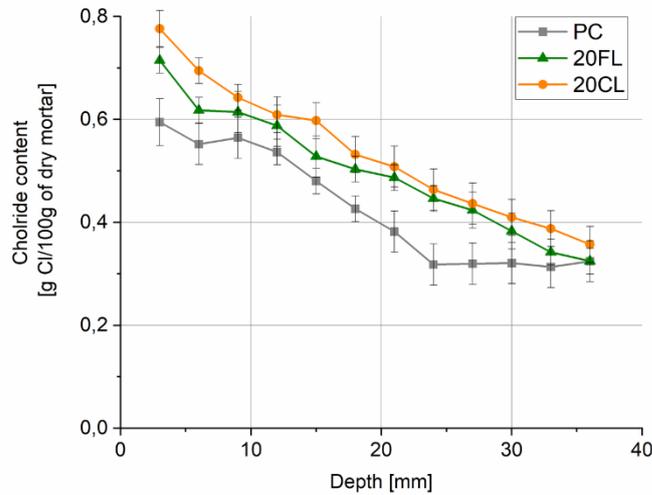


Figure 2-8. Chloride content for PC and limestone cement mortars after 6 months of exposure to 3 wt.% NaCl ponding solution

2.3.6 Combination of fine and coarse limestone

Previous results showed that 20% of clinker can be replaced by fine limestone particles while maintaining similar strength development up to 7 days. However, increasing the surface area could increase the water demand [43,44]. Therefore, a study was made in which fine limestone was progressively replaced by coarse limestone in increments of 5%.

Compressive strength for all blended cements is plotted in Figure 2-9. The dashed lines represent the strength for PC. The higher the fine limestone content or the lower the coarse limestone, the higher is the compressive strength. The mix 15% of fine particles and 5% of coarse limestone showed similar, or even slightly higher strength compared to the system with 20% of fine limestone.

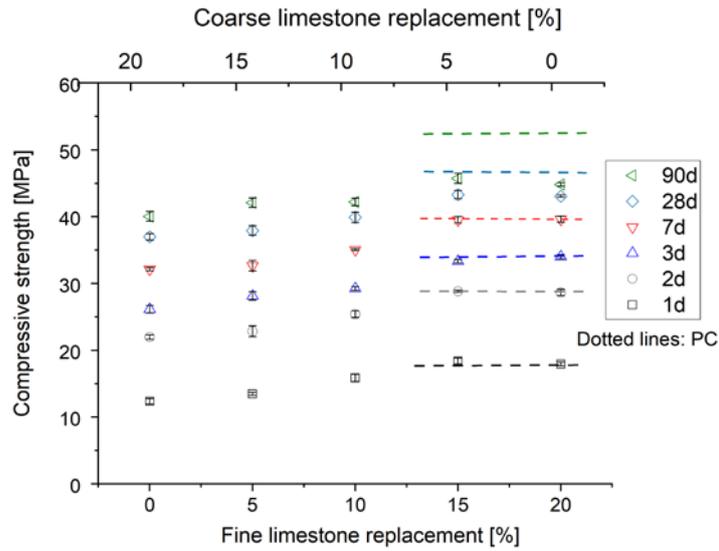


Figure 2-9. Compressive strength as a function of fine/coarse limestone powder from 1 up to 90 days

The volume amount of C-S-H and hemi- and mono-carboaluminate phases determined by mass balance approach is plotted at 1, 3 and 28 days in Figure 2-10. The highest amount of C-S-H is observed with PC. For all ages, a similar C-S-H amount is obtained between the two mixes with 20% and 15% of fine limestone. Similar observations are obtained for the blends with 20% and 15% of coarse limestone. Between 3 and 28 days, there is no significant evolution of C-S-H amount in limestone cements. AFm amount is higher with higher amount of fine limestone addition.

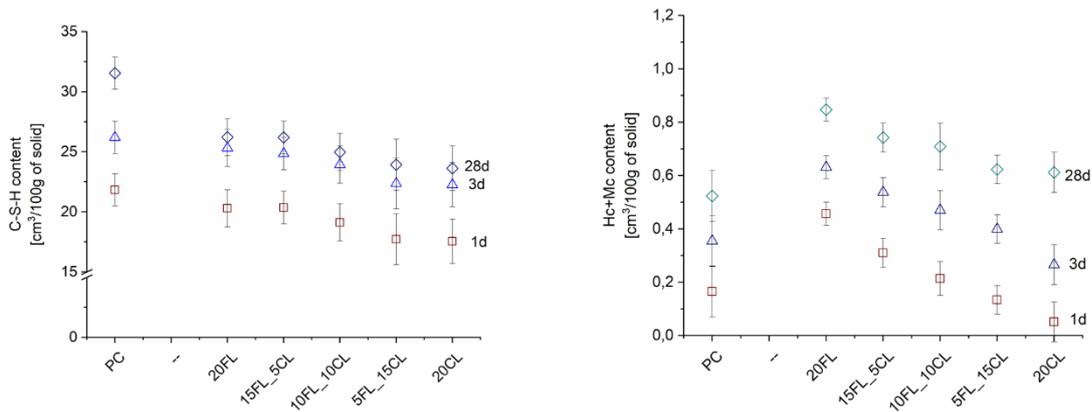


Figure 2-10. C-S-H and Hc+Mc amounts for PC and limestone cements at 1, 3 and 28 days

2.3.7 Correlation between strength and phase assemblage

The gel to space ratio permits to determine to which extent the available space is filled up by the hydrates [24,45,46]. The gel to space approach is the ratio of volume of hydration products to the space available for these hydrates as indicated in Equation 2-1. The gel is defined as the sum of the volume occupied by the hydration products including C-S-H, portlandite, AFm phases and AFt phases “ $\Sigma V_{\text{hydration products}}$ ”. The space is defined as the sum of the initial water volume $V_{\text{water},i}$ and the volume left by the reacted binder $V_{\text{reacted binder}}$. The binders here are clinker, limestone and anhydrite.

$$\text{GSR}_{\Sigma \text{hydrates}} = \frac{\Sigma V_{\text{hydrates}}}{V_{\text{water},i} + V_{\text{reacted binder}}} \quad \text{Equation 2-1}$$

The influence of the errors of measurements of the input data from mass balance approach on the determination of gel space ratio was established using a sensitivity analysis. The error values considered for the determination of the clinker phase content, the ettringite quantification, the C-S-H composition and the portlandite quantification were adapted from previous study [21]. Based on these errors, the maximum variations were applied to study their impact on the gel to space ratio. Figure 2-11 shows the compressive strength against gel space ratio for PC and all investigated blends in this study. The dashed lines indicate the deviations based on sensitivity analysis for all phases. A clear linear trend of the compressive strength with the gel to space ratio is obtained with all systems.

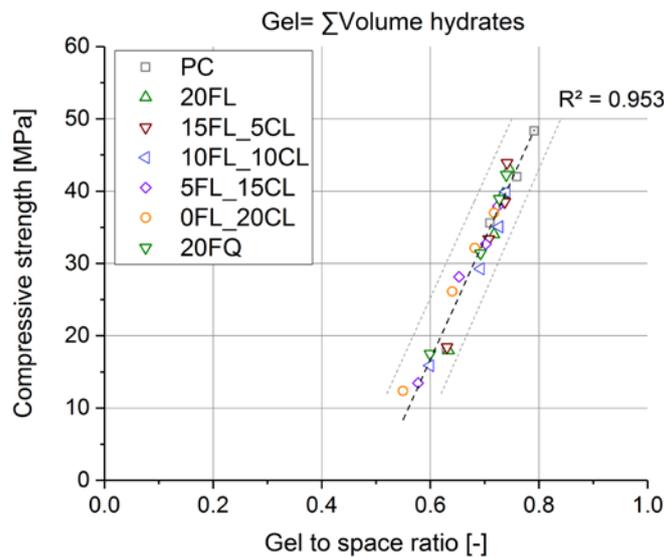


Figure 2-11. Correlation between compressive strength and gel space ratio considering the gel as the sum of hydration products

Blending 15% of fine limestone with 5% of coarse limestone maintained similar strength to the system with 20% of fine limestone for all ages. The results are explained with the similarity of phase

assemblage. A clear linear correlation between compressive strength and gel space ratio was obtained for all investigated systems.

2.4 Conclusions

This study describes the influence of limestone fineness on strength development and clinker hydration with a replacement level of 20%. Fine limestone was replaced with quartz with similar fineness (PSD and SSA) to understand the contribution of fine limestone on cement hydration. Similar compressive strength was obtained between PC and fine limestone blended cement up to 7 days. Replacing limestone with quartz decreased strength development with the main differences at 2, 3 and 7 days. The results were explained with the increase of C₃S hydration due to the enhancement effect of fillers and therefore compensating the dilution effect due to the decrease of clinker amount. Coarse limestone showed the lowest strength development for all ages. The influence of coarse limestone on cement hydration was mainly observed at late ages due to dilution effect.

In the second study, fine limestone was progressively replaced by coarse limestone in increments of 5%. Blending fine limestone (15%) and coarse limestone (5%) showed similar strength with the system containing 20% of fine limestone. A similar phase assemblage was obtained for all systems leading to a linear correlation between compressive strength and gel space ratio.

To sum up, this research showed that the substitution limit with limestone can be increased up to 20% without compromising strength development.





Chapter 3 Understanding of the slowing down of metakaolin reaction in limestone calcined clay cement (LC³) at late ages

Disclaimer: This chapter is adapted from the preprint version of the following article being submitted to Cement and Concrete Research journal – with permissions of all co-authors:

Y.Briki ^a, F.Avet ^a, M.Zajac ^b, P.Bowen ^a, M.Ben Haha ^b, and K.Scrivener ^a “Understanding of the slowing down of metakaolin reaction in limestone calcined clay cement (LC³) at late ages”

^a Laboratory of Construction Materials, EPFL, 1015 Lausanne, Switzerland

^b Heidelberg Technology Center GmbH, Rohrbacher Str.95, 69181 Leimen, Germany

My contribution: Methodology, experiments, analysing, writing

Abstract

Factors which could explain the slowing down of the metakaolin reaction in LC³ blends are investigated. Portlandite availability and the presence of aluminium ions in the pore solution are shown not to be slowing down factors. In this study, the upper and lower limits of water filled pores were investigated as factors slowing down the reactivity of metakaolin at later ages. Internal relative humidity measurements indicate that at 28 days water is present only in pores below 13 nm. Above this limit, hydration products cannot deposit and the metakaolin reaction is slowed down. Below this limit, the growth of AFm and C-(A)-S-H seems to be limited below a range of pore radii between 3 to 7 nm due to the level of concentration in solution required to balance the increase of the surface energy associated with curvature of crystals to grow into small pores. An enhancement of metakaolin reaction was obtained at late ages when the capillaries are filled with solution.

Keywords: pore radius, saturation index, water-filled capillary pores

3.1 Introduction

To reduce the environmental impact of cement production, supplementary cementitious materials (SCMs) are increasingly used in blended cements. The high demand for SCMs cannot be met with traditional SCMs, such as fly ash and granulated blast furnace slag as the amount of these relative to cement is rather low [6]. Slag plus useable fly ash is at present about 15% of cement production globally and this is will decrease in the near future [4,6,9]. Recently, studies have focused on replacing clinker with a combination of calcined clay and limestone which have the advantage of being abundant: LC³ (limestone calcined clay cement) [6]. The replacement level of Portland cement by LC³ can be as high as 50% with similar compressive strength to plain Portland cement from 7 days onwards [15]. However, neither clinker nor metakaolin react completely in LC³ cement pastes with w/b of 0.4 at late ages [31].

Different mechanisms have been considered for the slowing down of reaction at late ages. Antoni et al. [47] suggested that the main factor for slowing down metakaolin reaction at late ages is the availability of portlandite. The presence of alumina in solution has also been suggested as a reason for reaction limitations. Dissolution experiments performed under far-from-equilibrium conditions showed that the dissolution of the pozzolanic glasses was inhibited by increasing amounts of aluminium ions solution [48]. The impact of aluminium was also observed to inhibit the dissolution of C₃S [49,50].

Cement hydration takes place via a dissolution-precipitation processes: the anhydrous phases dissolve and provide ions to the pore solution. These ions then combine to form hydration products which precipitate from the pore solution. The precipitation of hydrates can only occur in solution filled pores. There are two conditions limiting the availability of pores for hydrates precipitation. First, at the upper end, cement pastes are almost never completely saturated. After setting, the volume of the hydration products is less than that of the reactants (anhydrous phases plus water) leading to the creation of voids after setting and the decrease of internal relative humidity [51]. C₃S hydration has been reported to cease below about 80% of internal relative humidity [52]. Even when external curing water is provided (commonly after 1 day of hydration), large pores remain empty since water can penetrate only a millimetre or so due to the refinement of the porosity during cement hydration. The internal relative humidity can be described using Kelvin Laplace equation (Equation 3-1)

$$\ln \left(\frac{P}{P_0} \right) = \ln (RH) = \frac{2\gamma V_m}{r RT} \quad \text{Equation 3-1}$$

where P [Pa] is the vapour pressure, P₀ [Pa] is the saturated vapour pressure, V_m is the molar volume of the water V_m = 1.8 10⁻⁵ m³/mol, γ is the water interfacial energy γ = 0.07286 N/m, r [m] is the radius of the droplet, and the universal gas constant R = 8.314J/kMol (all at 293.15 K i.e. 20 °C).

The reduction of internal RH in cementitious systems depends on two major mechanisms: desaturation of pores due to chemical shrinkage (RH_k) and water activity of the pore solution (RH_s), RH = RH_k × RH_s [17,22]. The RH_s varies with the amount and species of salt dissolved and decreases

slightly and only during the first month after hydration [53]. RH_s is approximated by the following Equation 3-2[53]:

$$RH_s(t) = 0.9872 - 0.0025 \cdot \ln(t) \quad \text{Equation 3-2}$$

Generally, internal relative humidity in real concrete (even those cured underwater) is in the range 90-95% RH [51,53,54]. At 20°C, the Kelvin Laplace equation shows that for 95% of relative humidity, a limiting of pore radius of approximately 20 nm is obtained between empty and saturated pores. Above 20 nm, vapour rather than solution is present and hence precipitation of hydrates from solution is not possible.

At the lower end, the growth of hydration products is driven by the saturation of the pore solution with respect to the hydration products. As the pore structure gets finer, hydrates need to grow into smaller pores. To grow into small pores the radius of curvature of the crystals must increase and this increases the activity of the pore solution needed to continue crystal growth. This is illustrated in Figure 3-1 showing that after growing and filling a large pore, the hydrate can continue to grow into a smaller pore only if the activity of the pore solution is sufficient to balance the increase of the surface energy due to the curvature needed to enter the pore.

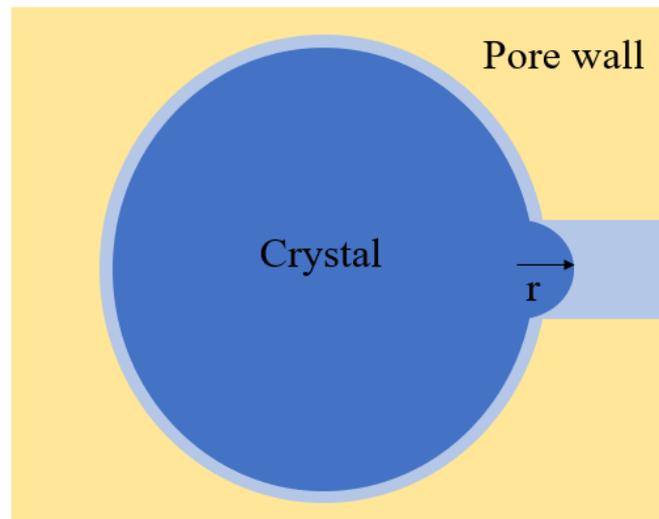


Figure 3-1. Schematic illustration of homogenous and spherical crystal growth exerting isotropic pressure in large and small pores, note the thickness of the liquid film between the crystal and the pore wall. Adapted from [55]

The ionic activity product in equilibrium with a curved crystal is given by the Kelvin-Laplace equation (Equation 3-3) linking the saturation index SI and the pore radius r in the cement:

$$\frac{RT}{V_m} \ln \left(\frac{IAP}{K_{sp}} \right) = \frac{2\gamma}{r} \quad \text{Equation 3-3}$$

Where V_m is the molar volume of the hydration product growing in the pore [m^3/mol]. IAP refers to the ion activity product calculated from the measured concentration, K_{sp} is the solubility product of the given phase. γ is the interfacial energy between the hydration product and the solution [N/m] and r is the pore radius in [m]. The classical crystal growth mechanism given by the Kelvin Laplace equation over simplifies the situation as it is assumed that the crystal is spherical and under uniform pressure. Nevertheless, this gives an indication of the order of magnitude of effects. Recently, Avet and Scrivener [31] showed an agreement between the slowing down of hydration (experimentally) and the calculation given by Kelvin-Laplace equation. In their study on LC³ cement paste, the authors showed that the pore entry radius investigated by MIP technique reached a minimum pore radius after 7 days (6 nm) and then did not decrease further. This point where the minimum pore entry was reached corresponded to the slowing down of hydration and it was suggested that hydration became limited by the growth of hydration products in fine pores (insufficient saturation index required for hydrate growth), as previously suggested by Berodier and Scrivener [56].

Overall, the factors limiting metakaolin reaction at late ages are not fully explored. In this chapter, the lack of portlandite and the impact of aluminium on metakaolin reaction are first studied. Then the upper and lower aspects of the water filled pores are investigated as factors limiting reactivity of metakaolin at later ages.

3.2 Materials and methods

3.2.1 Materials

Clinker was provided from HeidelbergCement. Soluble anhydrite came from Saint-Gobain. The calcined clay came from Bhuj, India and contained 48% of metakaolin as determined by thermogravimetric analysis (TGA) according to [31]. Limestone powder came from Omya. The content of calcium carbonate was above 98% as measured by thermogravimetric analysis (TGA). Quartz was from Sibelco and silica fume from Sigma-Aldrich. The oxide composition of the materials determined by X-ray fluorescence (XRF) analysis is shown in Table 3-1. The clinker composition is indicated in Table 3-2.

Component	Clinker	Calcined clay	Silica fume	Quartz
Chemical analysis (%)				
CaO	64.4	0.2	-	-
SiO ₂	20.6	49.7	92.5	1
Al ₂ O ₃	5.7	41.8	0.3	-
Fe ₂ O ₃	3.7	2.3	-	-
MgO	1.6	0.1	-	-
Na ₂ O	0.2	0.3	-	-
K ₂ O	1.3	0.1	-	-
SO ₃	1.0	-	-	-
TiO ₂	0.3	3.4	0.3	-
P ₂ O ₅	0.1	0.1	0.3	-

Table 3-1. Chemical composition of clinker, calcined clay, silica fume and quartz

C ₃ S (%)	C ₂ S (%)	C ₃ A (%)	C ₄ AF (%)
71.1	6.2	6.6	12.9

Table 3-2. Composition of clinker phases

The particle size distribution of the powders determined by laser diffraction with a Malvern Master-size is plotted in Figure 3-2. The specific surface area determined by nitrogen adsorption is also indicated in Figure 3-2 .

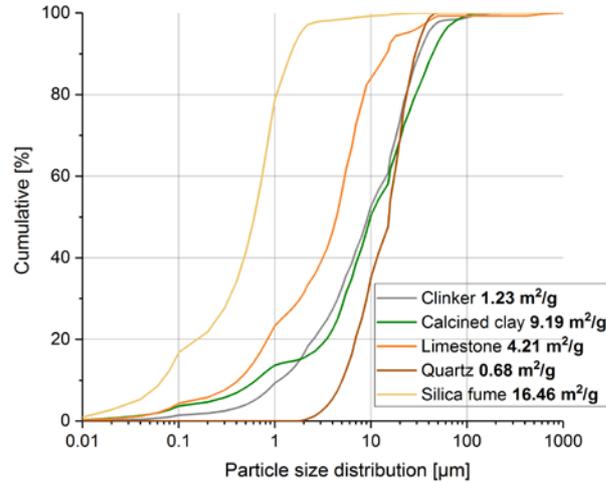


Figure 3-2. PSD and BET of all used materials

The mix composition for all the systems is detailed in Table 3-3. The clinker replacement level was fixed at 50%. A content of 4.5% of soluble anhydrite (2.64% of SO₃) by binder was added to PC and blended cement. To assess the lack of portlandite in LC³ system, 5% of calcium hydroxide (Roth company) was added to the LC³ (LC³+5%CH). To assess the impact of Al on metakaolin reaction, silica fume (SFC) replaced only the metakaolin part of the calcined clay. The secondary phases of the calcined clay were replaced by quartz.

The impact of increasing water binder ratio was investigated as well for LC³ cement: 0.3, 0.4 and 0.6 in sealed-curing conditions. For 0.3 and 0.4, Mapei SP914 Dynamon polycarboxylate superplasticizer was used (max 1.4 wt% of total solid mass) to ensure similar workability to PC.

Notation	Clinker	Calcined clay	Limestone	Silica fume	Quartz	Calcium hydroxide	Anhydrite
PC	95.5	-	-	-	-	-	4.5
LC ³	47.8	28.6	19	-	-	-	4.5
LC ³ +5%CH	47.8	28.6	19	-	-	5	4.5
SFC	47.8	-	19	13.8	14.9	-	4.5

Table 3-3. Mix composition for all investigated blended cement

3.2.2 Methods

All pastes were mixed for 2 min at 1600 rpm, and then sealed cured with parafilm or cured in pore solution at 20 °C until tested. For pore solution curing, the LC³ sample was immersed in a pore

solution, similar to that extracted from pastes [24] after setting. Once the samples were sufficiently hardened, they were cut into slices and then broken into 2mm pieces which were put back in the pore solution. The idea of making such small pieces is to allow the solution to access all the capillary pores.

The quantification of crystalline phases was investigated using X-Ray Diffraction (XRD). Measurements were carried out on freshly cut paste slices at 1, 3, 7, 28, 90 and 180 days.

The following experiments were carried out after stopping the hydration using solvent exchange with isopropanol:

TGA was used to quantify portlandite using the tangent method [57]. For pore structure characterization, MIP was used with the contact angle of 120° between mercury and paste. The internal relative humidity (RH) of the paste samples was monitored using a HC2-AW-USB water activity probes from Rotronic.

The amount of reacted metakaolin/silica fume was estimated by the mass balance approach [46,58]. The amount of reacted metakaolin and silica fume is determined by iteration, by comparing for each metakaolin increment the predicted portlandite content with experimental XRD/TGA results.

The methods employed in this study are detailed in Appendix 1: Methods.

The evolution of the populations of water in the samples was investigated by tracking the relaxation time of hydrogen spin using ¹H-nuclear magnetic resonance (¹H-NMR). This allows the distinction of capillary water from gel water and interlayer water of the C-S-H and the “solid” water bound to portlandite, ettringite and AFm phases [59]. The use of grey cement was not compatible with ¹H-NMR measurements since the iron content (3.7% Fe₂O₃) is too high degrading the accuracy of the results [60]. Thus, a white cement from Aalborg Cement was used for ¹H-NMR experiments. The sulfate and alkali levels were adjusted to ensure similar hydration to grey cement [60]. Bhuj clay was simulated using kaolinitic clay (95%) diluted with quartz.

3.3 Results

3.3.1 Degree of reaction of metakaolin and degree of hydration of clinker

The degree of reaction of metakaolin in calcined clay in LC³ cement with w/b ratio of 0.4 is shown in Figure 3-3. The results are presented in linear scale in Figure 3-3a) to show the slowing down of the reaction and in logarithmic scale in Figure 3-3b) to highlight the reaction at early age. At 1day, the degree of reaction of metakaolin was observed to be at 27%. After 28 days, metakaolin reaction slows down and levels off at around 64%.

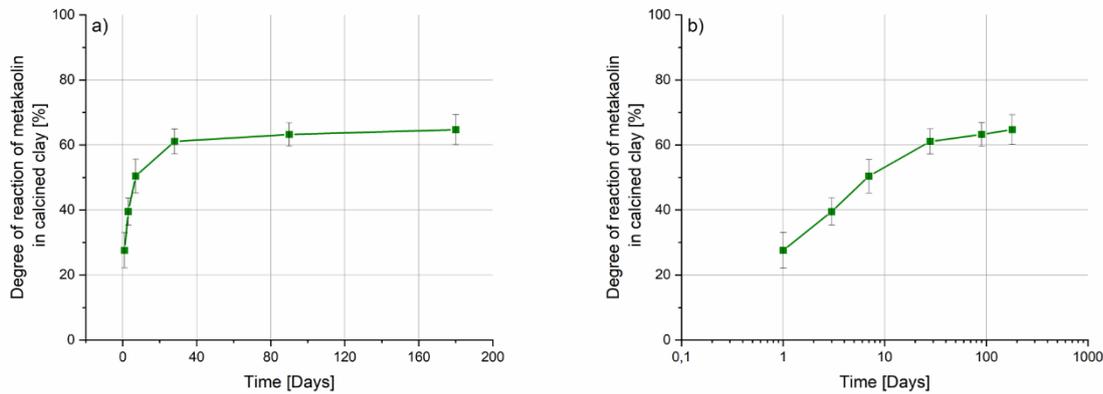


Figure 3-3. Degree of reaction of metakaolin in LC³ cement in a) linear scale and b) logarithmic scale (w/b=0.4)

Figure 3-4 shows the degree of reaction of the clinker phases: silicate (C₃S and C₂S) and aluminate (C₃A and C₄AF) phases in PC and LC³ cement. Alite hydration is higher in LC³ blended cement than the reference system. This is due to filler effect of the calcined clay and fine limestone as recently reported [35]. However, the hydration of C₂S and to a less extent C₃A, seems to be much less in the LC³ system.

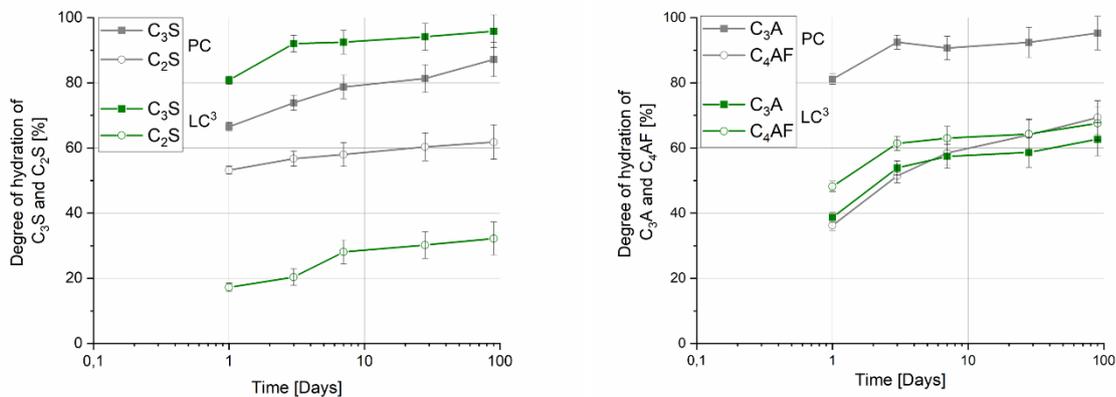


Figure 3-4. Degree of hydration of silicate and aluminate phases in PC and LC³ cements

3.3.2 Factors slowing down metakaolin reaction and clinker hydration at late ages

3.3.2.1 Lack of portlandite for pozzolanic reaction

The portlandite content determined by TGA is shown in Figure 3-5 for PC, LC³ and LC³ with 5% of portlandite. The portlandite content increases in PC due to the hydration of the silicate phases. Up to 7 days, portlandite is consumed in LC³ cement due to the pozzolanic reaction but afterwards, the consumption of portlandite effectively stops. A similar trend was observed also in the systems with

added-portlandite. The difference of portlandite content between LC³ and LC³ added-portlandite corresponds to the extra portlandite added.

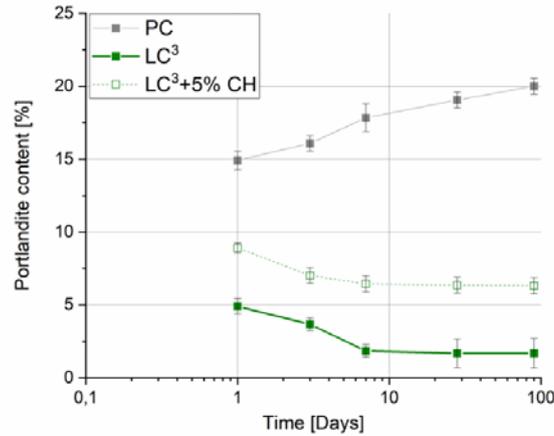


Figure 3-5. Portlandite content for PC, LC³ and LC³+5% CH

The degree of reaction of metakaolin in the LC³ with system with added-portlandite is plotted in Figure 3-6. A higher degree of reaction of metakaolin is observed in the system with added portlandite up to 7 days. Afterwards, the degree of reaction levels off at the same level as the reference system. The extra portlandite does not enhance the degree of reaction of metakaolin at late ages. The lack of portlandite is not the reason for the slowing down of metakaolin reaction at late ages.

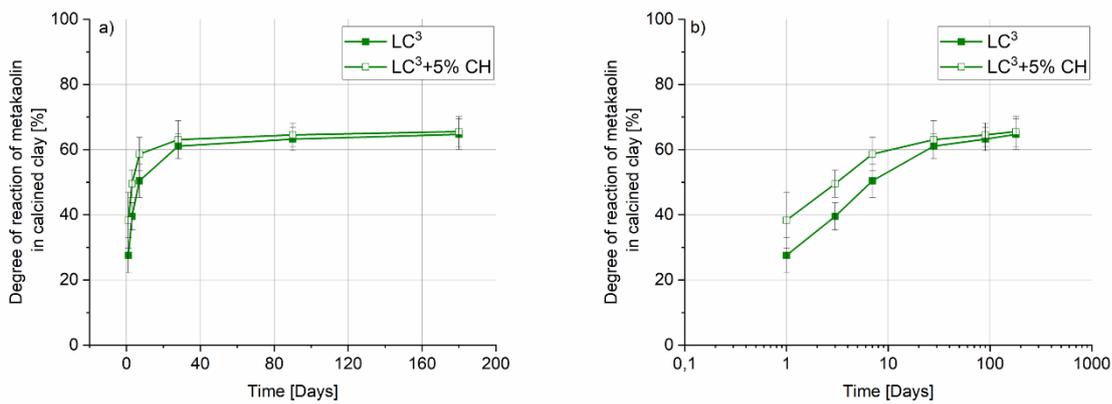


Figure 3-6. Degree of reaction of metakaolin in LC³ and LC³+5% CH

3.3.2.2 Impact of aluminium ions on metakaolin reaction

To assess the impact of aluminium on metakaolin reaction, a system was prepared where silica fume, where Al ions are absent, replaced the metakaolin part of the calcined clay. The secondary phases of the calcined clay were replaced by quartz. The degree of reaction of silica fume in this blend is plotted and compared to the metakaolin in LC³ in Figure 3-7. The reaction of silica fume is similar to that of the metakaolin and also slows down at late ages. This experiment indicates that the aluminium present in the pore solution is not responsible for the slowing down of metakaolin reaction, since similar slowing down is also observed with silica fume cement.

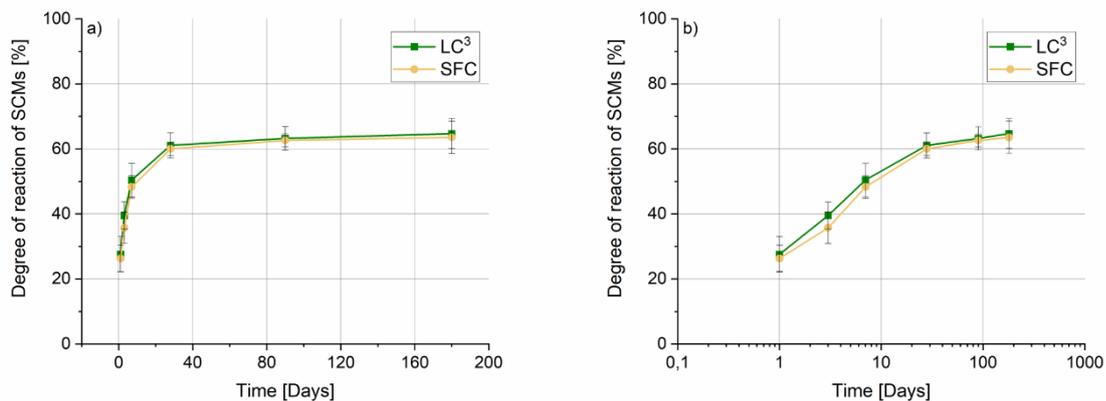


Figure 3-7. Degree of reaction of metakaolin and silica fume

To check whether Al from the metakaolin has any impact on the clinker hydration, the degree of clinker phases hydration in the silica fume system is plotted in Figure 3-8. The results show very similar evolution in both systems for all phases. A limitation on the DoH at later ages was observed also in silica fume cement, indicating that neither is the clinker hydration affected by aluminium at late ages.

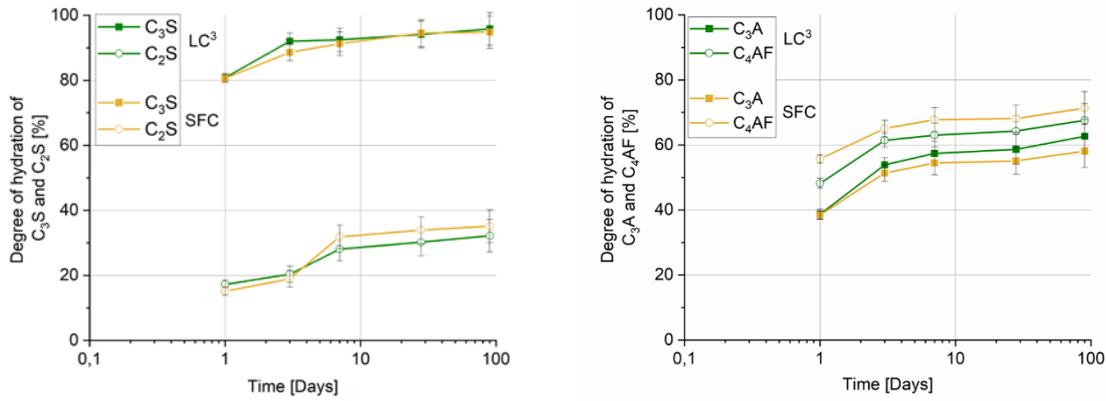


Figure 3-8. Degree of clinker hydration in LC³ and silica fume cement

3.3.2.3 Water filled porosity

3.3.2.3.1 At the upper end: Saturation of capillary pores

After setting, the capillary pores are progressively emptied due to chemical shrinkage [61,62], leading to the decrease of the relative humidity. The internal relative humidity of the LC³ and PC pastes is plotted in Figure 3-9. The relative humidity is higher in LC³ than PC system. The relative humidity (RH) in LC³ decreases with time to stabilize at around 90% as already observed in [24]. The relative humidity drop caused by the desaturation of the pores (RH_K) was corrected for relative humidity of the pore solution (RH_S) using the approximation given by Equation 3-3. The pore radius corresponding to relative humidity (RH_K) of 92% and 86% are 13 and 7 nm for LC³ and PC respectively. Above this range of pore radius, vapour rather than solution is present.

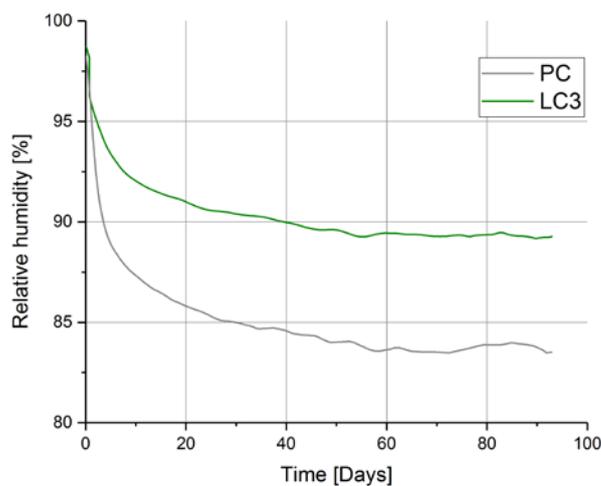


Figure 3-9. Internal relative humidity of PC and LC³ systems

Slices of 2 mm thickness cured under pore solution after setting time were studied to check how filling the capillary pores with solution affects the metakaolin and clinker reactions. The degree of reaction of metakaolin and portlandite content in the LC³ system are shown in Figure 3-10 and compared for both curing conditions. The reaction of metakaolin is enhanced for the pore solution cured sample to reach 100% of reaction at 90 days. This high degree of reaction leads to depletion of portlandite after 28 days of hydration as shown in the right graph.

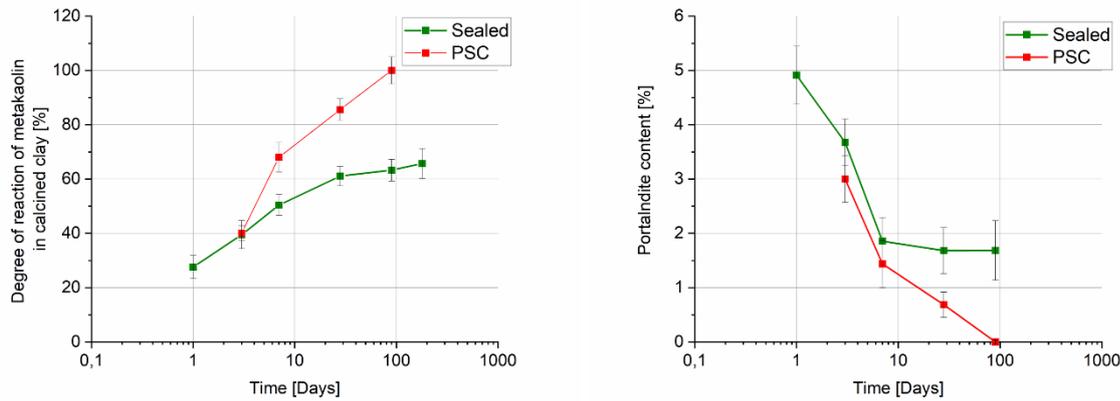


Figure 3-10. Degree of reaction of metakaolin (left) and portlandite content (right) in sealed and pore solution cured systems (PSC)

¹H-NMR results (Figure 3-11) compare the evolution of capillary and gel water (right) and of solid and interlayer water (left) for sealed systems and those cured in pore solution. Up to 10 days, capillary and gel pores in both systems follow the same trend. Afterwards, the evolution for both water populations is different between the two curing conditions. The capillary water decreases progressively in the sealed system to reach about 1% at 90 days due to the chemical shrinkage causing pores to empty. On the other hand, approximately 15% of capillary water remains in the cured system leading to the higher degree of reaction (Figure 3-10). The higher amount of gel pores in the sealed system can be explained by the fact that when capillary pores are filled with vapour, they actually still contain a water film on the surface, which is “detected” by ¹H-NMR as gel rather than capillary water. The solid and the interlayer water population are slightly higher in the pore solution cured systems due to the higher degree of reaction.

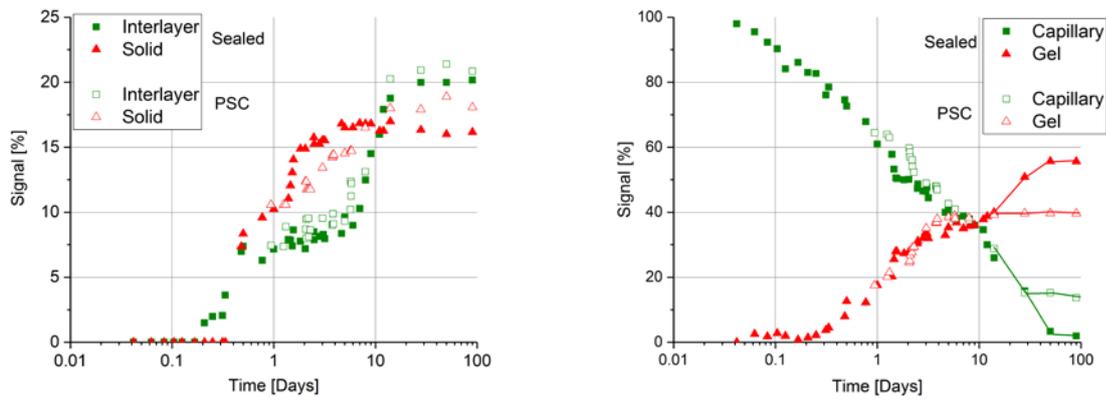


Figure 3-11. Solid and interlayer pores (left) capillary and gel pores (right) for sealed and cured LC³ white cement

The porosity of pore solution cured systems is compared to sealed cured pastes in Figure 3-12. Both systems seem to converge toward a similar critical entry radius. The total porosity in the pore solution cured samples is slightly lower due to the higher degree of reaction, but this reduction in porosity is mainly in the large pores, before the up turn in the MIP curve. The porosity in the pore solution cured system is about 4% in the PSC systems in contrast to 5.5% in the sealed cured systems.

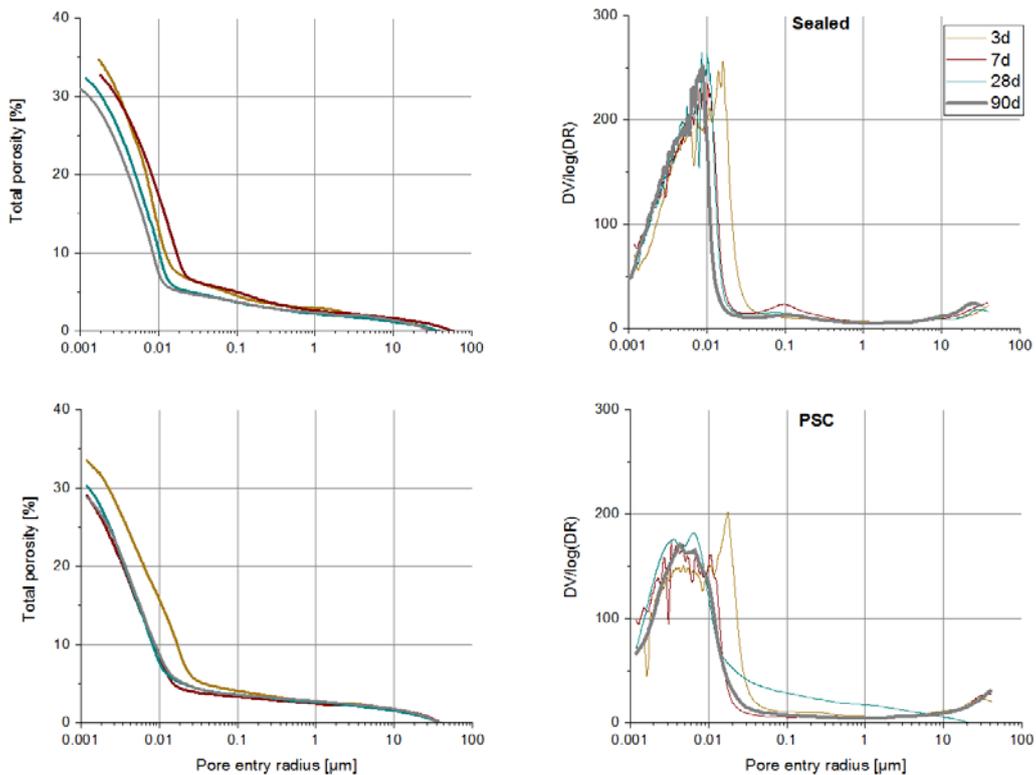


Figure 3-12. Porosity of sealed and pore solution cured LC³ cements

3.3.2.3.2 At the lower end: Growth of hydrates below a critical radius

The water to binder ratio was increased from 0.3 to 0.6 in LC³ cement paste in order to check the impact of the addition of water and space on the extent of metakaolin reaction. The degree of reaction of calcined clay for w/b 0.3, 0.4 and 0.6 is plotted in Figure 3-13. The degree of reaction of metakaolin in calcined clay using a w/b ratio of 0.5 was added from previous results [24]. As expected, the reaction of calcined clay is increased when increasing the water to binder ratio. Nevertheless, the reaction of metakaolin in calcined clay slows down after 28 days even with the water to binder ratio of 0.6. For w/b 0.3, the metakaolin reaction is slowed down more rapidly compared to the other w/b ratios (after only 7 days).

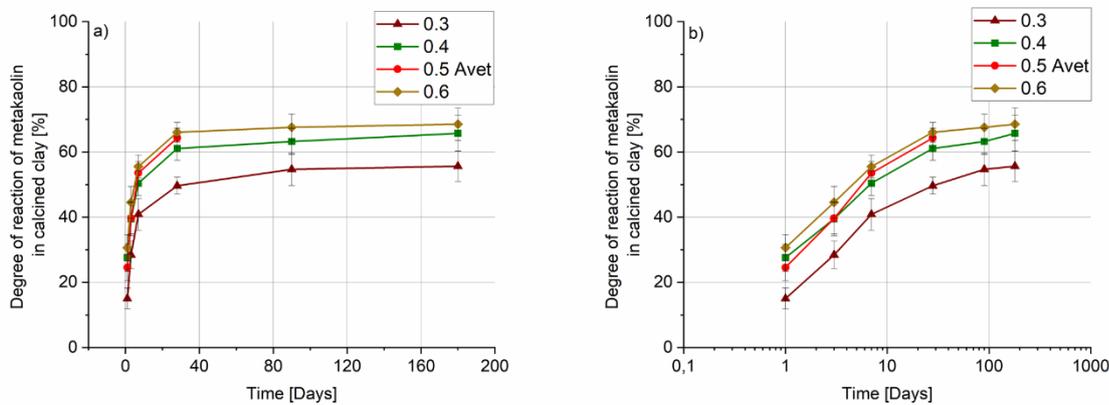


Figure 3-13. Degree of reaction of metakaolin for w/b=0.3,0.4,0.5 [12] and 0.6

For the lowest water binder ratio, relative humidity was investigated to check if the slowing down is linked to the desaturation of pores (Figure 3-14). The relative humidity of 0.3 drops very fast compared to the system with 0.4. About 71% was obtained for LC³_0.3 after 28 days. The results give an estimation of 3nm of pore radius above which the water is absent causing the slowing down of metakaolin reaction.

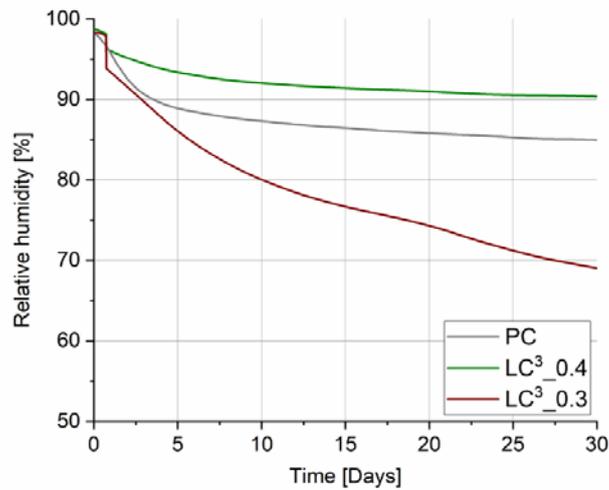
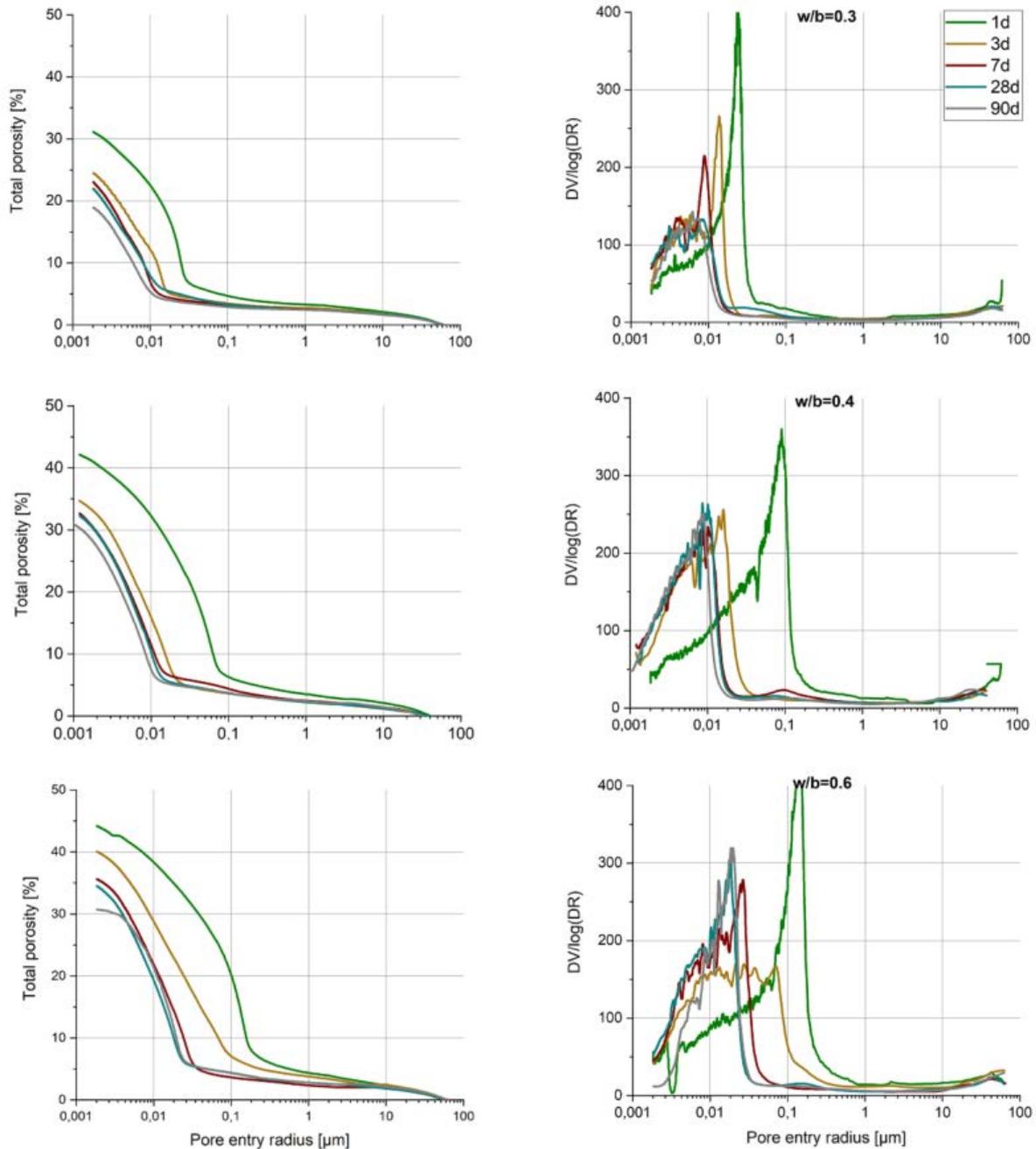


Figure 3-14. Relative humidity of PC, LC³ with w/b=0.3 and 0.4

The pore size distribution plots are shown in Figure 3-15. Almost no further refinement is observed after 28 days of hydration for all water binder ratios. A critical entry pore radius (the maximum of the capillary peak of the derivative curve) of approximately 3, 8 and 10 nm are obtained at 90 days for w/b 0.3, 0.4 and 0.6 respectively.

Figure 3-15. Porosity in LC³ for w/b=0.3, 0.4 and 0.6

The phase assemblage using mass balance approach of LC³ with different water binder ratio of 0.3, 0.4 and 0.6 was investigated at 90 days of hydration and plotted in Figure 3-16. According to this calculation, there is still free water present even at w/b ratio of 0.3. Moreover, a higher portlandite amount is observed at lower w/b ratio supports the finding that lack of portlandite is not limiting the metakaolin reaction. On the other hand, lower amounts of hemi- and mono-carboaluminate are observed with lower w/b ratio. There is a higher amount of clinker and metakaolin remaining unreacted with lower w/b ratio. The amount of C-A-S-H is less affected than AFm phases, but a somewhat

smaller amount is observed with lower w/b ratio. These observations suggest that the growth of AFm and C-A-S-H is more limited at low w/b ratios.

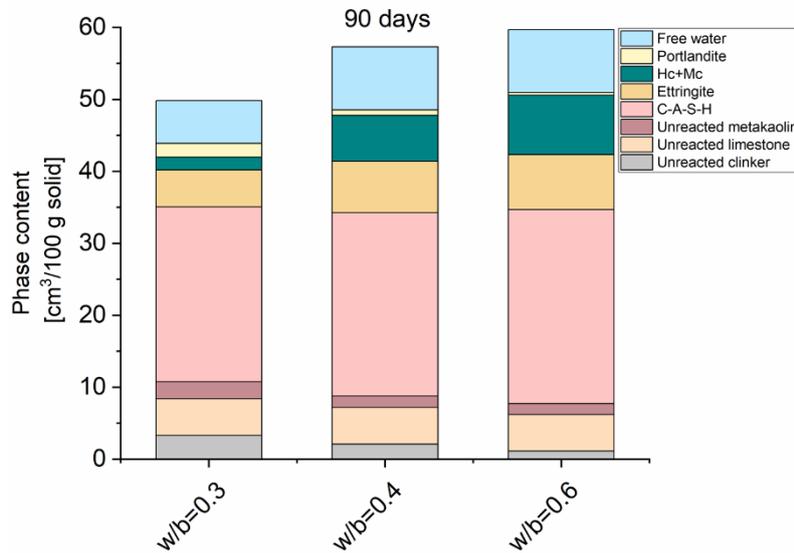


Figure 3-16. Phase assemblage of LC³ for w/b=0.3, 0.4 and 0.6 at 90 days of hydration assuming 2g/cm³ for C-A-S-H density (bulk density [18,24])

In order to estimate the critical pore radius below which the growth of hydrates could be limited, the saturation index required for hydrate growth can be compared with the saturation index calculated from the pore solution measurements using GEMS software. As shown in the Kelvin-Laplace equation (Equation 3-1), to obtain the SI_{required} , the molar volume (m^3/mol) and the surface energy (N/m) between the solution and the crystal of the hydrate product are required. The molar volumes can be obtained from the density and the molecular weight of the hydrates. The layer structure of AFm phases could help to get approximate interfacial energies. AFm phases have a structure composed of layers. The main layer consists of sheets of Ca (OH) octahedral ions, as in portlandite, in which 1/3 of the Ca^{2+} ions are replaced by $\text{Al}^{3+}/\text{Fe}^{3+}$ ions. The anionic composition of AFm phases in cementitious materials is dominated by anions such as CO_3^{2-} (coming from calcite), SO_4^{2-} , Cl^- and OH^- depending on the type of cement [63,64]. Values of interfacial energies for calcite and portlandite are documented and they are between 0.08 and 0.1 N/m for calcite [64] and 0.065 N/m for portlandite [65]. Thus, the range 0.065 – 0.1 N/m was used in this study.

Regarding C-S-H phases, different values have been reported in the literature [66,67]. Using the classical theory of homogenous nucleation, Gauffinet and Nonat [66] obtained 0.012N/m as a value for interfacial energy between synthetic C-S-H and solution. Andalibi et al. [67] used the population balance approach to describe the precipitation of a model synthetic C-S-H system with Ca : Si = 2. The authors obtained a value of 0.055 N/m for the interfacial energy of C-S-H-solution.

In this study, the interfacial energies were also estimated using Nielsen and Mersmann approach [68,69]. Nielsen [68] suggested a linear correlation between solubility and interfacial energy as indicated in Equation 3-4 and Equation 3-5

$$\frac{\sigma}{K T} = 2.82 - 0.272 \ln(K_{sp}) \quad \text{Equation 3-4}$$

$$\gamma = \sigma/a^2 \quad \text{Equation 3-5}$$

Where σ is the edge work, K Boltzmann constant, T the temperature, k_{sp} the solubility of the crystal, a is the molecular unit cell distance and finally γ is the interfacial energy.

Throughout this work, the molecular unit cell distance “ a ” used in Nielsen’s approach [68] was calculated as the cube root of the molecular unit cell volume (Ω) of C–S–H (composition $(CaO)(SiO_2)_{0.5}(H_2O)_{1.5}$) as reported in the study of Andalibi et al. [67]. The unit cell volume obtained was $8.1699 \times 10^{-29} \text{ m}^3$, calculated according to the formalism by Thomas et al. [70]. The value was acceptable in the light of typical values for various precipitates used in crystallization community.

Later, Mersmann [69] derived an equation for interfacial energy γ where the first term considers the adsorption of ions at the interface and the second term considers the approach of a point charge towards this interface (Equation 3-6):

$$\gamma = \gamma_0 - \underbrace{\frac{RT}{zF} \left\{ \sigma_{\max} \ln \left(\frac{\sigma_{\max}}{\sigma_{\max} - |\sigma|} \right) \right\}}_{\text{Adsorption of ions}} + \underbrace{\frac{8FI}{\kappa} \left[\sqrt{\left(1 + \left(\frac{\kappa\sigma}{4FI} \right)^2} \right) - 1 \right]}_{\text{Approach of the ions}} \quad \text{Equation 3-6}$$

With γ_0 the maximum interfacial energy of a crystal at its point of zero charge, R the gas constant, T the temperature, F the Faraday constant, z the valence of a ($z:z$) electrolyte, σ and σ_{\max} are the surface charge of ionic crystals, I the ionic strength and $1/\kappa$ the Debye length.

The details of these approaches are given in the Appendix 3: Nielsen and Mersmann approach.

In order to estimate the influence of the errors of the input data on the determination of the interfacial energy, a sensitivity analysis was carried out. Table 3-4 shows the error values considered for the determination of the density, the solubility, the dielectric constant and the surface charge density. Based on these errors, the maximum variations are applied to study their impact on the interfacial energy. The estimated error was $\pm 0.03 \text{ N/m}$.

Variable	Error measurement
Density (g/cm ³) [59]	±0,2
Log ksp [71]	±0,1
Dielectric constant [72]	±0,2
Surface charge density (C/m ²) [73]	±0,07

Table 3-4. Sensitivity analysis for the determination of the interfacial energy using Mersmann's approach [31]

Thermodynamic modelling was used to calculate the saturation indexes, SI_{GEMS} , for Mc and C-S-H phases at 28 days of hydration, defined as the ratio of ion activity product or the measured concentrations to the solubility of the crystal [74]. Calculations were carried out using the geochemical modelling program GEMS version 3.3 with thermodynamic data from the PSI-GEMS database supplemented by the cement specific data from CEMDATA18 database [71].

The details of all investigated approaches in this study are given in the supplementary material. The models were also discussed in the supplementary material.

AFm growth

The graph in Figure 3-17 plots the SI required for Mc growth in terms of pore radius. Beside the values encountered in the literature, the interfacial energy estimated from Nielsen approach [68] was used. The graph shows that as the pore radius decreases, the saturation indexes required for Mc growth increases to balance the increase of the surface energy due to the curvature needed to enter the pore. Between 3 to 7 nm seems to be the range of pore radii below which the growth of Mc would be limited since SI required is higher than the SI existing in the pore solution. The value of interfacial energy using Nielsen approach lies between the values of portlandite and calcite suggesting that interfacial energy of portlandite and calcite could be reliable for the estimation of the pore radius related to monocarboaluminate growth limitation.

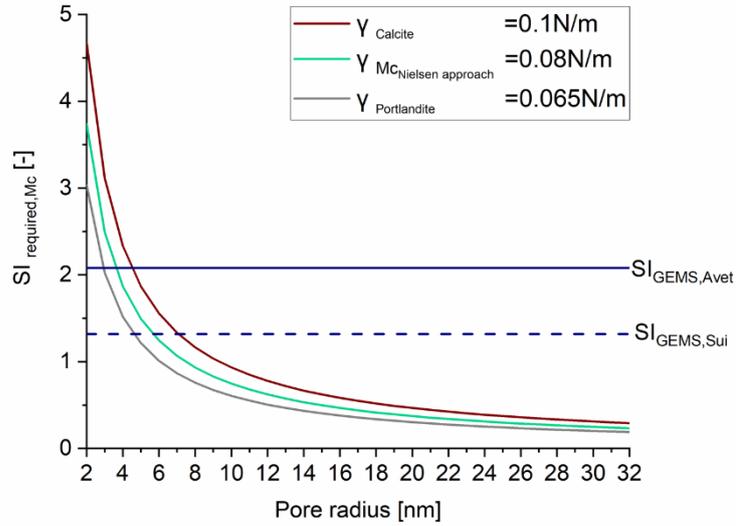


Figure 3-17. Saturation index required for Mc growth using interfacial energy of portlandite [65], calcite [64] and Mc with Nielsen's approach [68]

Hemi- and mono-carboaluminate amounts are plotted in Figure 3-18. The experimental results show an agreement with the approximations of the pore radius related to AFm growth limitation. For all water binder ratios, the formation of AFm phases is increasing up to 7 days. Afterwards, the amount is constant. Moreover, the lower the water binder ratio, the lower the amount of AFm.

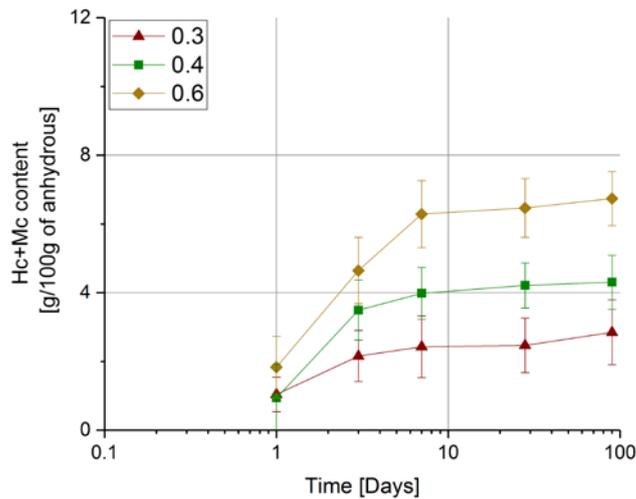


Figure 3-18. AFm content in LC³ for w/b=0.3,0.4 and 0.6

C-(A)-S-H growth

A similar graph (Figure 3-19) was plotted for C-S-H growth using the interfacial energy reported in literature [66,67] and Nielsen and Mersmann approaches [68,69]. The plot shows clearly that the interfacial energy is a crucial parameter for determining the required saturation index. Using the low interfacial energy of 0.012 N/m [66], the growth of C-S-H is not limited. On the other hand, when using the range of values between 0.055 N/m [67] and 0.14 N/m, the growth of C-S-H seems to be limited with a range pore radius between 3 to 7 nm.

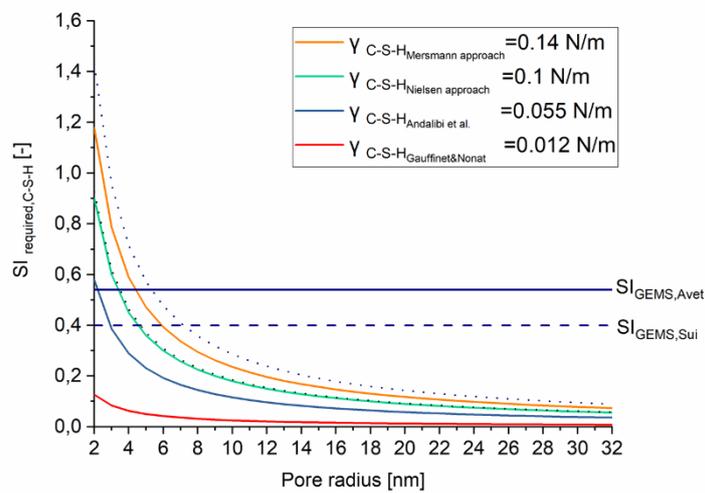


Figure 3-19. Saturation index required for C-S-H growth Vs. pore radius (black lines indicate the deviations based on sensitivity analysis)

The interfacial energy is an important parameter affecting nucleation and growth of crystals [75]. Values obtained for the same solid surface in contact with water can vary markedly, not only by using different techniques and models but even using the same method [75]. Determining the interfacial energy of a disordered variable stoichiometry material such as C-(A)-S-H is a difficult task. Over the years there have been efforts to investigate the interfacial energy of C-S-H but the values are not always in agreement with each other [66,67]. The additional approaches used in this study did not as well agree with the reported values. In addition to experimental difficulties, it is difficult to obtain reliable values of the solid-solution interfacial energy since both the rate of crystal growth and the supersaturation change with time [69].

Nevertheless, all of the approaches used in this study give bound limits for interfacial energies. The lowest limit given by Gauffinet and Nonat [66] was determined using the induction time of precipitation reactions. However, only the interfacial energy at the onset of the reaction can be determined

by this method [76]. Wu and Nancollas [75] criticized the use of homogenous nucleation to determine the interfacial energy as it is difficult to prepare systems free from impurities, which might act as nucleation catalysts. Moreover, uncertainties in the geometrical shape factor f , can also introduce errors in the calculated interfacial energy. Mersmann approach [69] gave the highest limit of interfacial energy which was also previously observed with Donnet et al. [76] for calcite.

From another point of view, some slight refinement is still observed at late ages on the MIP curves for all water binder ratios (Figure 3-15), explained by the slight increase of metakaolin reaction (Figure 3-13). It is possible that the growth of hydrates at late ages might occur via different growth mechanisms as a function of supersaturation [77] and refinement of pores may not be solely governed by the effect of curvature and pore size.

3.4 Conclusions

In this study, factors that could be considered to slow down metakaolin reaction in LC³ cement at late ages were investigated. It was shown that neither lack of portlandite nor Al ions in the pore solution can be the mechanisms slowing down metakaolin reaction. The addition of 5% of calcium hydroxide to LC³ system did not extend the reaction after 7 days. Similar slowing down of reaction was observed when replacing metakaolin with silica fume, an Al-free SCM, which invalidates the hypothesis that Al ions are responsible of the slowing down of metakaolin reaction at late ages.

This study looked in depth at the two conditions slowing down the availability of pores for hydrates precipitation as possible factors for slowing down the reactivity of metakaolin at late ages. At the upper end, relative humidity measurements on LC³ cement paste indicate that at 28 days above a pore radius of 13 nm, capillaries are not saturated with solution. At the lower end, Kelvin Laplace equation provides a thermodynamically approach between curvature and solubility to estimate the pore radius below which the growth of hydrates could be slowed down. Different approaches were used to estimate the interfacial energy for AFm and C-(A)-S-H. The results indicate that the growth of AFm seems to be limited below a range of pore radius between 3 to 7 nm. The limited growth of AFm was confirmed with XRD-Rietveld quantifications. The slowing down of AFm formation in LC³ blend at late ages was observed for all the investigated range of water binder ratios from 0.3 to 0.6. A range of pore radius from 3 to 7 nm where the growth of C-(A)-S-H could be slowed down was also obtained.

When the capillaries of the samples were refilled with solution after setting time, a full reaction was obtained at 90 days of hydration with a complete portlandite depletion.





Chapter 4 Strength and phase assemblage of limestone calcined clay cements (LC³) with clinker content from 50% down to 30%

Disclaimer: This chapter is adapted from the preprint version of the following article being submitted to Cement and Concrete Research journal – with permissions of all co-authors:

Y.Briki ^a, M.Ben Haha ^b and K.Scrivener ^a “Strength and phase assemblage of limestone calcined clay cements (LC³) with clinker content from 50% down to 30%”

^a Laboratory of Construction Materials, EPFL, 1015 Lausanne, Switzerland

^b Heidelberg Technology Center GmbH, Rohrbacher Str.95, 69181 Leimen, Germany

My contribution: Methodology, experiments, analysing, writing

Abstract

The phase assemblage and strength for LC³ system when decreasing clinker content from 50% down to 30% was investigated. A decrease of strength development was observed with the decrease of the clinker content while maintaining a constant amount of calcined clay of 30%. However, strengths with 30% clinker are still above those required for 32.5 cements in the current European standard. Furthermore, despite the depletion of portlandite in LC³ blends containing 30% of clinker, the metakaolin reaction did not slow down. Calcium ions for metakaolin reaction are most likely consumed from C-A-S-H. Combined water fraction (*CWF*) was used in this study as a simpler approach than gel space ratio (*GSR*) to explain strength development. The parameter was refined with the addition of the evaporated water in ettringite to the bound water in hydrates and the volume of reacted binder to the initial water. A good and linear correlation between compressive strength and combined water fraction was obtained for all systems.

Keywords: low clinker content, LC³, phase assemblage, combined water fraction

4.1 Introduction

Limiting global warming means that the emissions of greenhouse gases need to be reduced rapidly in the coming decades [78]. Cement producers are following several mitigation scenarios for CO₂ emissions. One, which is well-established, is to partially replace clinker with supplementary cementitious materials (SCMs) [4,6,79]. Slag and fly ash have been cost-effective substitutes for Portland cement for several decades [4]. However, the amounts of these SCMs are limited compared to the demand for cement and those available are almost fully used in cement [9]. In this context, LC³ a ternary blend of clinker, calcined clay, limestone, and gypsum can reduce CO₂ emissions by up to 40% compared to PC or CEM I (>90% clinker) [6]. This reduction is obtained thanks to the lower clinker content, the lower calcination temperature of clay compared to clinker, the absence of chemical CO₂ in the clay structure and the use of fine limestone as filler [47]. Studies on LC³ cement showed the beneficial impact of the combination of calcined clay and limestone on strength development and durability aspects such as chloride resistance and ASR [24,47,54,80]. Reducing further the clinker content in LC³ blends without compromising the development of early age strength requires a better assessment of the reactivity of metakaolin. An understanding of the factors slowing down metakaolin reaction at late ages was established the previous chapter. This study highlighted two aspects:

- Internal relative humidity measurements indicated that at 28 days pore radii above a few nm (13 nm for LC³_50) contain vapour rather than solution. Hydration products cannot deposit in vapour filled pore and the metakaolin reaction is slowed down.
- The growth of AFm and C-A-S-H phases was limited below a range of pore radius around 3 to 8 nm. This limitation is due to the level of supersaturation required to balance the increase of the surface energy related with the curvature of the pores.

On this basis, this chapter investigates the performance of LC³ formulations with clinker content down to 30%. The phase assemblage is characterized to better understand the mechanical results.

4.2 Materials and methods

4.2.1 Materials

Clinker was provided from HeidelbergCement. Soluble anhydrite from Saint-Gobain was used. Limestone powder Durcal 1 was from OMYA. The clay came from Bhuj, India. This clay was calcined using a rotary kiln. The calcined clay contains 48% of metakaolin as determined by thermogravimetric analysis (TGA). This composition is typical of widely-available clays, with a metakaolin content of 40-50% [31]. The oxide composition of the materials determined by X-ray fluorescence (XRF) analysis is shown in Table 4-1. The clinker composition is shown in Table 4-2.

	Clinker	Limestone	Calcined clay
CaO	64.41	54.21	0.2
SiO ₂	20.62	0.96	49.7
Al ₂ O ₃	5.71	0.25	41.8
Fe ₂ O ₃	3.7	0.22	2.3
MgO	1.63	0.89	0.1
Na ₂ O	0.18	-	0.3
K ₂ O	1.27	-	0.1
SO ₃	0.97	-	-
TiO ₂	0.3	-	3.4
P ₂ O ₅	0.12	-	0.1
LOI	0.8	42.6	1.5

Table 4-1. Chemical compositions of all powders

C ₃ S (%)	C ₂ S (%)	C ₃ A (%)	C ₄ AF (%)
71.1	6.2	6.6	12.9

Table 4-2. Composition of clinker phases

The particle size distribution of the powders determined by laser diffraction with a Malvern Master-size is plotted in Figure 4-1. The specific surface area determined by nitrogen adsorption is also indicated in Figure 4-1.

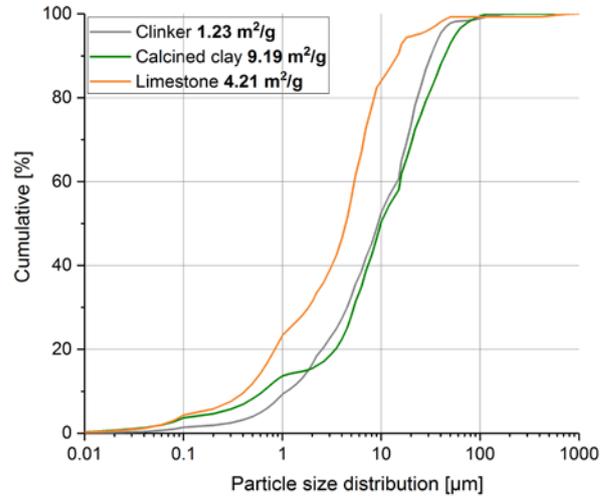


Figure 4-1. PSD and BET of all used materials

The mix composition for all the systems of LC³ is detailed in Table 4-3. In the notation LC³_XX_YY, the first number “XX” refers to the amount of clinker and the second number “YY” corresponds to the percentage of calcined clay. In systems with constant calcined clay amount (30%), clinker was progressively replaced by limestone in increments of 5%. In addition, a blend was made where the calcined clay amount was increased from 30 to 40% with a clinker content of 40%. The amount of soluble anhydrite by clinker was adjusted to the blends determined by calorimetry. The water binder ratio was fixed at 0.4 for all studied systems. The superplasticizer Mapei SP914 Dynamon polycarboxylate was used to ensure similar workability between all systems.

Notation	Clinker	Calcined clay	Limestone	Anhydrite	Superplasticizer
LC ³ _50_30	50	30	20	4.5	0.3
LC ³ _45_30	45	30	25	4.05	0.3
LC ³ _40_30	40	30	30	3.6	0.3
LC ³ _35_30	35	30	35	3.15	0.3
LC ³ _30_30	30	30	40	2.7	0.3
LC ³ _40_40	40	40	20	3.6	0.2

Table 4-3. Mix composition for all investigated blended cement

4.2.2 Methods

Compressive strength for all blends was tested following the European standard EN 196-1.

X-Ray diffraction (XRD) measurements combined with Rietveld refinement were carried out on freshly cut slices to quantify the main crystalline phases present and to determine the degree of hydration of clinker in the different systems.

TGA was used to quantify the portlandite content. The porosity was investigated using mercury intrusion porosimetry (MIP). The amount of reacted metakaolin was estimated by the mass balance approach [21,31].

The methods used in this chapter are detailed in Appendix 1: Methods.

4.3 Results

4.3.1 Decreasing clinker content with calcined clay amount constant

The strength development of LC³ blends with different clinker contents is shown in Figure 4-2. For all ages, the lower the clinker content, the lower the strength. Compressive strength is also plotted as a function of the clinker factor. Up to 7 days, a clear linear correlation between strength and clinker factor is obtained. At 28 and 90 days, the system LC³_45_30 becomes closer to the strength of LC³_50_30. Even with decreasing clinker content down to 30%, strength still meet 2- and 28-days strength requirements according to 32.5 N.

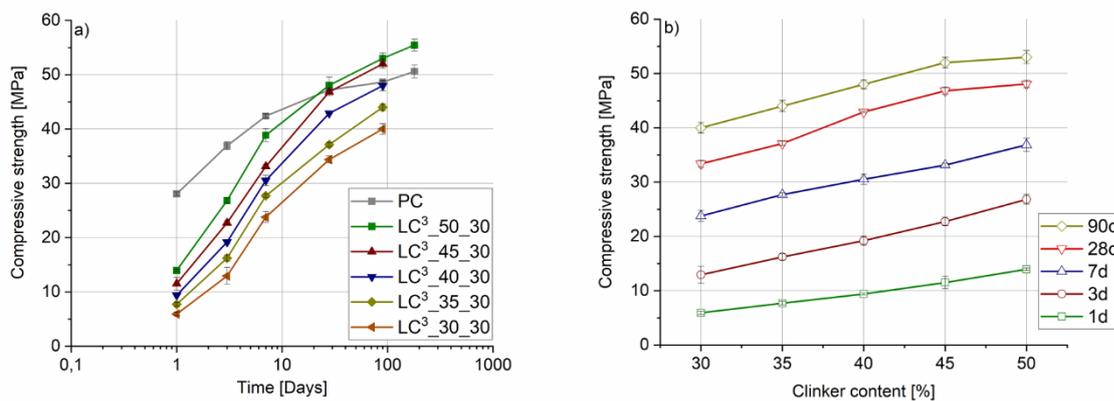


Figure 4-2. Compressive strength against a) days b) clinker content

The degree of hydration for silicate (C₃S and C₂S) and aluminate phases (C₃A and C₄AF) in LC³ cement pastes is plotted in Figure 4-3. Overall, the DoH of the anhydrous phases is relatively independent of the clinker content. Some slight differences observed for C₂S, C₃A and C₄AF are in the

range of error, as they are present in low amounts: for example, only about 2% of C₂S and C₃A and 4% of C₄AF are initially present in the system with 30% of clinker.

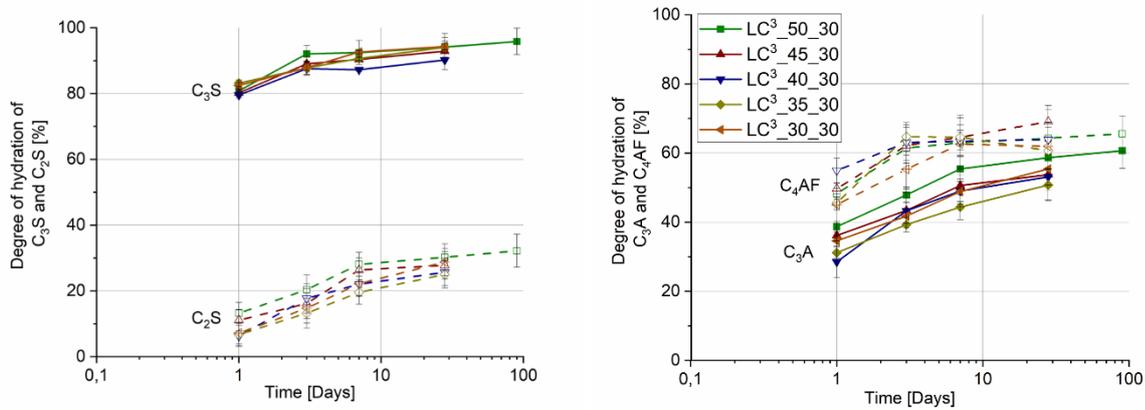


Figure 4-3. Degree of hydration of silicate and aluminate phases in LC³ cements

The amount of reacted clinker is shown in Figure 4-4. When the absolute amount, rather than the DoH is plotted, it is clear how the amount of reacted clinker decreases with decreasing the clinker content.

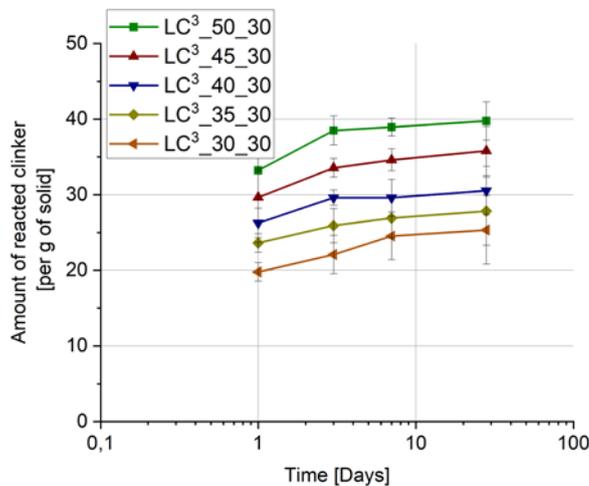


Figure 4-4. Amount of reacted clinker in LC³ cements

Figure 4-5 shows the portlandite amount normalized per g of solid for all LC³ blends. In absolute terms, calcium hydroxide seems to decrease approximately at the same rate in all LC³ blends. A slowing down of portlandite consumption can be observed from 7 days onwards for the systems LC³₅₀ to LC³₄₀. A lower amount of portlandite is observed with LC³₃₅ and LC³₃₀ due to the

lower amount of reacted clinker. At 7 and 28 days, calcium hydroxide is fully consumed in the systems LC³_30 and LC³_35 respectively.

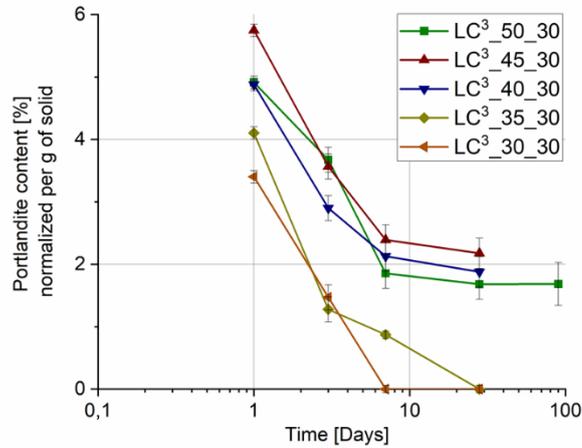


Figure 4-5. Portlandite content normalized per g of solid for all LC³ blends

For the mass balance approach, the C-A-S-H composition is required. Generally, the error measurements related to its quantification is mostly around ± 0.015 for both Al/Ca and Si/Ca [21,24,81]. However, the quantification of the C-A-S-H composition was a difficult task in this study due to the difficulties in finding clearly identifiable inner product around clinker phases, which is usually used for analysis as it avoids intermixing with calcined clay or limestone. Over 300 points per sample were measured to find the average composition of C-A-S-H. Then, C-A-S-H composition was assumed to be the same for all systems and this average used for the calculation of all systems. The reaction degree of metakaolin in LC³ blends determined by mass balance is shown in Figure 4-6. For all ages, the degree of reaction of metakaolin, appears to be similar and follow a similar trend, considering the errors. This is consistent with the similar rate of consumption of calcium hydroxide (Figure 4-5). Despite the depletion of portlandite in LC³_30 from 7 days (Figure 4-5), the metakaolin reaction did not slow down. Calcium ions for the metakaolin reaction are most likely coming from C-A-S-H.

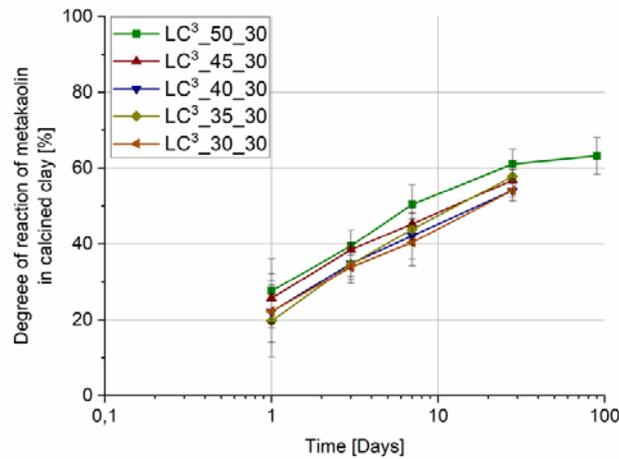


Figure 4-6. The reaction degree of metakaolin in calcined clay in all LC³ blends

The phase assemblage for all systems at 28 days of hydration is plotted in Figure 4-7. As discussed previously, the amount of reacted metakaolin is similar between all systems while the amount of reacted clinker decreases with the decrease of clinker content. The amount of ettringite is fairly similar between the systems because this phase forms during the early hydration (<1 day) and dependent on the initial sulfate content of the systems. The amount of C-A-S-H and carboaluminate phases seems to decrease with the decrease of the clinker content.

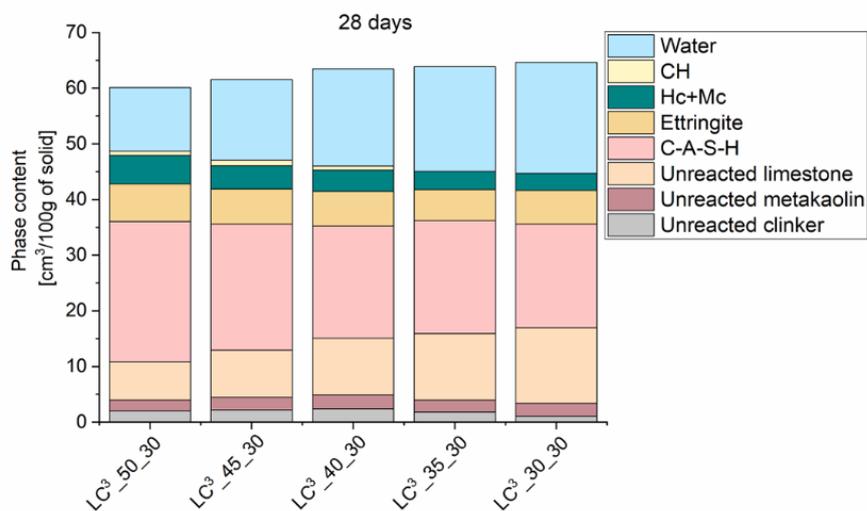


Figure 4-7. Phase assemblage for LC³ blends at 28 days of hydration

In order to clearly observe the changes in phase assemblage, the amount of AFm and C-A-S-H phases at 1 and 28 days are separately plotted as a function of the clinker factor in Figure 4-8. The higher the clinker content, the higher the amount of AFm formed at 1 and 28 days of hydration. This might be explained by the lower amount of reacted C₃A. With a lower amount of reacted clinker, the amount of C-A-S-H formed decreases with the decrease of the clinker content in both ages.

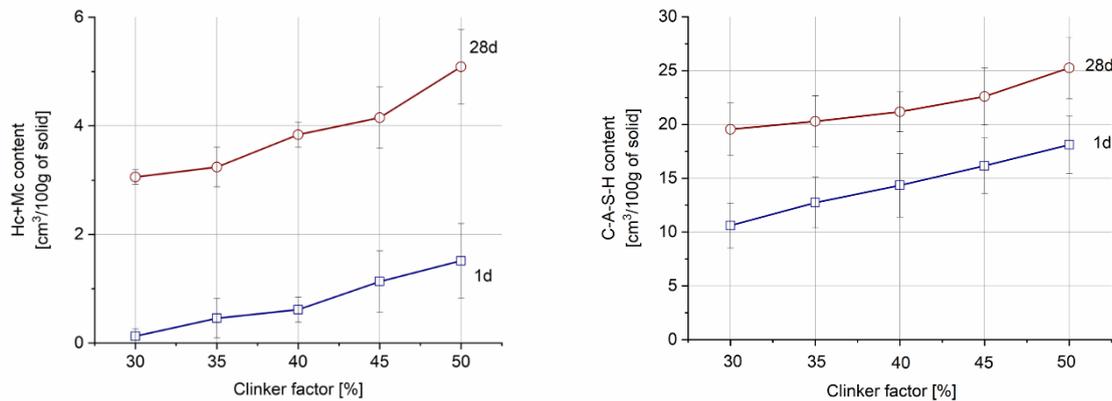


Figure 4-8. AFm and C-A-S-H contents determined by mass balance for LC³ blends at 1 and 28 days of hydration (density of C-A-S-H to 2 g/cm³[59,60])

In the first section of this study, the effect of further decreasing the clinker content in LC³ from 50% down to 30% while maintaining calcined clay amount constant (30%) was investigated. Strength development decreased with decreasing clinker amount. However, strength development still meets the 32.5N requirement even for the lowest clinker factor.

4.3.2 Decreasing clinker content with increasing calcined clay amount

Strength development for the previous systems LC³_{50_30} and LC³_{40_30} are compared with the blend LC³_{40_40} in Figure 4-9. Decreasing clinker content down to 40% but replace it with metakaolin, brings the strength development for all ages back to similar levels found for the LC³ blend with the highest amount of clinker. Compared to the neat cement PC, the blend with more calcined clay amount shows similar strength to PC at 7 days. Afterwards, strength development is higher than PC. The new formulation with the substitution of 10% of clinker by calcined clay could open the way to binders with even lower CO₂ emissions.

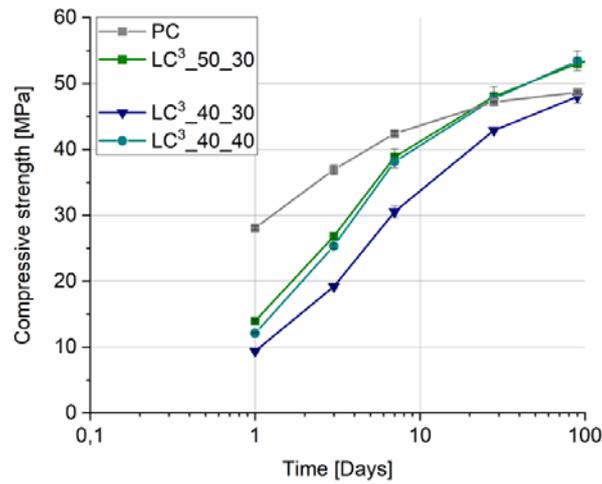


Figure 4-9. Compressive strength for LC³_50_30, LC³_40_30 and LC³_40_40

The degree of hydration of silicate and aluminate for LC³_50 and LC³_40 with 30% and 40% of calcined clay is plotted in Figure 4-10. Overall, the hydration of anhydrous phases of clinker seems to be similar. The slight differences are within the error measurements.

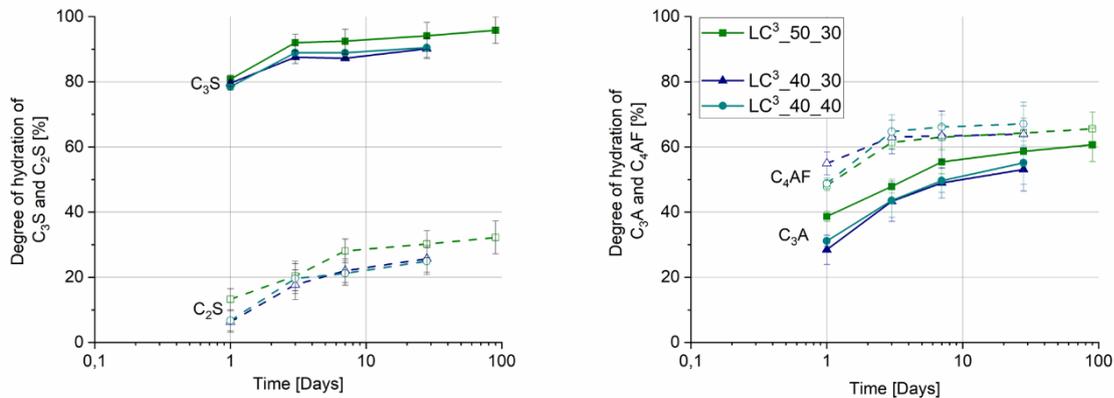


Figure 4-10. Amount of reacted clinker for LC³_50_30, LC³_40_30 and LC³_40_40

Portlandite consumption for LC³ blends is plotted in Figure 4-11. Portlandite consumption is comparable mainly between systems LC³_50 and LC³_40 with 40% of calcined clay. All systems shown a slowing down of calcium hydroxide consumption from 7 days and onwards.

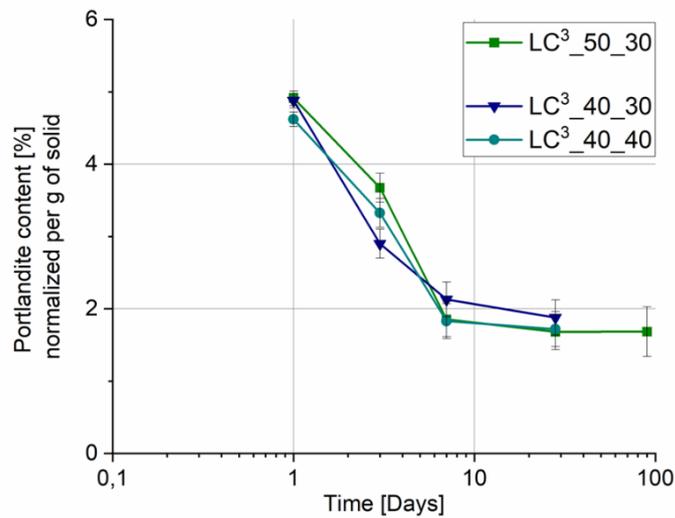


Figure 4-11. Portlandite consumption for LC³_50_30, LC³_40_30 and LC³_40_40

The amount of reacted metakaolin in LC³ blends is plotted in Figure 4-12. Replacing clinker with metakaolin did not decrease the amount of reacted metakaolin. The difference is within the error measurement.

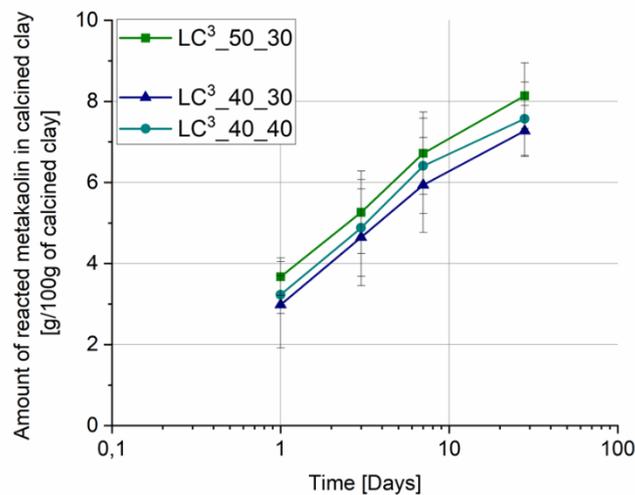


Figure 4-12. The amount of reacted metakaolin in calcined clay for LC³_50_30, LC³_40_30 and LC³_40_40

The pore structure for LC³_50_30, LC³_40_30 and LC³_40_40 at 1 and 28 days of hydration is investigated and plotted in Figure 4-13. The decrease of the clinker content down to 40% does not lead to an increase of the porosity. At 1 day, both blends of LC³ with lower clinker amount (40%) show

lower critical entry pore radius and total porosity than the system with higher clinker amount (50%). At 28 days of hydration, all systems seem to converge toward a similar critical entry radius and total porosity.

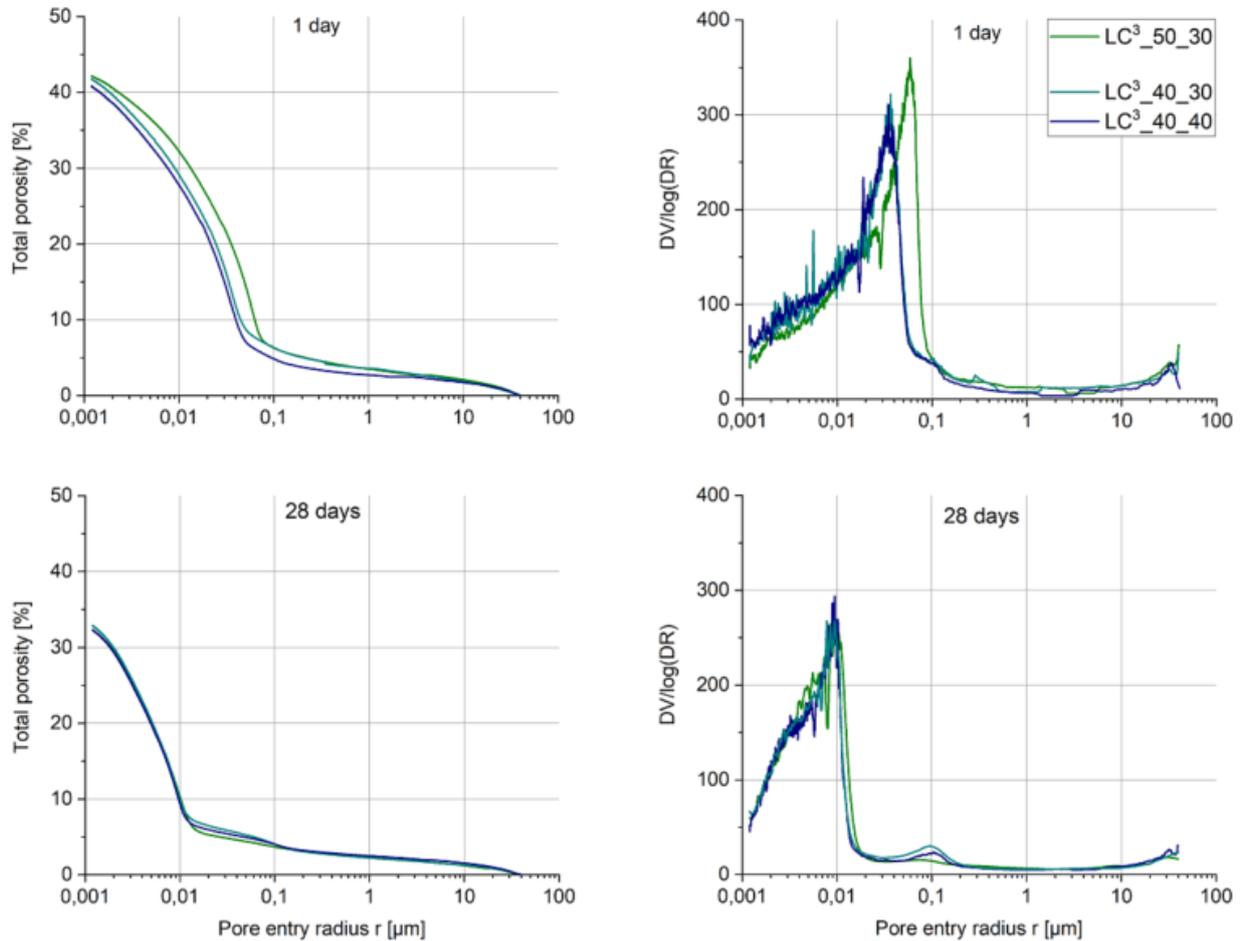


Figure 4-13. Pore structure for LC³_{50_30}, LC³_{40_30} and LC³_{40_40}

Replacing 10% of clinker with metakaolin gave strength development for all ages similar to LC³ the blend containing 50% of clinker. The porosity at early age was lower in the system containing more metakaolin in the blend.

4.3.3 Correlation between compressive strength and combined water fraction

Strength results are often interpreted in terms of gel space ratio which is the ratio of volume of hydration products to the space available for these hydrates [24,45,46]. However, in this approach the errors in determination of all the anhydrous and hydrate phases are compounded. In this study, difficulty in determining the C-A-S-H composition at low clinker contents, amplifies these uncertainties.

The correlation between compressive strength and gel space ratio is detailed in Appendix 4: Gel space ratio approach.

Recently, John et al. [82] introduced a simple and more practical parameter the combined water fraction “CWF”. This approach is the ratio of the water combined in hydrates divided by the total water added in the system. The authors obtained a linear correlation between strength development and combined water fraction for binary and ternary blends [82]. Combined water fraction is defined in Equation 4-1

$$\text{CWF} = \frac{\frac{W_{40} - W_{550}}{w_{550}}}{w} \quad \text{Equation 4-1}$$

where w_x is the percentage of mass loss at temperature $x^\circ\text{C}$ determined by TGA analysis, and w is the amount of mixing water.

In this study, an attempt to refine the combined water fraction parameter with the evaporated water of hydrates and the volume of reacted binder was investigated. The quantity of water combined in ettringite phase ($\text{C}_3\text{A} \cdot 3(\text{CaSO}_4) \cdot 32\text{H}$) is higher than in other hydrates [83] leading to the highest drying capacity with 85% for ettringite and 35% for C-S-H for example [83]. The volume of the reacted binder (clinker, metakaolin and limestone) was determined using mass balance approach. Consequently the Equation 4-1 becomes as following :

$$\text{CWF}^* = \frac{\frac{W_{40} - W_{550} + W_{\text{evaporated, Aft}}}{w_{550}}}{w + V_{\text{reacted binder}}} \quad \text{Equation 4-2}$$

The influence of the errors of measurements of the bound water from TGA on the determination of combined water fraction was established using a sensitivity analysis. The relative error of measurement of bound water was observed to be between $\pm 5\%$ and $\pm 10\%$ [84].

The compressive strength of LC³ blends is plotted as a function of CWF in Figure 4-14 a) and b) before and after refinement respectively. The dashed lines indicate the deviations based on the potential bound water error. A bi-linear correlation was obtained between the compressive strength and the combined water fraction of all the systems together with all the points falling within the uncertainty limits. It was suggested in a recent study [46] that the first regime could correspond to space filling of the cementitious matrix and the second regime would then correspond to the densification of the matrix. After the addition of the evaporated water in ettringite to the bound water in hydrates and the volume of reacted binder to the initial water, a good and linear correlation is obtained for all systems. The systems LC³_50_30 and LC³_40_40 fit the correlation in the same way.

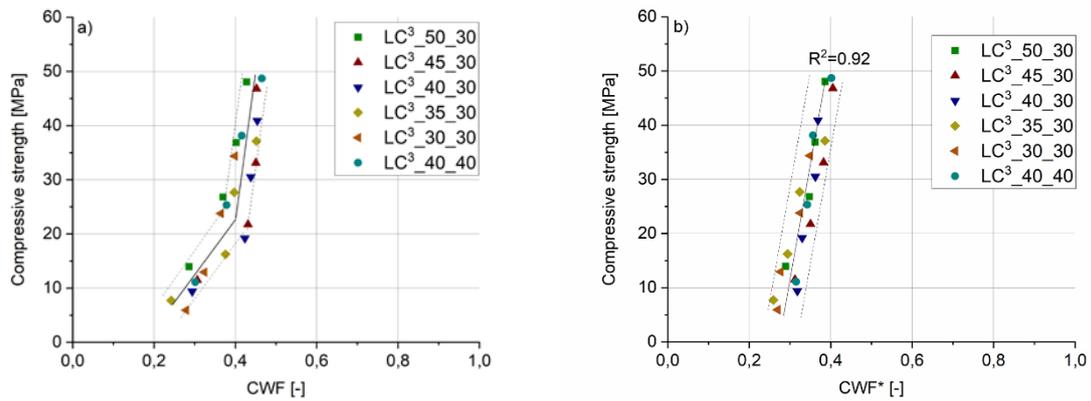


Figure 4-14. Compressive strength vs. combined water fraction a) without refinement b) with refinement (The sensitivity analysis is indicated by the dashed lines)

4.4 Conclusions

In this study, the effect of decreasing clinker content from 50% down to 30% in LC³ blend was studied. In the first section, the metakaolin amount was maintained constant at 30% and the phase assemblage was investigated. The strengths reduced with decreasing clinker content. However, it is interesting to note that even with the lowest clinker amount with 30% of clinker, strength results conform the strength standard requirements of 32.5N at 2 and 28 days.

The mass balance approach is used in this study for the phase assemblage of all LC³ blends. However, the quantification of C-A-S-H composition was not an easy task due to the low clinker amount. Therefore, the composition was assumed to be the same for all blends and was calculated as the average for all determined composition. Metakaolin reaction was similar between all investigated systems, given the errors. With 30% of clinker, portlandite was fully consumed. However, metakaolin reaction did not slow down. This confirms that the lack of portlandite is not the major factor responsible for the slowing down of metakaolin reaction at late ages as previously suggested for LC³₅₀ [85]. Metakaolin reacts most likely with calcium from C-A-S-H phases.

Replacing 10 % of clinker content with metakaolin gave strength development similar to LC³_{50_30} for all ages. Compared to PC, the blend showed similar strength at 7 days and higher strength development at 28 days. This formulation shows the significant potential of the combination of limestone and calcined clay to decrease the CO₂ emissions related to cement production. The combined water fraction (CWF) was investigated in this study as a simpler way for correlation with compressive strength. This approach is relatively more practical with less uncertainties compared to the more complex gel-space ratio approach. Only the bound water of hydrates is required in this approach. In this study, an attempt was made to update the parameter with the addition of the evaporated water in ettringite to the bound water in hydrates and the volume of reacted binder to the initial water. A good and linear correlation was obtained for all systems.





Chapter 5 Factors affecting the reactivity of slag at early and late ages

Disclaimer: This chapter is adapted from the preprint version of the following article being submitted to Cement and Concrete Research journal – with permissions of all co-authors:

Y.Briki ^a, M.Zajac ^b, M.Ben Haha ^b, and K.Scrivener ^a “Factors affecting the reactivity of slag at early and late ages”

^a Laboratory of Construction Materials, EPFL, 1015 Lausanne, Switzerland

^b Heidelberg Technology Center GmbH, Rohrbacher Str.95, 69181 Leimen, Germany

My contribution: Methodology, experiments, analysing, writing

Abstract

Slag reaction is slow in blended cement. This chapter compares the reactivity of slag in NaOH solution ($w/s=100$) and in cement paste ($w/b=0.4$). The reactivity of slag is higher in NaOH solution than in cement paste. Addition of calcium hydroxide to NaOH solution, slows down the rate of slag dissolution. The higher the amount of calcium hydroxide added to NaOH solution, the lower the rate of reaction. An implication of these results with that in blended cements, the reactivity of slag is maybe slowed down by calcium ions released by clinker in the pore solution. At 28 days, relative humidity measurement indicate that water is only present in pores less than 6 nm. The small size of water filled pore, may limit the slag reaction.

Keywords: calcium ions, dissolution, saturation index, water-filled capillary pores

5.1 Introduction

Supplementary cementitious materials (SCMs) are crucial components of modern low carbon cements. One of the most common SCMs used, is ground-granulated blast-furnace slag. Ground-granulated blast-furnace slag (GGBFS) is a glassy material obtained by quenching molten iron slag (a by-product of iron and steel-making) from a blast furnace in water or steam, to produce a granular product that is then dried. The finished product is ground to similar fineness as cement and presents latent hydraulic properties [86]. Blending cement with slag is common in cement industry and there are three main categories of cement blended with slag defined in the European standard EN 197-1: CEM II, CEM III and CEM V. Composite cements containing slag show similar or better durability properties to the reference neat Portland cement such as chloride ingress, sulfate attack, alkali silica reaction and expansion [21,87,88]. However, slag blended cement is characterized by lower strength at early ages (≤ 7 days) when compared to neat Portland cement. Durdziński [21] showed that the compressive strength of blended cement with slag is similar to a system mixed with quartz at 1 day of hydration. Berodier [35] obtained similar heat cumulative released between slag and quartz up to 1 day which confirms the inert behavior of slag at early age. However, a degree of reaction of slag between 30% and 50% can be obtained when slag is mixed in alkali activated materials [89,90]. The early strength can be 30MPa at 1 day when mixing slag with waterglass solution [91]. It is of considerable interest to understand the reason for such difference in the reactivity of slag in the two conditions.

Factors affecting slag reactivity have been identified and reported in the literature [26,92–94]. Increasing fineness of slag increases the reactivity of slag in cement paste and thus the early age strength development [95]. The chemical composition of the amorphous phase, being the main constituent of GGBFS, was also shown to play a role [93,94,96]. It was suggested that the higher CaO content in slag composition (network-modifying cation), the higher the network depolymerization or structure disorder resulting in an increased rate of reactivity [93,94]. The pore solution was shown to influence the rate of slag. Adu-Amankwah et al. [14] found a decrease in slag reaction with the presence of aluminum in the pore solution. Similarly, Snellings [92] showed that the glass dissolution rates was affected by the solution composition. In experiments under far-from-equilibrium conditions, to prevent the precipitation of hydration products, with a water to glass mass ratio of 1000 he showed that the dissolution rates of synthetic glasses decrease with the addition of calcium ions. Suranenni et.al [97] observed similar results using the micro-reactor approach. With calcium addition (20mM), a strong inhibiting effect on the slag dissolution was obtained.

The reasons for the low kinetics of slag in cement paste remain unclear and an open question.

This study pointed out the influence of calcium addition on slag reactivity at early age. The factors slowing down slag reaction at late ages are also investigated.

5.2 Materials and methods

5.2.1 Materials

Clinker and GGBFS were provided by HeidelbergCement Company. Soluble anhydrite was from Saint-Gobain, it is produced by heating natural gypsum at 200°C, which makes it highly soluble and much more reactive than natural anhydrite [39]. Quartz (B250, Sibelco) was used instead of slag as inert filler. The oxide composition of the materials determined by X-ray fluorescence (XRF) analysis is indicated in Table 5-1.

	Slag	Quartz
CaO	39.8	-
SiO ₂	37.7	99.8
Al ₂ O ₃	10.5	-
Fe ₂ O ₃	0.41	-
MgO	5.7	-
Na ₂ O	0.21	-
K ₂ O	0.46	0.1
SO ₃	3.05	-
TiO ₂	1.31	-
P ₂ O ₅	0.01	-
LOI	0.2	0.03

Table 5-1. Chemical composition of slag and quartz

The particle size distribution of the powders determined by laser diffraction with a Malvern Mastersizer is plotted in Figure 5-1. The specific surface area determined by nitrogen adsorption is also indicated in Figure 5-1.

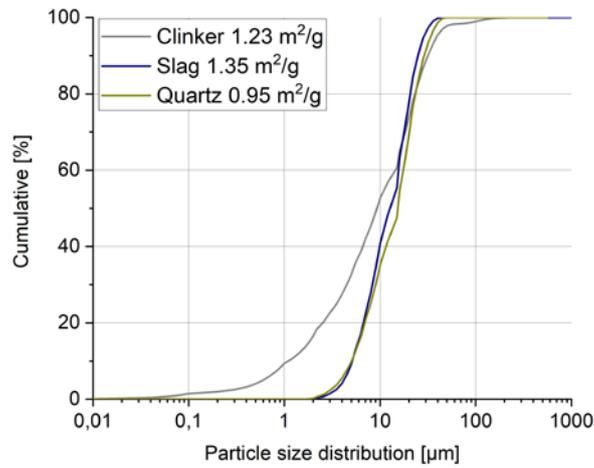


Figure 5-1. PSD and BET of clinker, slag and quartz

5.2.2 Methods

5.2.2.1 Slag in NaOH solution

The experimental setup consisted of mixing slag in NaOH solution (0.025M for NaOH) with a solution to slag mass ratio of 100 which is not as high as previous studies [92–94,97,98]. The precipitation of hydrates was not avoided in order to observe the impact of calcium addition on the extent of precipitation. The impact of calcium ions on slag reactivity was investigated by adding 0.1, 1 and 10 mM of Ca (OH)₂. The release rate of ions (r in mol/m²/s) is calculated as indicated in Equation 5-1 [92,94]:

$$r = \frac{C \cdot V}{SSA \cdot m \cdot x \cdot t} \quad \text{Equation 5-1}$$

where C is the concentration of the element in solution (mol/L), V is the volume of solution used (L), SSA is the specific surface area (m²/g), m is the mass of slag powder (g), x is the atomic fraction of the element in slag (calculated from the chemical composition of slag) and t is the time in seconds.

At corresponding sample ages (30min, 1, 2, 4, 6, 8 hours, 2, 4 and 7 days), 15 ml of the solution was collected in a syringe and filtered through a 0.45 μm nylon filter. The concentrations in the solution samples were measured by inductively coupled plasma-optical emission spectrometry. The samples were not acidified to avoid the evaporation of the reduced sulfur species [99,100]. Moreover, measurements were performed immediately after filtration to avoid the oxidation [100]. In this study, it is important to be able to measure reduced sulfur ions since they are an indicator for slag dissolution. The evolution of pH was checked for all samples at each age as well.

The degree of reaction of slag in NaOH solution (%) was calculated as indicated in Equation 5-2. The parameters are as defined in Equation 5-1 .

$$DoR = \frac{C.V}{m.x} \quad \text{Equation 5-2}$$

The degree of reaction of slag in NaOH solutions was estimated using the concentration of sulfur ions.

For microstructure investigations, the hydration of the sample was stopped using solvent exchange with isopropanol. 2g of sample put in a filtrating funnel (filter paper retention 5 μm). The funnel was immediately filled with isopropanol and the sample was stirred in the funnel for 2 minutes. Then the isopropanol was removed with a vacuum pump. The washing was repeated three times. Once the isopropanol was removed, the dried sample was collected from the filter paper and stored under vacuum in a desiccator for maximum 24 hours. For micrograph investigations, specimens were prepared from the dried powder and were dispersed on an adhesive carbon tab and coated with an iridium layer of 5 nm. The samples were analyzed afterwards using Zeiss Merlin which is an ultra-high-resolution FE-SEM (Field Emission SEM).

The hydration was followed by calorimetry (TAM Air, TA Instruments). The solution to solid ratio was decreased from 100 to 10 to reduce the noise of the baseline. Kinetics were expected to be slightly impacted since the critical concentrations are achieved at different times. However, the results remain comparable.

5.2.2.2 Slag in cement paste

The mix composition for all blended cement pastes is detailed in Table 5-2. The clinker replacement level was fixed at 50%. A content of 4.5% of ground soluble anhydrite by cement was added to PC and blended cements.

Notation	Clinker	Slag	Quartz
PC	100	-	-
Slag cement	50	50	0
Quartz cement	50	0	50

Table 5-2. Mix design for all investigated systems

The impact of increasing water binder ratio was investigated for the composite cement with different w/b ratios of 0.3, 0.4 and 0.6. For pore solution curing, the slag sample was immersed in a representative pore solution similar to the pore solutions extracted [21] after setting.

For each age, the hydration of the pastes was stopped by solvent exchange with isopropanol and the following investigations were carried out:

The degree of reaction of slag was measured by image analysis of a combined input from BSE grey level images and magnesium concentration maps collected by EDS. Kocaba et al.[101] described in detail the principle of this method.

The degree of clinker hydration was investigated on slices of 2mm thickness using X-ray powder diffraction. Pore structure was investigated using MIP.

The internal relative humidity (RH) of the paste samples was monitored using a HC2-AW-USB water activity probes from Rotronic.

The details of this method are detailed in Appendix 1: Methods.

5.3 Results

The degree of reaction of slag in cement paste was first investigated and plotted in Figure 5-2 a) linear scale to show the slowing down of the reaction and b) logarithmic scale to highlight the reaction at early age. At 1 day, only 3% of slag reaction is measured, but there is a high error ($\sim 4\%$) especially at early ages, due to the limited resolution of fine particles (below $1\ \mu\text{m}$) which may not be considered [101]. After 1 day, the evolution of slag reaction follows a linear trend. A slowing down of reaction is observed at late ages. Slag has reacted $50\pm 7\%$ at 180 days.

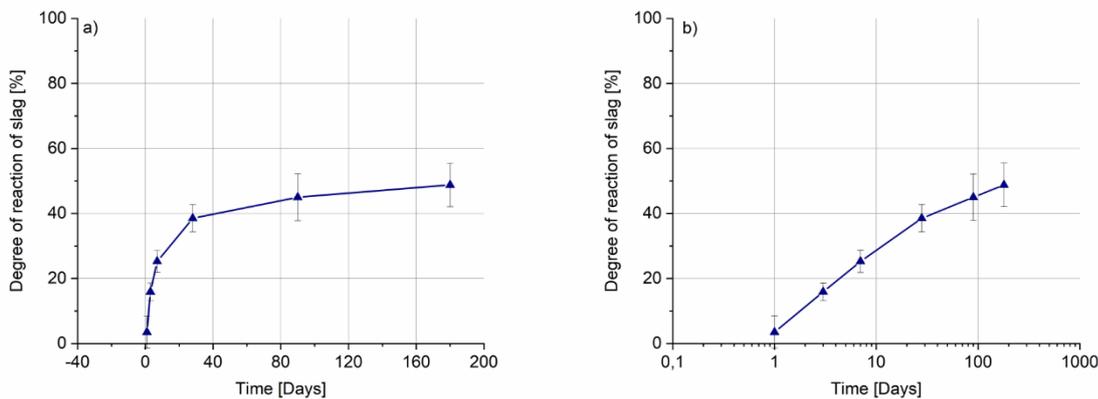


Figure 5-2. Degree of reaction of slag in cement paste a) linear scale and b) logarithmic scale ($w/b=0.4$)

The heat release determined using isothermal calorimetry for PC and blended cements is plotted in Figure 5-3. The heat is similar up to 1 day for slag and quartz system. Slag follows a similar behavior to quartz at early age, i.e. its reactivity is very low. After 1 day, slag seems to start reacting since its heat release is higher than the one of quartz.

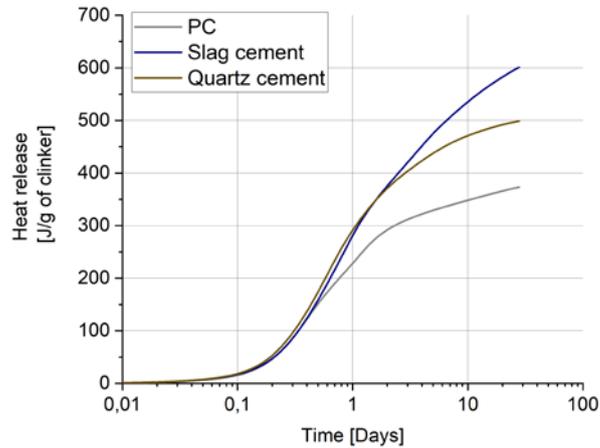


Figure 5-3. The heat release per g of clinker for PC and blended cements ($w/b=0.4$)

Figure 5-4 shows strength development for PC, slag and quartz cements. At 1 day, strength development is similar for the slag and quartz cements. Afterwards, the compressive strength of quartz cement remains consistently at just under half the strength of the PC due to the low clinker amount. The slag blend develops strength more rapidly than the Quartz blend and overtakes the PC at 28 days.

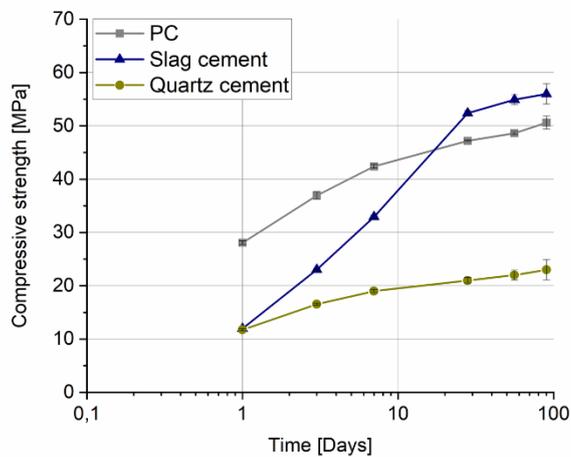


Figure 5-4. Compressive strength of PC and blended cement

5.3.1 Factors affecting the rate of slag reaction at early age

The logarithmic release rate of aluminum, silicon and sulfur ions in slag-NaOH solution was calculated using Equation 1 and plotted in Figure 5-5. A “non-steady state” dissolution stage is observed for the investigated elements followed by a linear decrease in solution concentrations but only for Al

and Si ions. The release rate of Al and Si are similar up to two days and start deviating later on. This is not the case for reduced sulfur ions. The release of the reduced sulfur species is constant up to 7 days. This indicates that sulfur species can be an indicator for slag dissolution.

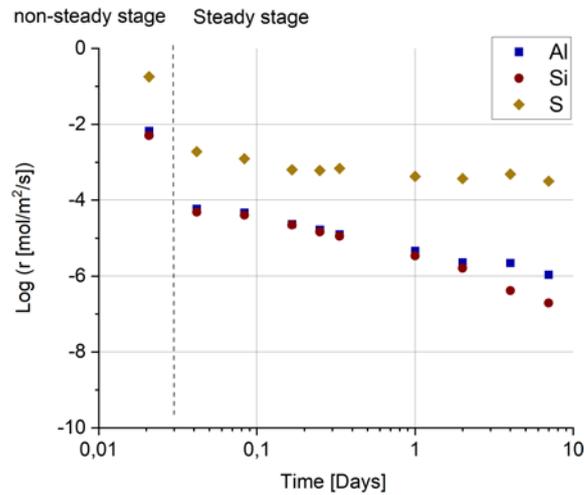


Figure 5-5. Logarithm of the release rate of Al, Si and S in slag-NaOH solution (w/s=100)

The saturation indexes with respect to hydrates that could precipitate in slag-NaOH solution were calculated and plotted in Figure 5-6. The graph shows that hydrotalcite with assumed stoichiometry “ $\text{Mg}_4\text{Al}_2\text{O}_7(\text{H}_2\text{O})_{10}$ ” [102,103] and all other type of magnesium aluminum layered double hydroxide phases are likely to precipitate, i.e. with high SI values. C-S-H phases are likely to precipitate as well.

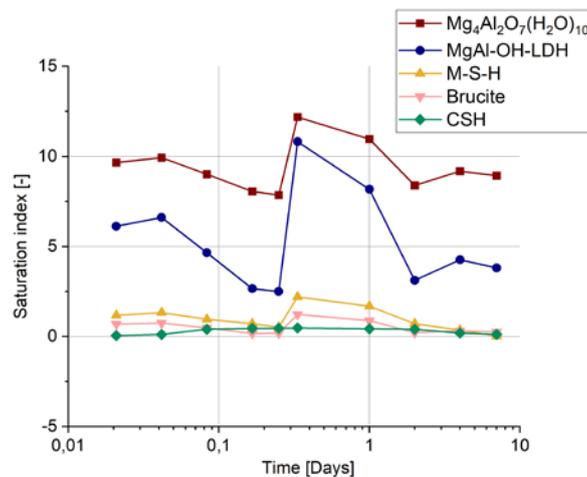


Figure 5-6. Saturation index of hydrates in slag-NaOH solution

Approximative mass balance calculations were carried out to estimate the amount of C-S-H and hydrotalcite phases (Figure 5-7). The stoichiometry of C-S-H was calculated from calcium silicon ratio of slag from XRF data (Table 5-1) and was $1/1.05\text{CaO SiO}_2 (\text{H}_2\text{O})_4$. Up to 1-day, similar amount is obtained between both hydrates. Afterwards, C-S-H amount is higher than hydrotalcite phase.

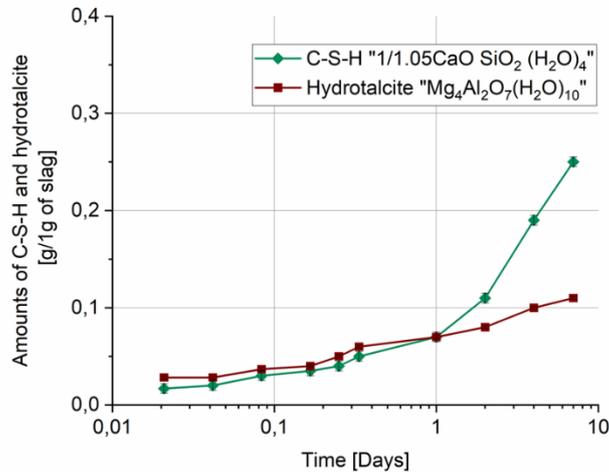


Figure 5-7. The amount of C-S-H and hydrotalcite in slag NaOH solution (w/s=100)

Micrographs of slag in NaOH solution after 30 min and 6 hours are presented in Figure 5-8. Precipitates can be observed on slag particles after 30 min. A platelet-like morphology can be observed which might be the characteristic of hydrotalcite-like phases. Other precipitates seem to have a foil like morphology which might be C-S-H phases. After only 6 hours, slag particles are covered by hydrates. The hydrates have morphology more like C-S-H. Hydrotalcite phases are likely to be covered by C-S-H phases. The decrease of the release rate of Al and Si ions observed previously in Figure 5-5 is explained by their consumption to form hydrotalcite and C-S-H phases.

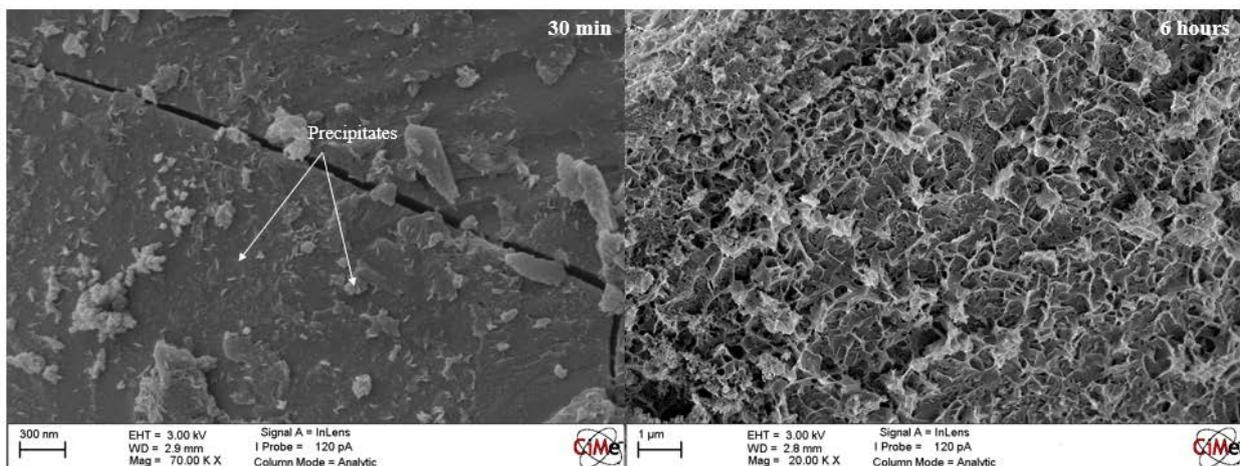


Figure 5-8. High resolution micrographs of slag in NaOH solution after 30 min and 6 hours

The degree of reaction of slag in NaOH solution was calculated as indicated in Equation 5-2. A comparison of the degree of reaction in NaOH solution and cement paste is shown in Figure 5-9. The reactivity of slag is much higher in NaOH solution for all ages. At 1 day, slag reaction is about six times higher in NaOH solution than in cement paste. The results suggest that slag reactivity might be limited due to the presence of clinker phases.

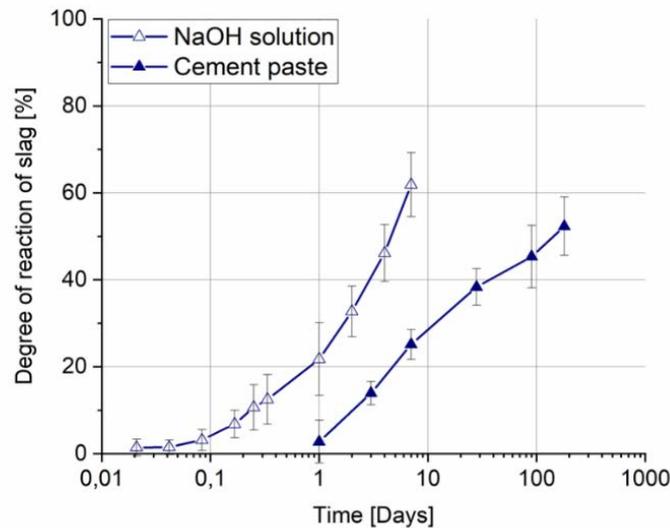


Figure 5-9. Degree of reaction of slag in NaOH solution and cement paste

One of the elements present in high quantities at 1 day in slag cement paste is calcium, sulphates and alkalis ions [100]. Here in this study, the effect of calcium addition on slag reactivity was studied. The presence of clinker phases was simulated by the addition of calcium hydroxide (0.1, 1 and 10mM) in slag NaOH solution. It was firstly verified that the addition of calcium did not significantly modify the pH, Figure 5-10.

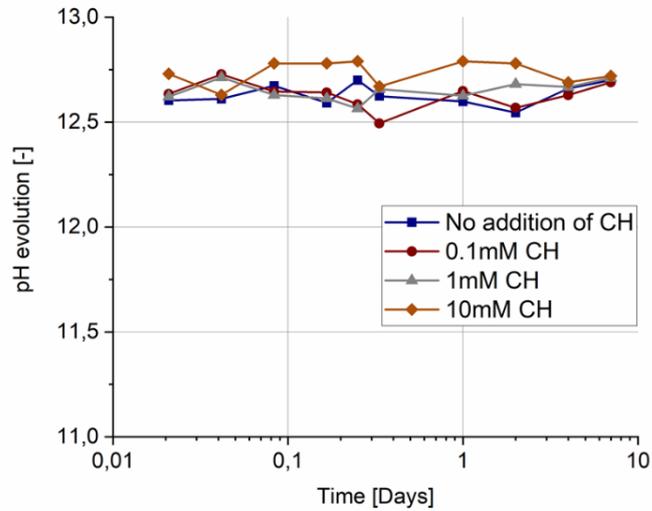


Figure 5-10. pH evolution for slag in NaOH solution with and without addition of calcium hydroxide

The driving force for solid dissolution is the undersaturation [50]. Slag reactivity might be affected by the solution undersaturation (modified by changing solution calcium concentrations) as suggested for alite [50,104]. Saturation index with respect to slag with the addition of calcium hydroxide (0.1, 1 and 10mM) in NaOH solution is plotted in Figure 5-11. The saturation index is similar between the reference sample and calcium hydroxide added samples with 0.1 and 1mM. This is not the case with the addition of 10mM of CH where the saturation index of slag is decreased. The results suggest that as the saturation index of slag decreases, the undersaturation is maybe increased which would mean that slag should dissolve more and higher hydration precipitates is expected.

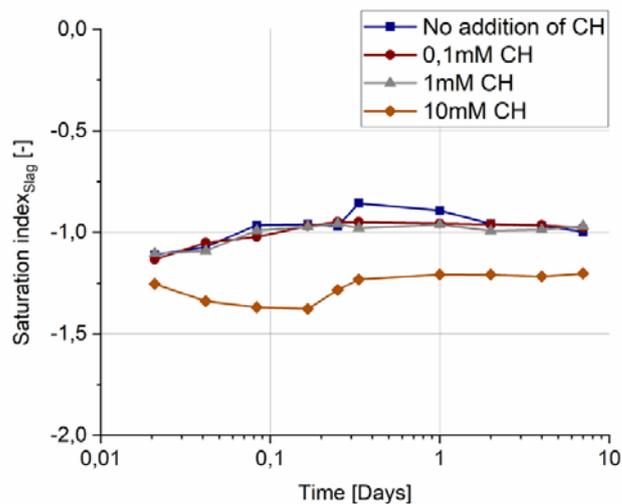


Figure 5-11. Saturation index of C-S-H and in slag-NaOH solution with and without addition of calcium hydroxide

The previous results showed that reduced sulfur species could be an indicator for slag dissolution since the other ions were consumed to form hydrates. The logarithmic release rate of S ions is plotted in Figure 5-12 for slag with and without addition of $\text{Ca}(\text{OH})_2$. The release rate of S ions seems to decrease in the presence of $\text{Ca}(\text{OH})_2$ with all investigated amounts. The lowest release rate was obtained with the presence of 10mM of $\text{Ca}(\text{OH})_2$.

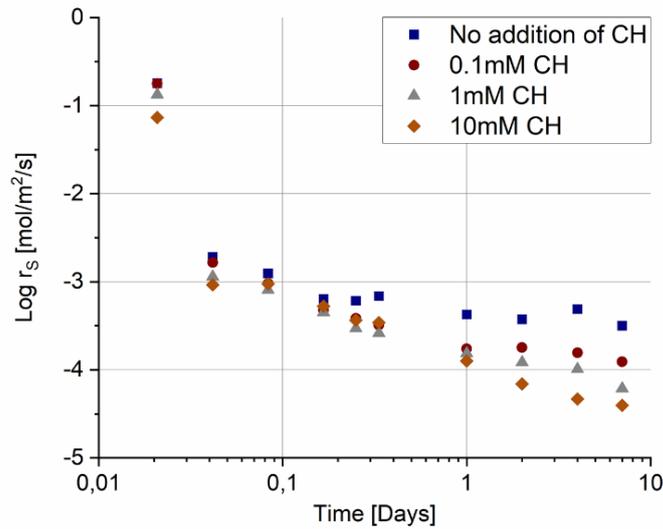


Figure 5-12. Logarithmic release rate of sulfur in slag-NaOH solution and in the presence of 0,1, 1 and 10mM of $\text{Ca}(\text{OH})_2$

The release rate of sulfur ions was plotted against calcium additions for 1, 4 and 7 days (Figure 5-13). For all ages, the release rate of sulfur decreased. The higher the addition of calcium hydroxide, the lower the release rate of sulfur.

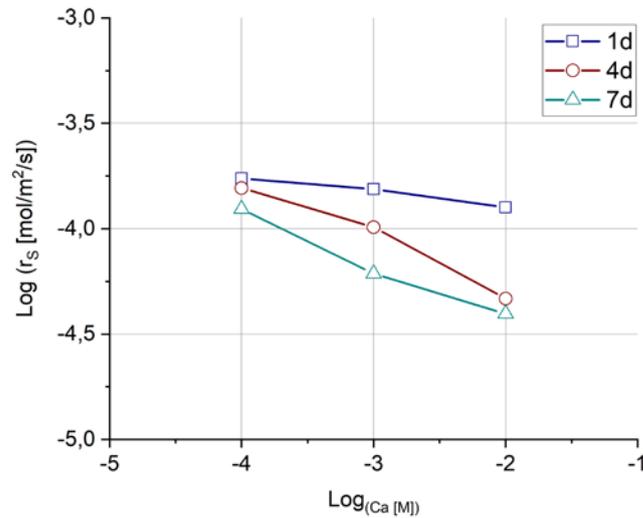


Figure 5-13. Logarithmic release rate of S vs. calcium addition

The precipitation of hydrates was investigated with GEMS thermodynamic modeling. The saturation index of C-S-H and the silicon concentrations with the additions of calcium hydroxide is plotted in Figure 5-14. Silicon concentration decreased with increasing the amount of calcium hydroxide. The precipitation of C-S-H is predicted to decrease also with the addition of calcium hydroxide and mainly with the addition of 10 mM.

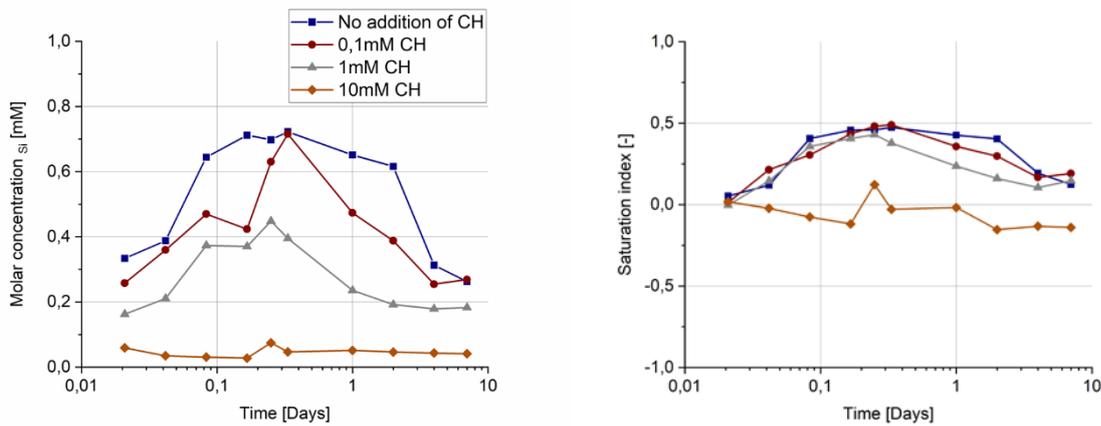


Figure 5-14. Si concentration and saturation index of C-S-H and in slag-NaOH solution with and without addition of calcium hydroxide

Micrographs of slag in NaOH solution are compared with slag in the presence of 10mM of calcium hydroxide and shown in Figure 5-15. After 30 min, slag particles seem to be smooth for addition of

10mM of CH to the solution (Figure 5-15 c). After 6 hours, lower precipitation can be observed in the presence of calcium hydroxide (Figure 5-15 d).

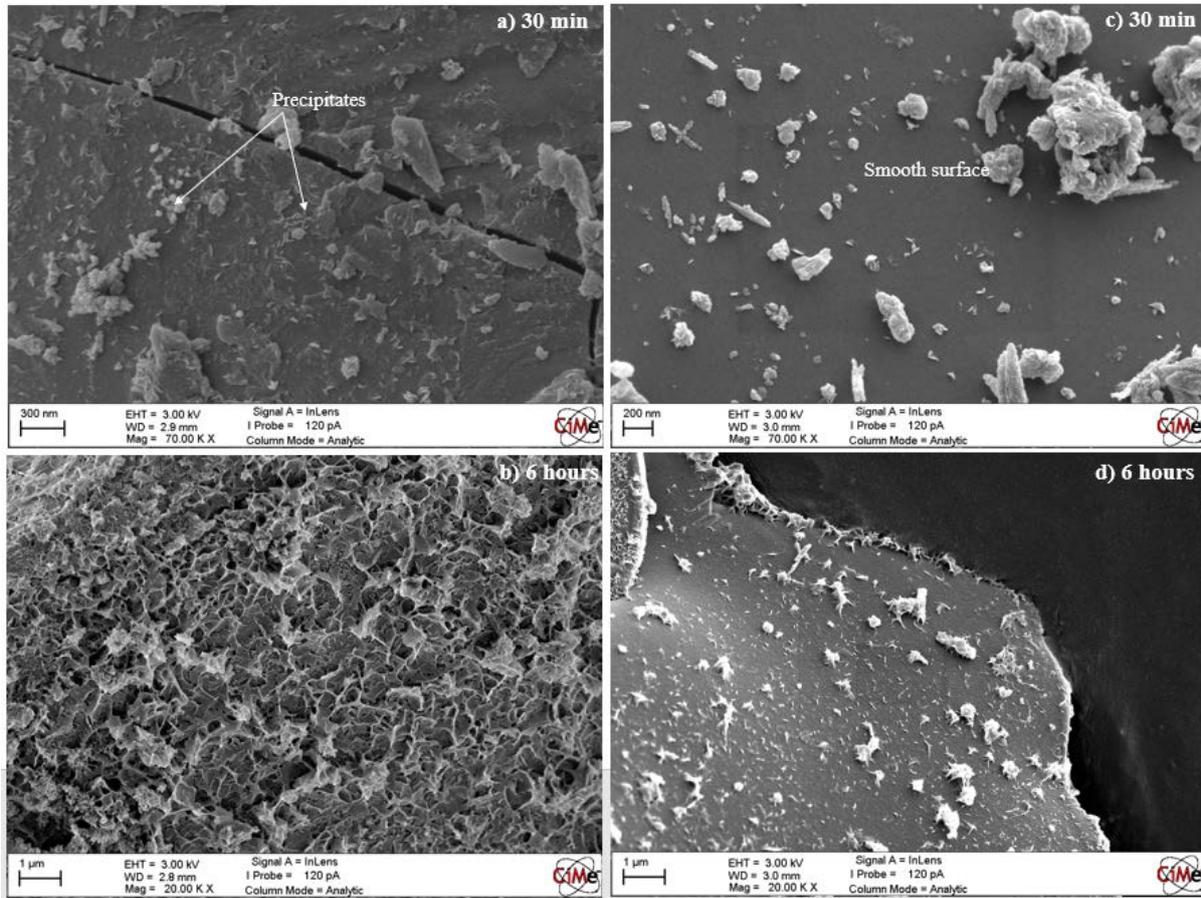


Figure 5-15. High resolution micrographs of slag in NaOH solution a) after 30 min and b) 6 hours and with addition of 10mM of calcium hydroxide c) after 30 min and d) 6 hours

The heat cumulative per gram of calcium hydroxide is plotted for the samples with and without addition of calcium hydroxide (Figure 5-16). The heat release decreased with the increase of the amount of calcium hydroxide.

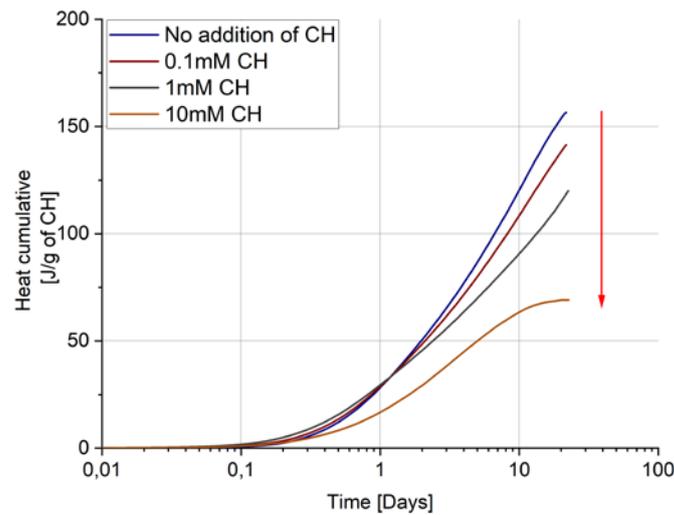


Figure 5-16. Heat cumulative of slag-NaOH solution with and without addition of calcium hydroxide (w/s=10)

Figure 5-17 compares the degree of reaction between slag in NaOH solution with the different amount of calcium hydroxide and slag in cement paste. The higher the amount of calcium hydroxide added in slag NaOH solution, the lower the degree of reaction. The degree of reaction of slag with 10mM CH comes closer to the reaction degree of slag in cement paste. The slow dissolution of slag due to the high concentration of calcium in the pore solution might be the reason for the slow kinetics of slag in cement paste at early age. This impact might be less significant at later ages since the alkali dominate the pore solution and the calcium concentrations decrease as they are limited by the portlandite precipitation [99,100,105,106].

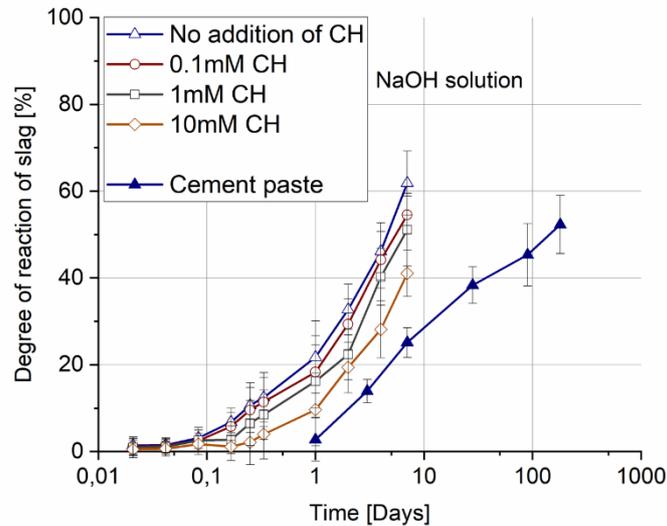


Figure 5-17. Degree of reaction of slag in NaOH solution with different amount of calcium hydroxide (w/s=100) and slag in cement paste (w/s=0.4)

This study showed that at high pH, the slag dissolution is slowed down with the addition of calcium hydroxide. In general, the rate-controlling mechanisms of the dissolution can be classified by either the transport of ions or the surface reactions [50,107,108]. When the dissolution is limited by surface reactions, several mechanisms were suggested to limit the dissolution of glasses such as the surface coverage by hydration products [109] or the adsorption of solution ions on reactive sites [110]. Similar hypotheses were suggested for the inhibition of alite dissolution [111–113]. The hypothesis of covering slag surface by hydration products can be excluded in this study as the micrographs showed the lowering of precipitation with the decrease of dissolution. In a recent study, Chave et al. [114] reported that the slower dissolution of synthetic glasses with the addition of calcium in solution is explained by the incorporation of calcium ions into the glass surface layer and therefore decreasing dissolution rates. However, these observations were at different conditions: pH=8.7 and temperature of 90°C. Armelao et al. [115] showed that calcium hydroxide reacts with the silica glass network using different surface techniques: X-ray photoelectron spectroscopy (XPS), secondary ion mass spectrometry (SIMS) and atomic force microscopy (AFM).

A more detailed analysis of the surface chemistry would be needed in this study to check if the calcium from solution reacts with silica network in the hydrated layer at the glass surface.

5.3.2 Factors affecting the rate of slag reaction at late ages

The two limits of water filled pores were investigated in this research as studied in Chapter 3 for metakaolin reaction in LC³ systems.

The water to binder ratio was firstly varied from 0.3 to 0.6 in slag cement paste to investigate the impact of the addition of water and space on the extent of slag reaction (Figure 5-18). Up to 7 days, increasing the water binder ratio from 0.3 to 0.4 did not enhance slag reaction. The system with 0.6 showed a slight increase of reaction but in the range of error measurement technique. After 7 days, the system with $w/b=0.6$ showed a higher degree of slag reaction than those systems with w/b of 0.3 and 0.4.

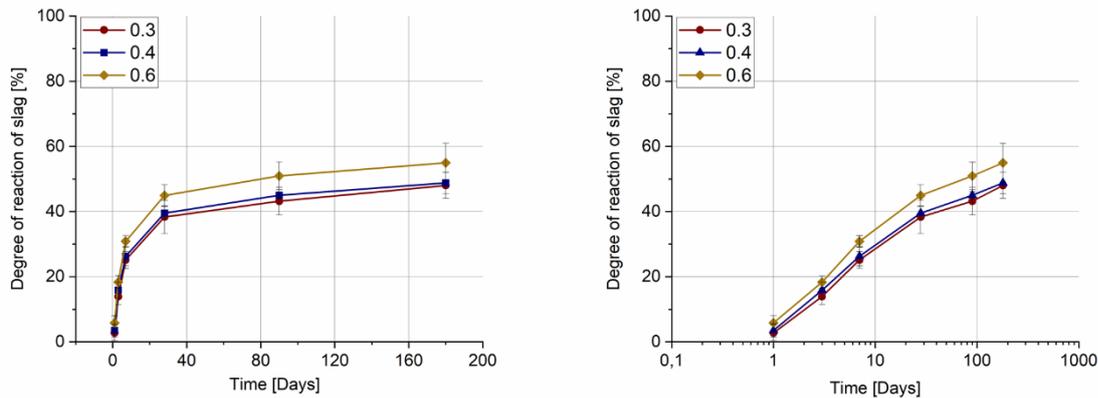


Figure 5-18. Degree of reaction of slag in cement paste with $w/b=0.3$, 0.4 and 0.6

The pore size distribution plots for all investigated water binder ratios are shown in Figure 5-19. Almost no further refinement was observed after 28 days of hydration for w/b 0.3 and 0.4. Both systems showed critical entry pore radius of 10 and 15 nm respectively at 90 days. This was not the case with slag cement with 0.6 where a refinement of porosity is still observed after 28 days.

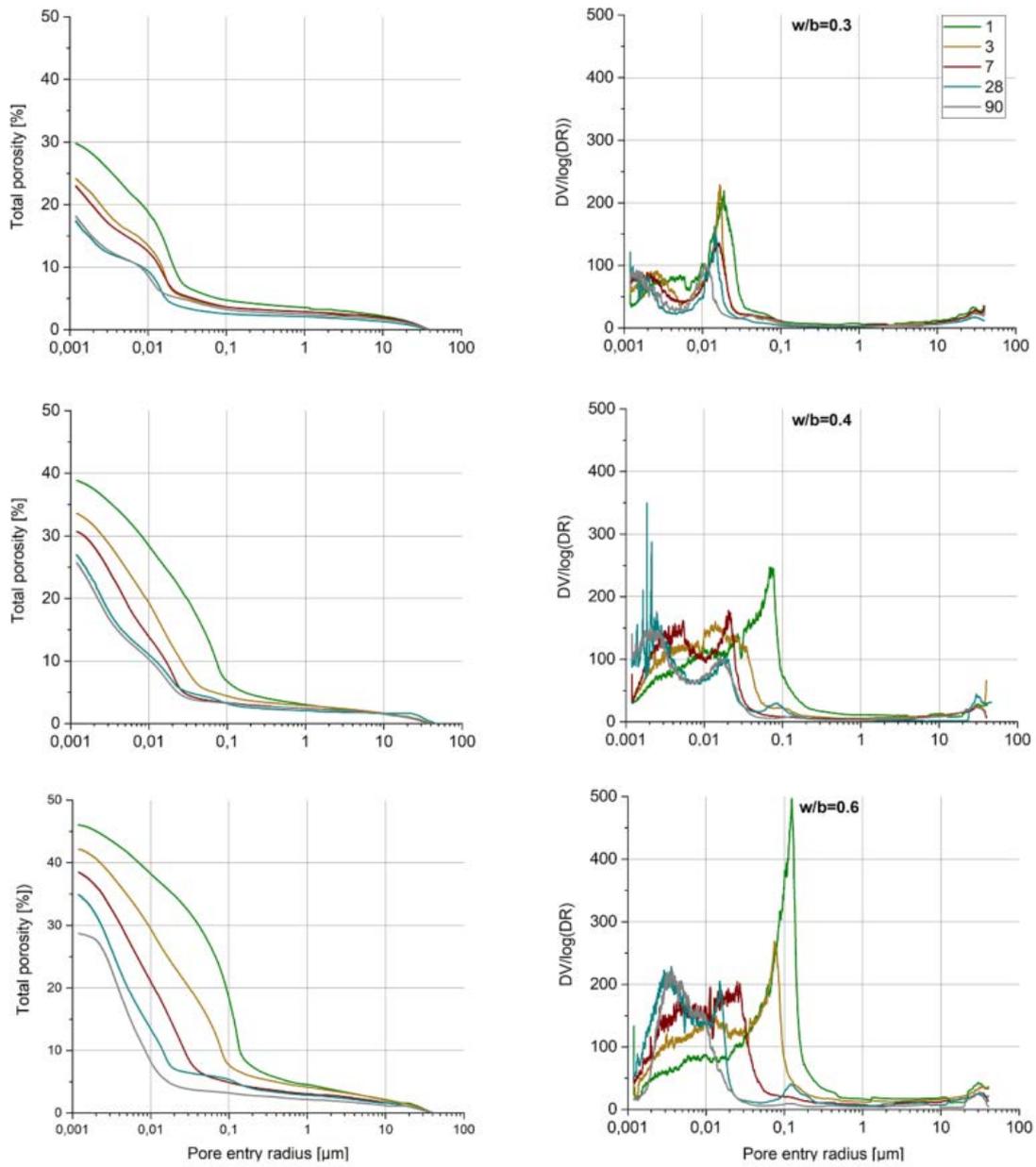


Figure 5-19. Porosity measurements of slag cement with w/b=0.3, 0.4 and 0.6

The internal relative humidity of slag cement and PC pastes is plotted in Figure 5-20. The relative humidity of both systems is similar up to 7 days. Afterwards, the decrease in relative humidity of PC slowed down whereas the relative humidity of slag cement keeps decreasing more strongly. At 28 days of hydration, the internal relative humidity of slag reached 81%. The relative humidity due to saturation of pores from chemical shrinkage was corrected to the water activity [53,54]. The corrected relative humidity 82% corresponds to a threshold of pore radius of ~6 nm. Above 6 nm, capillary pores are not saturated with solution.

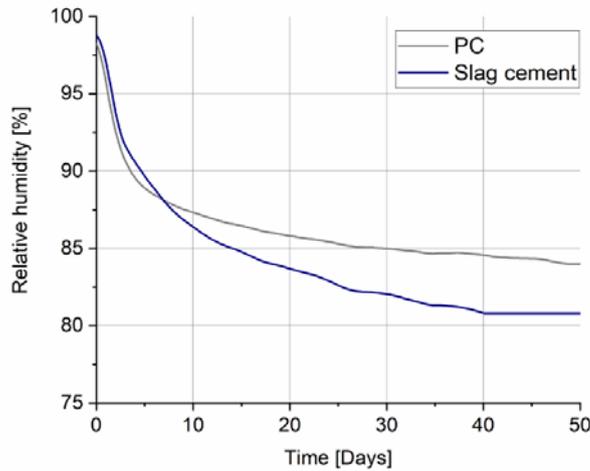


Figure 5-20. Internal relative humidity for PC and slag cement

Slag was immersed in pore solution as described in methods section and then the degree of reaction of slag was compared between sealed and pore solution cured and plotted in linear and logarithmic scale in Figure 5-21. Up to 28 days, the reaction of slag was similar in both conditions. Afterwards, the reaction of slag in sealed conditions slowed down. Meanwhile slag showed a log-linear reaction in pore solution cured conditions and reached 70 % at 180 days of hydration.

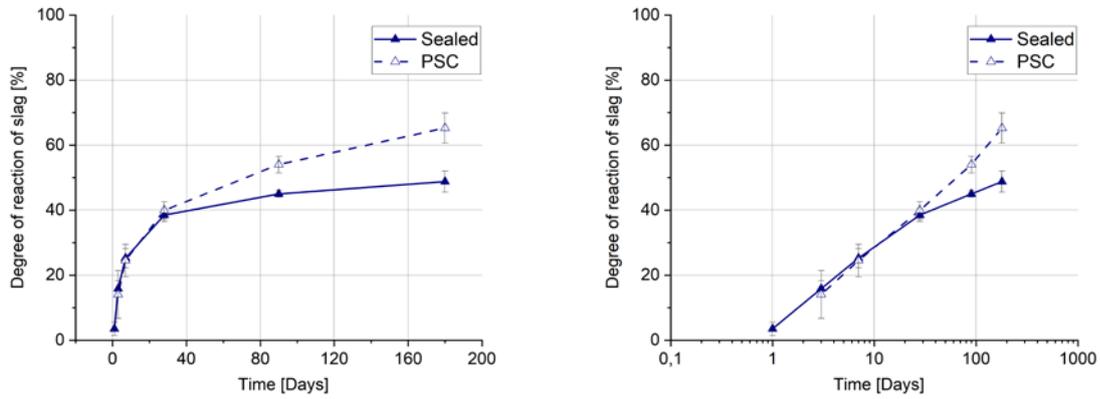


Figure 5-21. Degree of reaction of slag in sealed and pore solution cured conditions a) linear scale and b) logarithmic scale ($w/b=0.4$)

The porosity of sealed and pore solution cured at 3 and 90 days of hydration is plotted in Figure 5-22. For both ages, sealed and pore solution cured systems showed similar critical entry pore radius and total porosity.

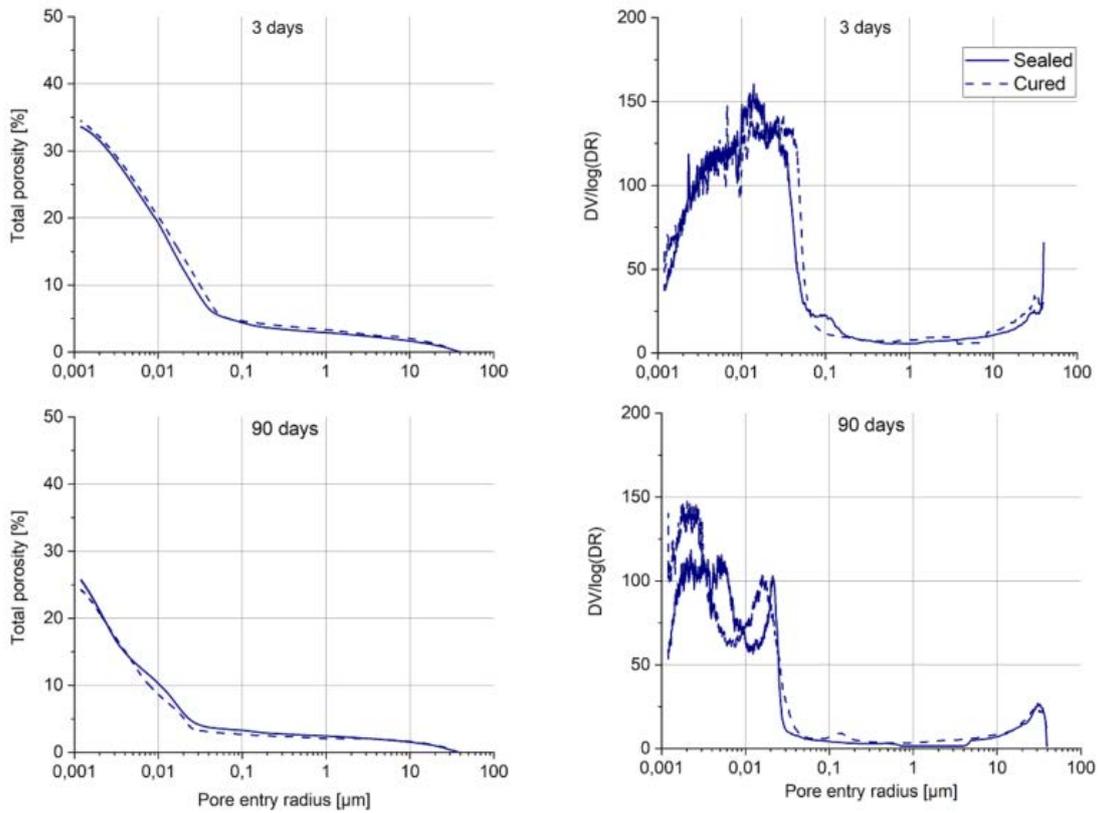


Figure 5-22. Porosity measurements of slag cement in sealed and pore solution conditions at 3 and 90 days of hydration ($w/b=0.4$)

The possible limited growth of hydrates below a critical pore radius was estimated as studied for LC³ in Chapter 3. The growth of C-S-H and AFm phases could be limited in slag cement at late ages. Due to the low solubility of hydrotalcite, the saturation index of hydrotalcite calculated by thermodynamic modelling are not reliable [100]. Therefore, AFm phases were limited to carboaluminate and monosulfoaluminate phases.

The interfacial energy between crystal and solution is necessary to estimate the saturation index required for hydrates growth. Nielsen approach [68] was used to investigate the interfacial energy for monosulfoaluminate. The parameters used in this approach are listed in Table 5-3. The saturation index for monosulfoaluminate using thermodynamic modelling was calculated using the pore solution data at 28 days of hydration from Durdzinski et al. [21]. The interfacial energy for monocarboaluminate is adapted from Chapter 3.

Log K_{sp} [71]	-29,26
Unit cell volume V (Å ³) [71]	769,5
Density ρ (g/m ³) [116]	2,02
Molecular weight M_w (g/mol)	622,52
[116]	

Table 5-3. Solubility product, unit cell volume, density and molecular weight of monosulfoaluminate

Figure 5-21 shows the SI required for Ms and Mc growth against the pore radius. As the pore radius decreases, the saturation index required for hydrate growth increases to balance the increase of the surface energy due to the curvature increase. The growth of monocarboaluminate seems to be limited below 10 nm. The growth of monosulfoaluminate seems to be not occurring for all pore radii. However, this can be explained by the presence of small amount of limestone in clinker. The monophase is therefore dominated by carbonates leading to low saturation index for monosulfoaluminate.

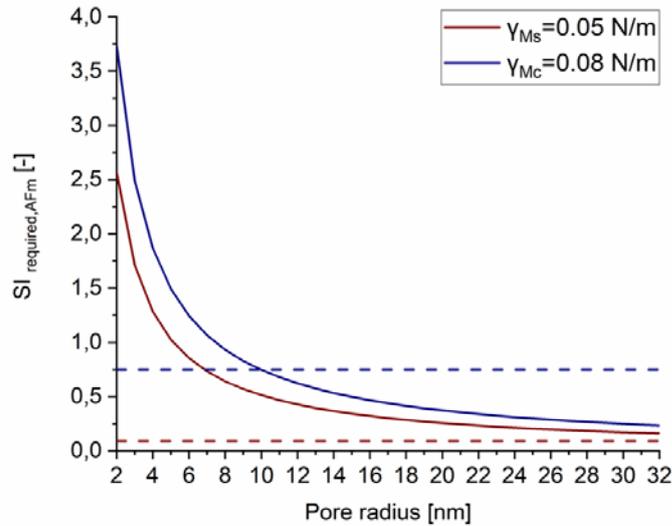


Figure 5-23. Saturation index required for Ms and Mc growth using interfacial energy estimated by Nielsen's approach [68]

AFm amounts with different water binder ratios determined by XRD-Rietveld analysis are plotted in Figure 5-24. The lower the water binder ratio, the lower the amount of Hc+Mc phases. A slowing down of carboaluminate formation was observed at late ages for all water binder ratios. Before 3 days, monosulfoaluminate phase was not identified for w/b 0.4 and 0.6 (up to 7 days for 0.3). Afterwards, the amount increases for all water binder ratios but remains lower than carboaluminate phases. The formation of monosulfate seems to be limited only because of the presence of limestone in cement paste.

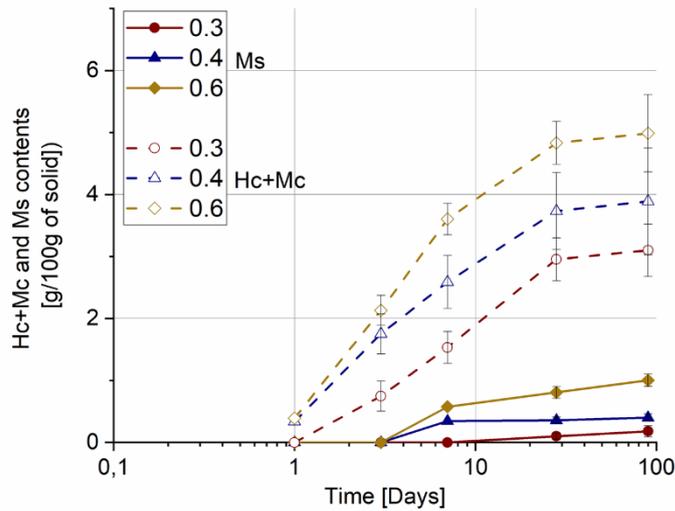


Figure 5-24. Hc+Mc and Ms amounts in slag cement w/b=0.3, 0.4 and 0.6

Regarding C-S-H phase, the different values of interfacial energy obtained in Chapter 3 was used here. Figure 5-25 shows the saturation index required for C-S-H growth against pore radius in nm. The growth of C-S-H seems to be limited below the pore radius of 10 nm. These observations agree with MIP results (Figure 5-19) where the minimum pore entry radius reached after 28 days for the lowest water binder ratio was 10 nm.

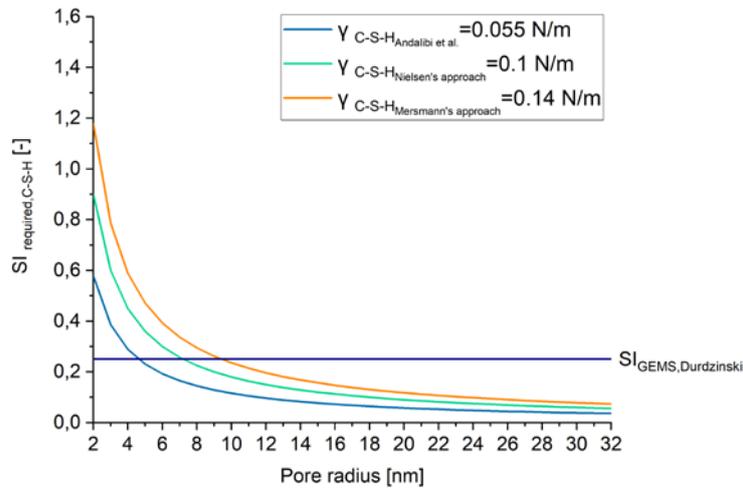


Figure 5-25. Saturation index required for C-S-H growth

The RH indicates that pores larger than 6 nm do not contain solution, at the same time the solution concentration and thermodynamic modelling indicate that the grow of both AFm phases and C-S-H is not likely to be possible in pores below 10 nm.

5.4 Conclusions

In this study, the mechanisms slowing down slag reaction at early and late ages were investigated. The influence of calcium ions addition on slag reactivity when isolated in NaOH solution (w/s=100) was studied. The dissolution of slag was followed with reduced sulfur ions as the results showed that they were not consumed to form hydrates. The addition of calcium hydroxide in slag NaOH solution, seems to decrease slag dissolution and therefore reduce the extent of precipitation. The higher the added amount of calcium ions into the solution, the lower the dissolution. The implication of these observations with slag in blended cement paste, suggests that the low reaction of slag at early age could be due to the high amount of calcium in the pore solution. This impact might be less significant at later ages since the alkali dominate the pore solution and the calcium concentrations decrease as they are limited by the portlandite precipitation [105,106].

The lack of water filled capillaries might slows down slag reaction at late ages. After 28 days, the internal relative humidity measurements indicated the absence of water in pores with the radius above 6 nm. Pore solution curing linearly increased slag reaction but only at late ages. The growth of monocarboaluminate and C-S-H phases might to be limited below the pore radius of 10 nm. However, these estimated limitations are associated with the curvature of the crystal using Kelvin Laplace model.





Chapter 6 Main findings and conclusions

6.1 Conclusions

The goal of this project was to understand the mechanisms slowing down or enhancing the reactivity of SCMs in order to maximize their use in blended cements. With the aim of making the concepts universal, this project focused on one hydraulic and one pozzolanic SCM, slag and calcined clay, respectively. The following conclusions can be drawn :

6.1.1 Maximizing the use of limestone in binary cements

- The fine limestone allowed to increase the replacement level up to 20% in blended cement while maintaining satisfactory mechanical results. Similar compressive strength to PC was obtained up to 7 days.
- The hydration of C_3S was enhanced by the presence of fine limestone. The physical and chemical effects of limestone compensate the dilution of the clinker up to 7 days.
- Blending fine limestone (15%) and coarse limestone (5%) showed similar strength with the system containing 20% of fine limestone and thus to PC up to 7 days. Reducing the content of fine limestone in this way, should improve water demand and workability and reduce the grinding energy during process.
- Strength results were explained by the phase assemblage using the gel space ratio approach.

6.1.2 Factors slowing down metakaolin reaction at late ages

The reaction of metakaolin in calcined clay slows down at late ages. The main findings in this study can be summarized as follows:

- Portlandite is not the factor slowing down the reaction of metakaolin in LC^3 . The addition of portlandite did not lead to an increase of the reaction degree of metakaolin.
- Similar slowing of reaction was observed when replacing metakaolin with silica fume, an Al-free SCM, suggesting that Al ions are not responsible for the slowing down of the reaction.
- The lack of water-filled capillaries is the most likely reason for the slowing down of metakaolin reaction. Internal relative humidity measurements indicated that at 28 days pores above 13 nm are not saturated with water.

- Interfacial energies of AFm and C-A-S-H phases were estimated in this study using different approaches. Different values were obtained for C-A-S-H phases. These values should be interpreted with caution as the parameters considered in these approaches are challenging and involve several uncertainties.
- The growth of AFm and C-A-S-H phases is possibly limited below a range of pore radius around 3 to 7 nm. These limitations are based on classical growth mechanism using Kelvin Laplace equation.

6.1.3 Effect of decreasing clinker content from 50% down to 30% in LC³

- The decrease of clinker content leads to a decrease of compressive strength. However, the substitution of 70% of CEM I 42.5 R by 30% calcined clay and 40% limestone still permits to pass the strength criteria of 32.5 N class. This shows the significant potential of the combination of limestone and calcined clay to decrease the CO₂ emissions related to cement production.
- LC³ with 30% of clinker showed a depletion of portlandite at 7 days. However, metakaolin keeps reacting after this time. Calcium is most likely consumed from C-A-S-H phases. The observation supports the previous conclusion that the lack of portlandite is not the major factor responsible for the slowing down of metakaolin reaction at late ages.
- LC³₄₀ with 40% metakaolin has a similar mechanical performance to LC³₅₀ with 30% metakaolin. This new formulation opens the path towards even to further reduction of CO₂ emissions while maintaining sufficient strength.
- Strength results are often interpreted in terms of gel space ratio. However, this approach includes several uncertainties based on the measurement of the phase assemblage. The C-A-S-H composition is especially challenging to determine for cementitious blends very low clinker content. Combined water fraction used in this study as a simpler and more practical approach to predict compressive strength. A good correlation was obtained for LC³ blends with low clinker content.

6.1.4 Factors slowing down slag reaction at early and late ages

Early ages:

- The addition of calcium hydroxide to slag in NaOH solution, seems to limit slag dissolution. The higher the added amount of calcium ions in the solution, the lower the dissolution. The extent of precipitation of hydrates is reduced in presence of calcium hydroxide.
- Slag reactivity at early age might suffer from the dissolution of clinker phases because of the high amount of calcium released in the pore solution. This impact might be less significant at later ages since the alkali dominate the pore solution and the calcium concentrations decrease as they are limited by the portlandite precipitation.

Late ages:

- After 28 days, internal relative humidity indicated that a threshold of pore radius of 6 nm is the limit between empty and solution filled pores. Hydrates cannot grow in empty pores and this will slow down the reaction.

6.2 Perspectives

6.2.1 Metakaolin reactivity at early age

- Compressive strength of LC³ is low at early age compared to PC.

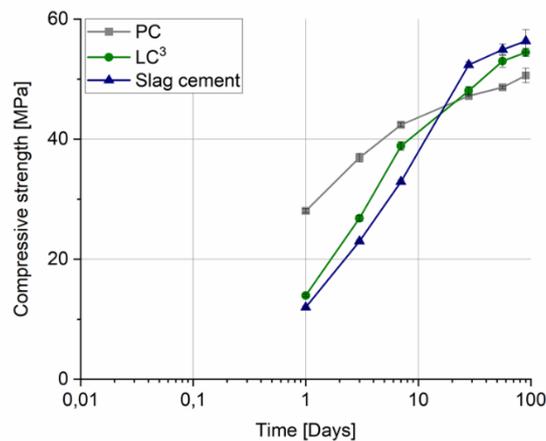


Figure 6-1. Compressive strength of PC, slag cement and LC³ blend

- What factors influence metakaolin reaction at early age?

The dissolution of metakaolin in calcined clay in NaOH solution (w/s=100) proceeds at a constant rate. The release rate of Al and Si ions is constant over time.

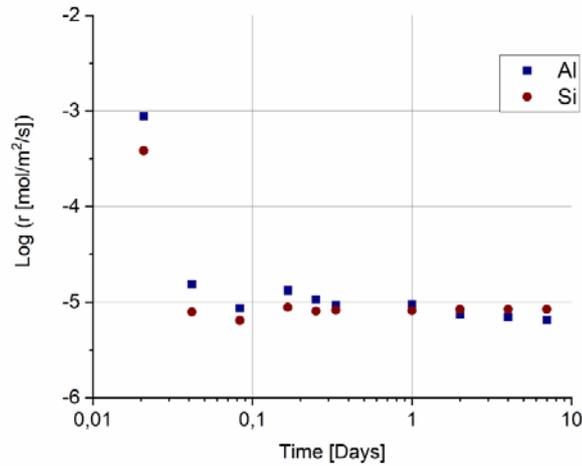


Figure 6-2. Log release rate of Al and Si in metakaolin in calcined clay (w/s=100)

The addition of calcium hydroxide enhances metakaolin reaction. The release rate as well as the degree of reaction are increased with the addition of calcium hydroxide. During hydration of cementitious blends, the Ca of the pore solution permits to observe similar trend to the dissolution experiments with portlandite addition.

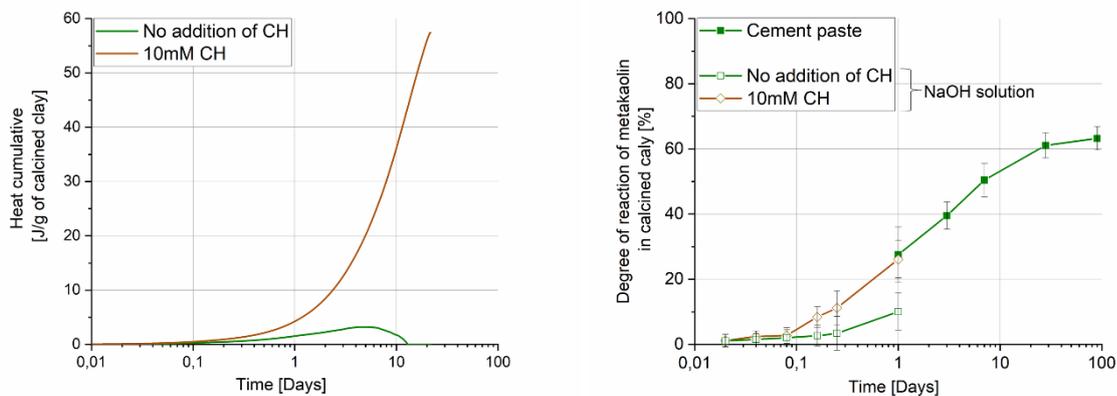


Figure 6-3. Heat cumulative of calcined clay in NaOH solution and degree of reaction of metakaolin in NaOH solution and cement paste

Using these findings, grinding optimization could provide quickly the adequate pore solution composition for higher metakaolin reactivity. Increasing the fineness of clinker would increase the dissolution and the release of calcium ions. Therefore, metakaolin reactivity could be enhanced. As a consequence, the replacement level with metakaolin can be further increased in LC³ blends.

6.2.2 Slag reactivity at early age

- Slag dissolution is decreased in presence of calcium hydroxide. More investigations on the surface chemistry of slag would be needed to investigate the complexation of calcium ions with different ions on slag surface. Calcium ions from solution could be incorporated into the glass surface layer.
- The heat release of slag in NaOH solution (w/s=100) decrease with the addition of 0.2mM of aluminium nitrate in the solution. Investigations on the impact of aluminum ions on slag dissolution would needed to be developed.

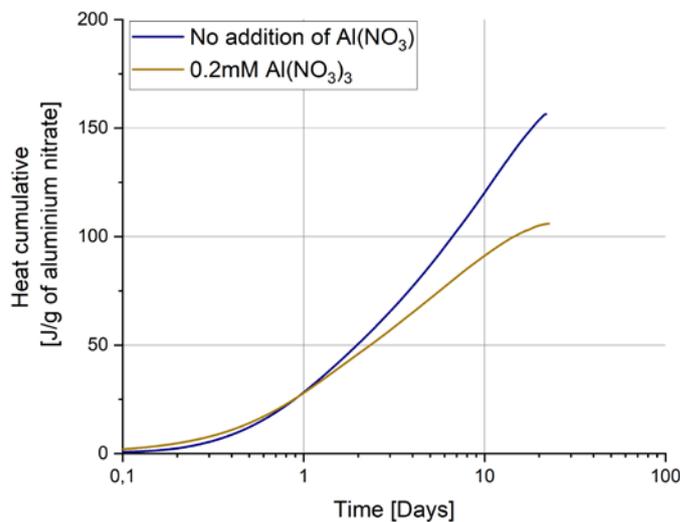


Figure 6-4. Heat cumulative of slag with and without addition of aluminium nitrate (w/s=100)

6.2.3 Metakaolin and slag reactivity at late ages

The reaction of slag and metakaolin does not stop at late ages but slows down. It is possible that the growth of hydrates at late ages might occur via different (slower) growth mechanisms.

TEM-tomography can help to investigate if other regimes for the growth of C-(A)-S-H are occurring in confined pores at late ages. The high resolution would be useful especially for LC³ system with a more refined pore connectivity.

These perspectives would allow to further develop the understanding of the reactivity of SCMs in cement paste. The key implications of this study and the recommendations for further research are essential to increase the replacement level of SCMs.

Appendix

7.1 Appendix 1: Methods

7.1.1 Characterization of powders

Particle size distribution of raw materials was determined using laser diffraction (Malvern Master-Sizer S). Mie theory was used to predict the size of the particle [40]. Limestone particles were dispersed using sodium metaphosphate (NaPO_3)₆. Isopropanol was used for clinker, quartz and silica fume. Solution of sodium carbonate Na_2CO_3 was used for calcined clay.

The specific surface area of powders was investigated using gas adsorption technique. Micromeritics TriStar II Plus was used. Powder was degassed at 200°C under constant N₂ flow for 2-4 hours. BET method was used to calculate the specific surface area.

7.1.2 Compressive strength test

Compressive strength was tested on 4 × 4 × 16 cm mortar bars following the EN 196-1 protocol. The results were obtained as an average of four compression tests.

7.1.3 Cement paste preparation and curing methods

The cement paste was mixed for 2 min at 1600 rpm and placed in plastic cylinder bottles (2 cm of diameter, 5 cm height). Two methods of curing were compared in this study:

Sealed curing : samples were cast in plastic cylinder bottles and then sealed with parafilm

Pore solution curing : after setting time, samples were demolded from the plastic bottles and placed in a container filled with pore solution.

For each testing age, four slices of the sample of 2-mm thickness were cut with a diamond saw using deionized water as a lubricant. One fresh slice was used for XRD measurements and the other three slices were put in isopropanol for 4 days. Isopropanol was changed after 1 hour, 1 day, and 3 days and then the slices were stored in a vacuum desiccator for at least 2 days.

7.1.4 Methods for cement hydration and microstructure investigations

Isothermal calorimetry

The hydration was followed by isothermal calorimetry (TAM Air, TA Instruments). Ten grams of paste were placed in the calorimeter. The instrument was maintained in a temperature-controlled room (20 °C) to ensure the stability of the baseline. The reference sample used in this study is water.

X-Ray diffraction (XRD)

X-Ray Diffraction (XRD) was used to characterize the crystalline phases consumed or formed during hydration. Measurements were carried out on freshly cut paste slices at 1, 3, 7, 28, 90 and 180 days. The slices were mounted on a sample holder and measured in Bragg-Brentano mode using a X'Pert PANalytical diffractometer with CuK α source operated at 45 kV and 40 mA. Samples were scanned from 7 to 70 $^{\circ}2\theta$ with a step size of 0.0167 $^{\circ}2\theta$ using a X'Celerator detector. The results were analyzed using X'Pert HighScore Plus 4.1 software with rutile as an external standard.

Thermogravimetric analysis (TGA)

TGA was used to quantify portlandite and bound water. The measurements were carried out on powder samples using a Mettler Toledo TGA/SDTA 851. Samples were crushed to obtain fine powder in an agate mortar. 50mg was filled in a specific alumina crucible. The program was run at a ramp rate 10 $^{\circ}$ C/min from 30 $^{\circ}$ C to 1000 $^{\circ}$ C under a 30 ml/min flow of N $_2$.

Sample preparation for SEM observations

A small piece of sample was impregnated under vacuum with a low viscosity and transparent epoxy resin (EpoTek 301). The setting of resin takes 24 hours. After resin setting, samples were pre-polished on an abrasive sandpaper grade P1200 using isopropanol as lubricant. The samples were then polished through three consecutive steps. To obtain a mirror-like sample surface, a 9 μ m diamond spray was used for polishing for 30min and then changed to 3 μ m for 2 hours and to 1 μ m for 3 hours. Petroleum was used as lubricant. Polished samples were cleaned using isopropanol in an ultrasonic bath and were kept under vacuum in desiccator for at least 48 h prior to analysis under the SEM. A 15nm thick carbon layer was applied in order to provide a conductive surface.

Scanning electron microscopy (SEM)

SEM was used for microstructure observation and phase composition. The backscattered electron imaging (SEM-BSE) and energy dispersive X-ray spectroscopy (SEM-EDS) were carried out on polished cross-section using a FEI Quanta 200 equipped with Bruker XFlash 4030 EDS detector.

The composition of C-(A)-S-H was determined by EDS point analysis following the optimization method recommend by Rossen et al. [81]. The authors suggested that the estimation of C-(A)-S-H atomic composition is best conducted using data acquired by manual choice of the regions of interest (particularly the inner and outer product C-(A)-S-H). Points should be measured in many zones across the sample and at sufficiently high magnification (at least 4000 \times in our setup) [81]. The typical plot between the atomic ratio of Al/Ca versus Si/Ca to define the composition is shown in Figure 7-1. An acceleration voltage of 15 kV and a working distance of 12.5 mm were used. To achieve relevant statistics, over 200 points were collected by SEM-EDS from the inner product of C-(A)-S-H.

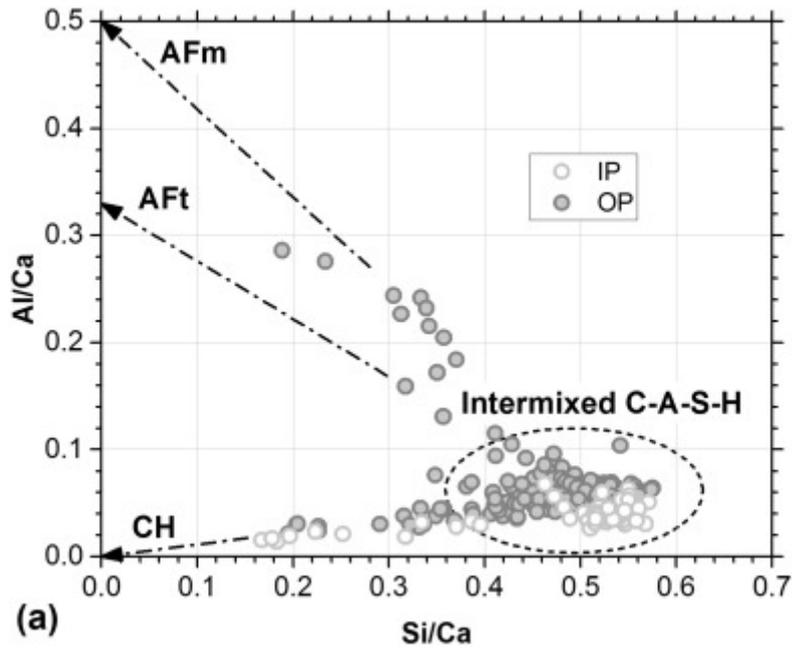


Figure 7-1. Determination of the composition of C-(A)-S-H from the plot of Al/Ca versus Si/Ca [81]

Mercury intrusion porosimetry (MIP)

Samples were crushed in small pieces with similar weight for consistency (1g). The dried samples were placed in the dilatometer. The measurement was carried out in two steps. In the first step a pressure of 100 kPa was applied to intrude the largest pores. Then, the pressure progressively increased up to 400 MPa which allows the intrusion of pore entry down to 2 nm. A contact angle of 120° was used between mercury and cement paste. The critical entry pore radius, the total porosity and the threshold pore radius can be determined from the derivative and the cumulative curves of MIP results (Figure 7-2).

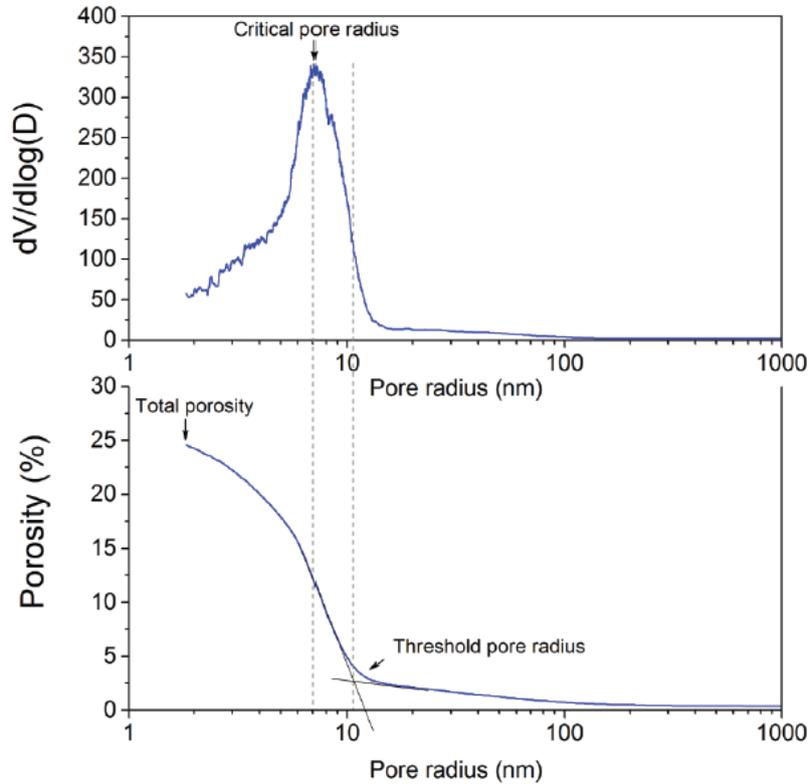


Figure 7-2. MIP results showing derivative and cumulative curves of LC³-50 paste samples at 28 days [80]

Relative humidity

Between 16 and 24h after casting, samples to be tested were crushed to sub-centimeter pieces and placed in the device, in a plastic container fitting the cavity of the probe. The probes measure the RH of the air surrounding the sample. Due to the limited size of the chamber, it is assumed that the RH of the air is at equilibrium with the RH of the pore network. A water-cooling system was used to keep the samples and the sensor at a constant temperature of 20°C. The set-up is equipped with 3 cells, and every studied system was replicated on the 3 cells in parallel. The recording interval was set to 10 min during the first 5 to 7 days of hydration, and then reduced to one recording per hour. A calibration routine is carried out in-between each run, using the built-in software calibration tool (HW4v.3). Saturated solutions of different salts (K_2SO_4 , K_2NO_3 , KCl, NaCl) were used to calibrate the sensors at fixed RH points between 98% and 75%.

7.1.5 Mass balance approach

The phase assemblage of all studied systems was estimated by the mass balance approach [21,31]. The inputs of this method are: the consumption of clinker phases, limestone and anhydrite and the

ettringite content from XRD measurement; the Al/Ca, Si/Ca ratios of the C-(A)-S-H of the different systems by SEM-EDS.

The principle of this method is well detailed in [21,31]. The sum of the different oxides coming from all the reacting phases are considered: CaO, SiO₂, Al₂O₃, Fe₂O₃, SO₃, CO₂ and MgO. Then a series of steps are used to calculate the amounts of the different phases formed, analogous to the Bogue calculation for the anhydrous phases in Portland cement. The sequence of steps is as follows:

- All MgO is considered to form hydrotalcite like phase M₄AH₁₀, subtracting the Al₂O₃ contribution from the initial Al₂O₃ amount available for the formation of hydration products.
- All Fe₂O₃ is then considered to form Fe-siliceous hydrogarnet C₃FS_{0.84}H_{4.32}, which is more stable than Fe-ettringite and Fe-AFm phases [63]. The required amounts of silicon and calcium oxides used for hydrogarnet formation are subtracted from their initial available content.
- All the remaining SiO₂ is then considered to be in C-A-S-H. Knowing the Al/Ca, Si/Ca ratios for the different systems at all ages by SEM-EDX described previously, the aluminium and calcium contributions are subtracted.
- The quantity of ettringite C₃A.3(C\$)H₃₂ (AFt) is taken as that measured by X-ray Diffraction - Rietveld method and from this the amounts of SO₃, CaO and Al₂O₃ are subtracted.
- The remaining Al₂O₃ is used for the formation of monocarboaluminate C₄A \bar{C} H₁₁ (Mc), consuming the available CO₂. Al₂O₃ was used as the limiting factor of the reaction rather than CO₂ because of the relative difficulty for the quantification of calcite by XRD-Rietveld.
- The amount of remaining CaO is used to form portlandite (CH).

The H₂O/(Si+Al) was fixed to 4 (including gel water) and the density of C-S-H to 2 g/cm³ [60,117]. The remaining water is calculated by subtracting the water consumed for all hydrates (C-A-S-H, ettringite, AFm, portlandite, stratlingite and hydrogarnet) from the initial water. In order to determine the amount of reacted metakaolin, calculations are made at steps of 1% metakaolin reaction and then plotted against the amount of portlandite. The real amount of metakaolin reactions can then be estimated from the portlandite content measured by XRD-Rietveld results [58].

7.2 Appendix 2: Preliminary study on fly ash cement

The impact of decreasing clinker content from 50% down to 30% was investigated in systems blended with fly ash and fly ash-limestone. Compressive strength was firstly investigated in these systems.

7.2.1 Chemical composition and mix design

The chemical composition of fly ash is presented in Table 7-1.

	Calcareous Fly ash
CaO	15.46
SiO ₂	47.61
Al ₂ O ₃	21.9
Fe ₂ O ₃	8.25
MgO	2.17
Na ₂ O	0.33
K ₂ O	1.61
SO ₃	1.08
TiO ₂	0.73
P ₂ O ₅	0.24
LOI	0.05

Table 7-1. Chemical composition of fly ash

The mix design of all investigated systems is shown in Figure 7-3. In binary blends with fly ash, clinker content was decreased from 50% down to 30%. In ternary blends, clinker was progressively replaced by fly ash with maintaining a constant amount of limestone to 10%.

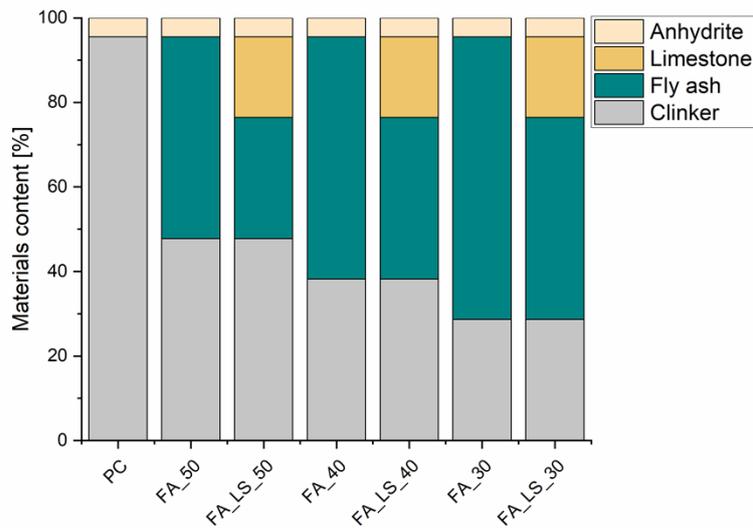


Figure 7-3. Mix formulations of cement blended with fly ash and limestone

7.2.2 Compressive strength

Strength development for PC and blended cements is shown in Figure 7-4. At 1 day, all blends show similar and very low compressive strength. The systems with clinker content 50% and 40% show comparable strength development for all ages. The system with 30% of clinker shows the lowest strength development. The partial replacement of fly ash with limestone in this system affects more negatively strength development.

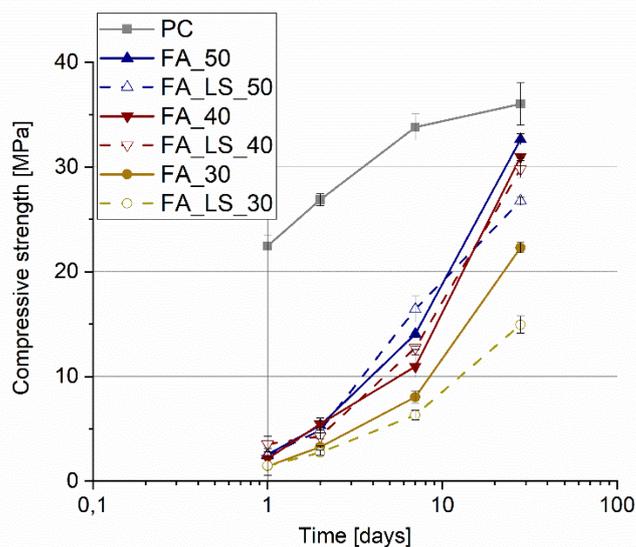


Figure 7-4. Strength development of PC, fly ash and fly ash-limestone blends

Compressive strength for fly ash blended systems was poor compared to PC due to the slow reaction of fly ash. This study was not continued because of the very slow performances of fly ash blends.

7.3 Appendix 3: Nielsen and Mersmann approach

7.3.1 Saturation index using thermodynamic modelling

Thermodynamic modelling was used to calculate the saturation indexes, SI_{GEMS} , for AFm and C-S-H at 28 days of hydration. Pore solution at 28 days of hydration from previous studies on LC³ and slag cements were used as inputs for calculating SI_{GEMS} [21,31,118]. Table 7-2 summarizes the elemental concentrations used. Concentrations were obtained with w/b ratio of 0.5 since the extraction of the pore solution becomes more challenging for lower w/b.

mmol/L	Al	Si	Ca	S	Na	K
LC ³ _50 [31]	1.02	0.45	1.2	2.25	53	93
50% metakaolin						
LC ³ _50 [118]	1.11	0.41	0.75	2.95	46	90
48% metakaolin						
Slag cement	0.02	0.05	4	2,4	50	112
55% cement-45%slag [21]						

Table 7-2. Element concentrations in LC³ and slag cement

7.3.2 Nielsen and Mersmann approach for interfacial energy estimation

Nielsen approach [68] was used to estimate the interfacial energy σ which is an approach involving solubility and interfacial energy as shown in Equation 7-1 and Equation 7-2:

$$\frac{\sigma}{K T} = 2.82 - 0.272 \ln(K_{sp}) \quad \text{Equation 7-7-1}$$

$$\gamma = \sigma/a^2 \quad \text{Equation 7-7-2}$$

Where σ is the edge work, K Boltzmann constant, T the temperature, k_{sp} the solubility of the crystal, a is the molecular unit cell distance and finally γ is the interfacial energy.

There are several models of C-S-H solubility reported in literature [119–123]. The solubility of tobermorite C-S-H $(CaO)_{0.83}(SiO_2)(H_2O)_{1.3}$ with the value -8 was selected in this study [119]. Solubility data (K_{sp}) of AFm was also adapted from the same study [119].

Mersmann approach [69] was also used to estimate the interfacial energy given γ in Equation 7-3. The first term considers the adsorption of ions at the interface and the second term considers the approach of a point charge towards this interface:

$$\gamma = \gamma_0 - \frac{RT}{zF} \left\{ \underbrace{\sigma_{\max} \ln \left(\frac{\sigma_{\max}}{\sigma_{\max} - |\sigma|} \right)}_{\text{Adsorption of ions}} + \underbrace{\frac{8FI}{\kappa} \left[\sqrt{\left(1 + \left(\frac{\kappa\sigma}{4FI} \right)^2} - 1 \right)}_{\text{Approach of the ions}} \right] \right\} \quad \text{Equation 7-7-3}$$

With γ_0 the maximum interfacial energy of a crystal at its point of zero charge, R the gas constant, T the temperature, F the Faraday constant, z the valence of a (z:z) electrolyte, σ and σ_{\max} are the surface charge of ionic crystals.

γ_0 is defined in Equation 7-4

$$\gamma_0 = 0.414 \cdot K_B \cdot T \left(\frac{1000 \rho N_{AV}}{M_w} \right)^{2/3} \ln \left(\frac{1000 \rho}{M_w K_{sp}} \right) \quad \text{Equation 7-7-4}$$

I is the ionic strength and $1/\kappa$ is the Debye length are defined in Equation 7-5

$$I = \sum_{i=1}^n C_i Z_i^2 ; \kappa^{-1} = \sqrt{\frac{\epsilon \epsilon_0 k T}{2 N_{AV} e^2 I}} \quad \text{Equation 7-7-5}$$

With K_B is the Boltzmann constant, N_{AV} is the Avogadro constant, ϵ_0 is the vacuum permittivity and e is the electron charge.

- The density ρ and the molecular weight M_w of hydrates [60,116,117]

- The molar concentration C_i are based from results of Harris et al. on C-S-H synthesis with Ca/Si:2 [124]

- The dielectric constant ϵ [125]

- The surface charge densities σ and σ_{\max} [73].

Poisson–Boltzmann equation can be applied to determine the surface charge density of ionic crystals (σ); a parameter required for Mersmann's approach. However, Poisson–Boltzmann equation assumes that ions are point charges interacting with the surface and the surrounding electrolyte solution [126]. As a consequence, the ion-ion interactions are neglected. This theory could be reliable for low surface

charge densities in the presence of only monovalent counterions in low concentrations (diluted solutions) but fails to describe high surface charge density which is the case for C-(A)-S-H [127]. Hence, in this study the surface charge density for C-S-H were not calculated using Poisson–Boltzmann equation but were adapted from recent work determined using Monte Carlo simulation [73] where the electrostatic interactions are considered.

7.4 Appendix 4: Gel space ratio approach

Strength results for LC³ 50-30 were correlated with phase assemblage using the gel space ratio approach. The plot for compressive strength against gel space ratio for all investigated systems is shown in Figure 7-5. The gel was defined here as a) sum of hydrates, b) C-A-S-H and c) sum of hydrates and the volume of unreacted limestone and metakaolin. Space is defined as the initial water volume with the volume of reacted particles. For each system and considering all the definitions studied for gel, compressive strength increases with increasing gel space ratio. However, a low correlation was obtained; i.e. the gel to space ratio fits with the compressive strength of all the systems together but with a considerable deviation.

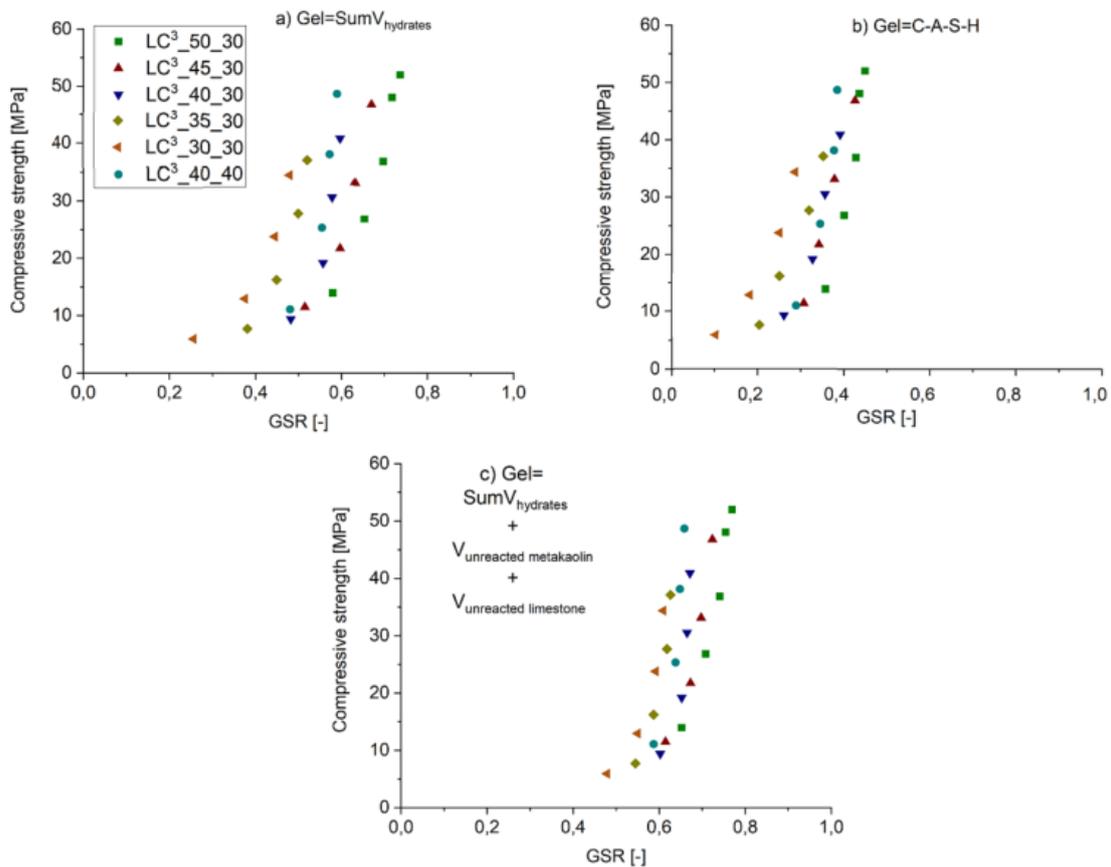


Figure 7-5. Correlation between compressive strength and gel space ratio considering the gel as a) sum of hydrates, b) C-A-S-H and c) sum of hydrates and the unreacted limestone and metakaolin

The deviation observed with gel space ratio is partially related to the challenging quantification of C-A-S-H composition for low clinker cements. Moreover, the definition of gel space ratio considers only the chemical reactions involved in the systems and does not deal with the physical impact of the

initial particle arrangement. More study would be needed to incorporate the physical impact of SCMs and fillers on the particle packing density in the gel to space ratio approach.

References

- [1] G. Hammond, C. Jones, A BSRIA Guide. Embodied Carbon: The Inventory of Carbon and Energy. University of Bath, UK., Ice. (2011) 136. <https://doi.org/10.1680/ener.2011.164.4.206>.
- [2] European Commission, A Roadmap for moving to a competitive low carbon economy in 2050, COM(2011) 112 Final. 34 (2011) 1–34. <https://doi.org/10.1002/jsc.572>.
- [3] CEMBUREAU, The Role of Cement in the 2050 Low Carbon Economy, (2013) 1–64.
- [4] WBCSD, IEA, Cement Technology Roadmap 2009: Carbon emissions reductions up to 2050, Technol. RoadmapsCement. 1 (2009) 1–36. <https://doi.org/978-3-940388-47-6>.
- [5] WBCSD, The Cement Sustainability Initiative, Cement Industry Energy and CO₂ Performance: “Getting the Numbers Right,” <Http://Www.Wbcdcement.Org/Index.Php>. (2016) 44. <https://doi.org/ISBN: 978-3-940388-48-3>.
- [6] K.L. Scrivener, V.M. John, E.M. Gartner, Eco-efficient cements: Potential economically viable solutions for a low-CO₂ cement-based materials industry, *Cem. Concr. Res.* 114 (2018) 2–26. <https://doi.org/https://doi.org/10.1016/j.cemconres.2018.03.015>.
- [7] J.W. Bullard, H.M. Jennings, R.A. Livingston, A. Nonat, G.W. Scherer, J.S. Schweitzer, K.L. Scrivener, J.J. Thomas, Mechanisms of cement hydration, *Cem. Concr. Res.* 41 (2011) 1208–1223. <https://doi.org/https://doi.org/10.1016/j.cemconres.2010.09.011>.
- [8] T. Emeritus, Cement chemistry, *Cem. Concr. Compos.* 20 (1998) 335. [https://doi.org/10.1016/s0958-9465\(98\)00023-7](https://doi.org/10.1016/s0958-9465(98)00023-7).
- [9] R. Snellings, Assessing , Understanding and Unlocking Supplementary Cementitious Materials, (2016) 50–55. <https://doi.org/10.21809/rilemtechlett.2016.12>.
- [10] T. Matschei, B. Lothenbach, F.P. Glasser, The role of calcium carbonate in cement hydration, *Cem. Concr. Res.* 37 (2007) 551–558. <https://doi.org/10.1016/j.cemconres.2006.10.013>.
- [11] B. Lothenbach, G. Le Saout, E. Gallucci, K. Scrivener, Influence of limestone on the hydration of Portland cements, *Cem. Concr. Res.* 38 (2008) 848–860. <https://doi.org/https://doi.org/10.1016/j.cemconres.2008.01.002>.
- [12] O. Chowaniec, Limestone Addition in Cement, 5335 (2012) 242. <https://infoscience.epfl.ch/record/174700>.
- [13] G. Kakali, S. Tsivilis, E. Aggeli, M. Bati, Hydration products of C3A, C3S and Portland cement in the presence of CaCO₃, *Cem. Concr. Res.* 30 (2000) 1073–1077. [https://doi.org/10.1016/S0008-8846\(00\)00292-1](https://doi.org/10.1016/S0008-8846(00)00292-1).
- [14] S. Adu-Amankwah, M. Zajac, C. Stabler, B. Lothenbach, L. Black, Influence of limestone on the hydration of ternary slag cements, *Cem. Concr. Res.* 100 (2017) 96–109. <https://doi.org/https://doi.org/10.1016/j.cemconres.2017.05.013>.
- [15] F. Avet, R. Snellings, A. Alujas Diaz, M. Ben Haha, K. Scrivener, Development of a new rapid, relevant and reliable (R3) test method to evaluate the pozzolanic reactivity of calcined

-
- kaolinitic clays, *Cem. Concr. Res.* 85 (2016) 1–11. <https://doi.org/10.1016/j.cemconres.2016.02.015>.
- [16] M. Zajac, A. Rossberg, G. Le Saout, B. Lothenbach, Influence of limestone and anhydrite on the hydration of Portland cements, *Cem. Concr. Compos.* 46 (2014) 99–108. <https://doi.org/10.1016/j.cemconcomp.2013.11.007>.
- [17] C.J. Werth, Equilibrium Partitioning and Mass Transfer of Organic Chemicals Leached from Recycled Hazardous Waste Materials, *Water Pollut.* 5 (2005) 1–32. <https://doi.org/10.1007/b11493>.
- [18] P. Chindapasirt, T. Cao, 8 - The properties and durability of high-pozzolanic industrial by-products content concrete masonry blocks, in: F. Pacheco-Torgal, P.B. Lourenço, J.A. Labrincha, S. Kumar, P.B.T.-E.-E.M.B. and B. Chindapasirt (Eds.), Woodhead Publishing, Oxford, 2015: pp. 191–214. <https://doi.org/https://doi.org/10.1016/B978-1-78242-305-8.00008-5>.
- [19] B. Lothenbach, K. Scrivener, R.D. Hooton, Supplementary cementitious materials, *Cem. Concr. Res.* 41 (2011) 1244–1256. <https://doi.org/10.1016/j.cemconres.2010.12.001>.
- [20] R.B. Holland, K.E. Kurtis, L.F. Kahn, 7 - Effect of different concrete materials on the corrosion of the embedded reinforcing steel, in: A.B.T.-C. of S. in C.S. Poursaei (Ed.), Woodhead Publishing, Oxford, 2016: pp. 131–147. <https://doi.org/https://doi.org/10.1016/B978-1-78242-381-2.00007-9>.
- [21] P.T. Durdziński, Hydration of multi-component cements containing clinker, slag, type-V fly ash and limestone, 6834 (2016) 1–225. <https://doi.org/10.5075/EPFL-THESIS-6834>.
- [22] K. Scrivener, F. Martirena, S. Bishnoi, S. Maity, Calcined clay limestone cements (LC3), *Cem. Concr. Res.* 114 (2018) 49–56. <https://doi.org/https://doi.org/10.1016/j.cemconres.2017.08.017>.
- [23] A. Alujas, R. Fernández, R. Quintana, K.L. Scrivener, F. Martirena, Pozzolanic reactivity of low grade kaolinitic clays: Influence of calcination temperature and impact of calcination products on OPC hydration, *Appl. Clay Sci.* 108 (2015) 94–101. <https://doi.org/https://doi.org/10.1016/j.clay.2015.01.028>.
- [24] F. Avet, Investigation of the grade of calcined clays used as clinker substitute in Limestone Calcined Clay Cement (LC3) -Ph.D Thesis, 8143 (2017) 169.
- [25] S. Aboudi, M. Hanafiah, A. Chowdhury, Environmental characteristics of clay and clay-based minerals, *Geol. Ecol. Landscapes.* 1 (2017) 155–161. <https://doi.org/10.1080/24749508.2017.1361128>.
- [26] J. Skibsted, R. Snellings, Reactivity of supplementary cementitious materials (SCMs) in cement blends, *Cem. Concr. Res.* 124 (2019) 105799. <https://doi.org/https://doi.org/10.1016/j.cemconres.2019.105799>.
- [27] K.L. Konan, C. Peyratout, A. Smith, J.-P. Bonnet, S. Rossignol, S. Oyetola, Comparison of surface properties between kaolin and metakaolin in concentrated lime solutions, *J. Colloid*

-
- Interface Sci. 339 (2009) 103–109. <https://doi.org/https://doi.org/10.1016/j.jcis.2009.07.019>.
- [28] J. Ambroise, M. Murat, J. Pera, Hydration reaction and hardening of calcined clays and related minerals. IV. Experimental conditions for strength improvement on metakaolinite minicylinders, *Cem. Concr. Res.* 15 (1985) 83–88. [https://doi.org/https://doi.org/10.1016/0008-8846\(85\)90011-0](https://doi.org/https://doi.org/10.1016/0008-8846(85)90011-0).
- [29] A.S. Silva, A. Gameiro, J. Grilo, R. Veiga, A. Velosa, Long-term behavior of lime–metakaolin pastes at ambient temperature and humid curing condition, *Appl. Clay Sci.* 88–89 (2014) 49–55. <https://doi.org/https://doi.org/10.1016/j.clay.2013.12.016>.
- [30] A. Tironi, M. Trezza, A.N. Scian, E. Irassar, Assessment of Pozzolanic Activity of Different Calcined Clays, *Cem. Concr. Compos.* 37 (2013) 319–327. <https://doi.org/10.1016/j.cemconcomp.2013.01.002>.
- [31] F. Avet, K. Scrivener, Investigation of the calcined kaolinite content on the hydration of Limestone Calcined Clay Cement (LC3), *Cem. Concr. Res.* 107 (2018) 124–135. <https://doi.org/10.1016/j.cemconres.2018.02.016>.
- [32] E. Berodier, K. Scrivener, Understanding the Filler Effect on the Nucleation and Growth of C-S-H, *J. Am. Ceram. Soc.* 97 (2014). <https://doi.org/10.1111/jace.13177>.
- [33] P. Juilland, A. Kumar, E. Gallucci, R.J. Flatt, K.L. Scrivener, Effect of mixing on the early hydration of alite and OPC systems, *Cem. Concr. Res.* 42 (2012) 1175–1188. <https://doi.org/https://doi.org/10.1016/j.cemconres.2011.06.011>.
- [34] T. Oey, A. Kumar, J.W. Bullard, N. Neithalath, G. Sant, The filler effect: The influence of filler content and surface area on cementitious reaction rates, *J. Am. Ceram. Soc.* 96 (2013) 1978–1990. <https://doi.org/10.1111/jace.12264>.
- [35] E. Berodier, Impact of the Supplementary Cementitious Materials on the kinetics and microstructural development of cement hydration, 6417 (2015) 154. https://infoscience.epfl.ch/record/204690/files/EPFL_TH6417.pdf%5Cnhttp://files/148/EPFL_TH6417.pdf.
- [36] K. De Weerd, M. Ben Haha, G. Le Saout, K.O. Kjellsen, H. Justnes, B. Lothenbach, Hydration mechanisms of ternary Portland cements containing limestone powder and fly ash, *Cem. Concr. Res.* 41 (2011) 279–291. <https://doi.org/10.1016/j.cemconres.2010.11.014>.
- [37] Y. Knop, A. Peled, Packing density modeling of blended cement with limestone having different particle sizes, *Constr. Build. Mater.* 102 (2016) 44–50. <https://doi.org/10.1016/j.conbuildmat.2015.09.063>.
- [38] S. Tsivilis, E. Chaniotakis, E. Badogiannis, G. Pahoulas, A. Ilias, A study on the parameters affecting the properties of Portland limestone cements, *Cem. Concr. Compos.* 21 (1999) 107–116. [https://doi.org/https://doi.org/10.1016/S0958-9465\(98\)00031-6](https://doi.org/https://doi.org/10.1016/S0958-9465(98)00031-6).
- [39] Y. Tang, J. Gao, C. Liu, X. Chen, Y. Zhao, Dehydration Pathways of Gypsum and the Rehydration Mechanism of Soluble Anhydrite γ -CaSO₄, *ACS Omega.* 4 (2019) 7636–7642. <https://doi.org/10.1021/acsomega.8b03476>.

-
- [40] M. Palacios, H. Kazemi-Kamyab, S. Mantellato, P. Bowen, Laser diffraction and gas adsorption techniques, in: 2016: p. 445. <https://doi.org/10.1201/b19074-11>.
- [41] F. Zunino, K. Scrivener, The influence of the filler effect on the sulfate requirement of blended cements, *Cem. Concr. Res.* 126 (2019) 105918. <https://doi.org/https://doi.org/10.1016/j.cemconres.2019.105918>.
- [42] J. Zhang, G.W. Scherer, Comparison of methods for arresting hydration of cement, *Cem. Concr. Res.* 41 (2011) 1024–1036. <https://doi.org/https://doi.org/10.1016/j.cemconres.2011.06.003>.
- [43] M. Hunger, H.J.H. Brouwers, Flow analysis of water–powder mixtures: Application to specific surface area and shape factor, *Cem. Concr. Compos.* 31 (2009) 39–59. <https://doi.org/https://doi.org/10.1016/j.cemconcomp.2008.09.010>.
- [44] S.A.A.M. Fennis, J.C. Walraven, Using particle packing technology for sustainable concrete mixture design, *Heron.* 57 (2012) 73–101.
- [45] T.C. Powers, American Ceramic Society, *J. Am. Ceram. Soc.* 41 (1958) 1–6.
- [46] P.T. Durdziński, M. Ben Haha, M. Zajac, K.L. Scrivener, Phase assemblage of composite cements, *Cem. Concr. Res.* 99 (2017) 172–182. <https://doi.org/10.1016/j.cemconres.2017.05.009>.
- [47] M. Antoni, J. Rossen, F. Martirena, K. Scrivener, Cement substitution by a combination of metakaolin and limestone, *Cem. Concr. Res.* 42 (2012) 1579–1589. <https://doi.org/10.1016/j.cemconres.2012.09.006>.
- [48] R. Snellings, Solution-Controlled Dissolution of Supplementary Cementitious Dissolution Rates, 2475 (2013). <https://doi.org/10.1111/jace.12480>.
- [49] L. Nicoleau, E. Schreiner, A. Nonat, Ion-specific effects influencing the dissolution of tricalcium silicate, *Cem. Concr. Res.* 59 (2014) 118–138. <https://doi.org/https://doi.org/10.1016/j.cemconres.2014.02.006>.
- [50] L. Nicoleau, A. Nonat, D. Perrey, The di- and tricalcium silicate dissolutions, *Cem. Concr. Res.* 47 (2013) 14–30. <https://doi.org/10.1016/j.cemconres.2013.01.017>.
- [51] P. Lura, O.M. Jensen, K. van Breugel, Autogenous shrinkage in high-performance cement paste: An evaluation of basic mechanisms, *Cem. Concr. Res.* 33 (2003) 223–232. [https://doi.org/https://doi.org/10.1016/S0008-8846\(02\)00890-6](https://doi.org/https://doi.org/10.1016/S0008-8846(02)00890-6).
- [52] R.J. Flatt, G.W. Scherer, J.W. Bullard, Why alite stops hydrating below 80% relative humidity, *Cem. Concr. Res.* 41 (2011) 987–992. <https://doi.org/https://doi.org/10.1016/j.cemconres.2011.06.001>.
- [53] Z. Hu, Prediction of autogenous shrinkage in fly ash blended cement systems, 7829 (2017) 213.
- [54] J. Ston, Basic creep and autogenous shrinkage of Limestone Calcined Clay Cement (LC3), (2019). <https://doi.org/10.5075/EPFL-THESIS-9321>.

-
- [55] K. Scrivener, A. Ouzia, P. Juilland, A. Kunhi Mohamed, Advances in understanding cement hydration mechanisms, *Cem. Concr. Res.* 124 (2019) 105823. <https://doi.org/https://doi.org/10.1016/j.cemconres.2019.105823>.
- [56] E. Berodier, K. Scrivener, Evolution of pore structure in blended systems, *Cem. Concr. Res.* 73 (2015) 25–35. <https://doi.org/10.1016/j.cemconres.2015.02.025>.
- [57] B. (Ed.). Scrivener, K. (Ed.), Snellings, R. (Ed.), Lothenbach, A Practical Guide to Microstructural Analysis of Cementitious Materials, 2018. <https://doi.org/10.1201/b19074>.
- [58] F. Avet, X. Li, K. Scrivener, Determination of the amount of reacted metakaolin in calcined clay blends, *Cem. Concr. Res.* 106 (2018) 40–48. <https://doi.org/https://doi.org/10.1016/j.cemconres.2018.01.009>.
- [59] A.C.A. Muller, K.L. Scrivener, A reassessment of mercury intrusion porosimetry by comparison with ¹H NMR relaxometry, *Cem. Concr. Res.* 100 (2017) 350–360. <https://doi.org/https://doi.org/10.1016/j.cemconres.2017.05.024>.
- [60] F. Avet, E. Boehm-courjault, K. Scrivener, Cement and Concrete Research Investigation of C-A-S-H composition , morphology and density in Limestone Calcined Clay Cement (LC 3), *Cem. Concr. Res.* 115 (2019) 70–79. <https://doi.org/10.1016/j.cemconres.2018.10.011>.
- [61] M. Wyrzykowski, P. Lura, Cement and Concrete Research Effect of relative humidity decrease due to self-desiccation on the hydration kinetics of cement, *Cem. Concr. Res.* 85 (2016) 75–81. <https://doi.org/10.1016/j.cemconres.2016.04.003>.
- [62] H. Chen, M. Wyrzykowski, K. Scrivener, P. Lura, Prediction of self-desiccation in low water-to-cement ratio pastes based on pore structure evolution, *Cem. Concr. Res.* 49 (2013) 38–47. <https://doi.org/https://doi.org/10.1016/j.cemconres.2013.03.013>.
- [63] B.Z. Dilnesa, B. Lothenbach, G. Le Saout, G. Renaudin, A. Mesbah, Y. Filinchuk, A. Wichser, E. Wieland, Iron in carbonate containing AFm phases, *Cem. Concr. Res.* 41 (2011) 311–323. <https://doi.org/https://doi.org/10.1016/j.cemconres.2010.11.017>.
- [64] A. Koishi, C. Physics, Carbonate mineral nucleation pathways Ayumi Koishi To cite this version : HAL Id : tel-01701947 Mécanismes de nucléation des carbonates Carbonate mineral nucleation pathways, (2018).
- [65] C. Estrela, C.R. de A. Estrela, L.F. Guimarães, R.S. Silva, J.D. Pécora, Surface tension of calcium hydroxide associated with different substances, *J. Appl. Oral Sci.* 13 (2005) 152–156. <https://doi.org/10.1590/S1678-77572005000200011>.
- [66] S. Garrault-Gauffinet, A. Nonat, Experimental investigation of calcium silicate hydrate (C-S-H) nucleation, *J. Cryst. Growth.* 200 (1999) 565–574. [https://doi.org/10.1016/S0022-0248\(99\)00051-2](https://doi.org/10.1016/S0022-0248(99)00051-2).
- [67] M.R. Andalibi, C. Ludwig, A. Testino, A. Kumar, B. Srinivasan, P. Bowen, K. Scrivener, On the mesoscale mechanism of synthetic calcium-silicate-hydrate precipitation: A population balance modeling approach, *J. Mater. Chem. A.* 6 (2018) 363–373. <https://doi.org/10.1039/C7TA08784E>.

-
- [68] A.E. Nielsen, Electrolyte crystal growth mechanisms, *J. Cryst. Growth.* 67 (1984) 289–310. [https://doi.org/https://doi.org/10.1016/0022-0248\(84\)90189-1](https://doi.org/https://doi.org/10.1016/0022-0248(84)90189-1).
- [69] A. Mersmann, *Crystallization technology handbook*, 2nd ed., r, New York : Marcel Dekker, New York, 2001.
- [70] J.J. Thomas, H.M. Jennings, A.J. Allen, Relationships between Composition and Density of Tobermorite, Jennite, and Nanoscale CaO–SiO₂–H₂O, *J. Phys. Chem. C.* 114 (2010) 7594–7601. <https://doi.org/10.1021/jp910733x>.
- [71] B. Lothenbach, D.A. Kulik, T. Matschei, M. Balonis, L. Baquerizo, B. Dilnesa, G.D. Miron, R.J. Myers, Cemdata18: A chemical thermodynamic database for hydrated Portland cements and alkali-activated materials, *Cem. Concr. Res.* 115 (2019) 472–506. <https://doi.org/10.1016/j.cemconres.2018.04.018>.
- [72] C. Gabriel, A. Peyman, Dielectric measurement: Error analysis and assessment of uncertainty, *Phys. Med. Biol.* 51 (2007) 6033–6046. <https://doi.org/10.1088/0031-9155/51/23/006>.
- [73] B. Jönsson, A. Nonat, C. Labbez, B. Cabane, H. Wennerström, Controlling the cohesion of cement paste, *Langmuir.* 21 (2005) 9211–9221. <https://doi.org/10.1021/la051048z>.
- [74] B. Lothenbach, M. Zajac, Application of thermodynamic modelling to hydrated cements, *Cem. Concr. Res.* 123 (2019) 105779. <https://doi.org/https://doi.org/10.1016/j.cemconres.2019.105779>.
- [75] W. Wu, G.H. Nancollas, Determination of interfacial tension from crystallization and dissolution data: a comparison with other methods, *Adv. Colloid Interface Sci.* 79 (1999) 229–279. [https://doi.org/https://doi.org/10.1016/S0001-8686\(98\)00072-4](https://doi.org/https://doi.org/10.1016/S0001-8686(98)00072-4).
- [76] M. Donnet, P. Bowen, J. Lemaître, A thermodynamic solution model for calcium carbonate: Towards an understanding of multi-equilibria precipitation pathways, *J. Colloid Interface Sci.* 340 (2009) 218–224. <https://doi.org/https://doi.org/10.1016/j.jcis.2009.09.005>.
- [77] O. Shnel, J. Garside, *Precipitation : basic principles and industrial applications*, Butterworth-Heinemann, Oxford [England]; Boston, 1992.
- [78] S. et. al. Rogelj, Joeri. Shindell, Drew. Jiang, Kejun. fifita, Solomone. Kheshgi, Haroon. Kobayashi, Chapter 2 : Mitigation pathways compatible with 1 . 5 ° C in the context of sustainable development, *Ipcc Sr1.5.* (2018) 1–112.
- [79] L. Barcelo, J. Kline, G. Walenta, E. Gartner, Cement and carbon emissions, *Mater. Struct.* 47 (2014). <https://doi.org/10.1617/s11527-013-0114-5>.
- [80] W. Hanpongpun, Investigation of the use of Limestone Calcined Clay Cement (LC3) applied to Thailand, 2019. <https://doi.org/10.5075/epfl-thesis-9005>.
- [81] J.E. Rossen, K.L. Scrivener, Optimization of SEM-EDS to determine the C–A–S–H composition in matured cement paste samples, *Mater. Charact.* 123 (2017) 294–306. <https://doi.org/https://doi.org/10.1016/j.matchar.2016.11.041>.
- [82] V.M. John, M. Quattrone, P.C.R.A. Abrão, F.A. Cardoso, Rethinking cement standards:

-
- Opportunities for a better future, *Cem. Concr. Res.* 124 (2019) 105832. <https://doi.org/https://doi.org/10.1016/j.cemconres.2019.105832>.
- [83] J.H. Ideker, K.L. Scrivener, H. Fryda, B. Touzo, 12 - Calcium Aluminate Cements, in: P.C. Hewlett, M.B.T.-L.C. of C. and C. (Fifth E. Liska (Eds.), Butterworth-Heinemann, 2019: pp. 537–584. <https://doi.org/https://doi.org/10.1016/B978-0-08-100773-0.00012-5>.
- [84] B. Lothenbach, F. Winnefeld, Thermodynamic Modeling of the Hydration of Portland Cement, *Cem. Concr. Res.* 36 (2006) 209–226. <https://doi.org/10.1016/j.cemconres.2005.03.001>.
- [85] K.S. Y.Briki, F.Avet, M.Zajac, P.Bowen, M.Ben Haha, Understanding of the factors slowing down metakaolin reaction in limestone calcined clay cement (LC3) at late ages, *Cem. Concr. Res.* (2020).
- [86] V. Kocaba, Development and evaluation of methods to follow microstructural development of cementitious systems including slags, *Techniques.* 4523 (2009) 1–263. <https://doi.org/10.5075/epfl-thesis-4523>.
- [87] J.O. Ukpata, P.A. Muhammed Basheer, L. Black, Expansion of CEM I and slag-blended cement mortars exposed to combined chloride-sulphate environments, *Cem. Concr. Res.* 123 (2019) 105794. <https://doi.org/https://doi.org/10.1016/j.cemconres.2019.105794>.
- [88] S. Ogawa, T. Nozaki, K. Yamada, H. Hirao, R.D. Hooton, Improvement on sulfate resistance of blended cement with high alumina slag, *Cem. Concr. Res.* 42 (2012) 244–251. <https://doi.org/https://doi.org/10.1016/j.cemconres.2011.09.008>.
- [89] G. Le Saoût, M. Ben Haha, F. Winnefeld, B. Lothenbach, Hydration Degree of Alkali-Activated Slags: A ²⁹Si NMR Study, *J. Am. Ceram. Soc.* 94 (2011) 4541–4547. <https://doi.org/10.1111/j.1551-2916.2011.04828.x>.
- [90] M. Ben Haha, G. Le Saout, F. Winnefeld, B. Lothenbach, Influence of activator type on hydration kinetics, hydrate assemblage and microstructural development of alkali activated blast-furnace slags, *Cem. Concr. Res.* 41 (2011) 301–310. <https://doi.org/https://doi.org/10.1016/j.cemconres.2010.11.016>.
- [91] S.-D. Wang, K.L. Scrivener, P.L. Pratt, Factors affecting the strength of alkali-activated slag, *Cem. Concr. Res.* 24 (1994) 1033–1043. [https://doi.org/https://doi.org/10.1016/0008-8846\(94\)90026-4](https://doi.org/https://doi.org/10.1016/0008-8846(94)90026-4).
- [92] R. Snellings, Solution-Controlled Dissolution of Supplementary Cementitious Material Glasses at pH 13: The Effect of Solution Composition on Glass Dissolution Rates, *J. Am. Ceram. Soc.* 96 (2013) 2467–2475. <https://doi.org/10.1111/jace.12480>.
- [93] A. Schöler, F. Winnefeld, M. Ben Haha, B. Lothenbach, The effect of glass composition on the reactivity of synthetic glasses, *J. Am. Ceram. Soc.* 100 (2017) 2553–2567. <https://doi.org/10.1111/jace.14759>.
- [94] K.C. Newlands, M. Foss, T. Matchei, J. Skibsted, D.E. Macphee, Early stage dissolution characteristics of aluminosilicate glasses with blast furnace slag- and fly-ash-like compositions, *J. Am. Ceram. Soc.* 100 (2017) 1941–1955. <https://doi.org/10.1111/jace.14716>.

-
- [95] M. Öner, K. Erdoğan, A. Günlü, Effect of components fineness on strength of blast furnace slag cement, *Cem. Concr. Res.* 33 (2003) 463–469. [https://doi.org/https://doi.org/10.1016/S0008-8846\(02\)00713-5](https://doi.org/https://doi.org/10.1016/S0008-8846(02)00713-5).
- [96] F. Winnefeld, M. Ben Haha, G. Le Saout, M. Costoya, S.-C. Ko, B. Lothenbach, Influence of slag composition on the hydration of alkali-activated slags, *J. Sustain. Cem. Mater.* 4 (2015) 85–100. <https://doi.org/10.1080/21650373.2014.955550>.
- [97] P. Suraneni, M. Palacios, R.J. Flatt, New insights into the hydration of slag in alkaline media using a micro-reactor approach, *Cem. Concr. Res.* 79 (2016) 209–216. <https://doi.org/https://doi.org/10.1016/j.cemconres.2015.09.015>.
- [98] P.T. Durdziński, R. Snellings, C.F. Dunant, M. Ben Haha, K.L. Scrivener, Fly ash as an assemblage of model Ca–Mg–Na-aluminosilicate glasses, *Cem. Concr. Res.* 78 (2015) 263–272. <https://doi.org/https://doi.org/10.1016/j.cemconres.2015.08.005>.
- [99] B. Lothenbach, G. Le Saout, M. Ben Haha, R. Figi, E. Wieland, Hydration of a low-alkali CEM III/B–SiO₂ cement (LAC), *Cem. Concr. Res.* 42 (2012) 410–423. <https://doi.org/https://doi.org/10.1016/j.cemconres.2011.11.008>.
- [100] A. Vollpracht, B. Lothenbach, R. Snellings, J. Haufe, The pore solution of blended cements: a review, *Mater. Struct.* 49 (2016) 3341–3367. <https://doi.org/10.1617/s11527-015-0724-1>.
- [101] V. Kocaba, E. Gallucci, K.L. Scrivener, Methods for determination of degree of reaction of slag in blended cement pastes, *Cem. Concr. Res.* 42 (2012) 511–525. <https://doi.org/https://doi.org/10.1016/j.cemconres.2011.11.010>.
- [102] M. Ben Haha, B. Lothenbach, G. Le Saout, F. Winnefeld, Influence of slag chemistry on the hydration of alkali-activated blast-furnace slag — Part II: Effect of Al₂O₃, *Cem. Concr. Res.* 42 (2012) 74–83. <https://doi.org/https://doi.org/10.1016/j.cemconres.2011.08.005>.
- [103] A. Jenni, U. Mäder, C. Lerouge, S. Gaboreau, B. Schwyn, In situ interaction between different concretes and Opalinus Clay, *Phys. Chem. Earth, Parts A/B/C.* 70–71 (2014) 71–83. <https://doi.org/https://doi.org/10.1016/j.pce.2013.11.004>.
- [104] P. Juilland, E. Gallucci, R. Flatt, K. Scrivener, Dissolution theory applied to the induction period in alite hydration, *Cem. Concr. Res.* 40 (2010) 831–844. <https://doi.org/10.1016/j.cemconres.2010.01.012>.
- [105] A. Schöler, B. Lothenbach, F. Winnefeld, M. Ben Haha, M. Zajac, H.-M. Ludwig, Early hydration of SCM-blended Portland cements: A pore solution and isothermal calorimetry study, *Cem. Concr. Res.* 93 (2017) 71–82. <https://doi.org/https://doi.org/10.1016/j.cemconres.2016.11.013>.
- [106] F. Deschner, F. Winnefeld, B. Lothenbach, S. Seufert, P. Schwesig, S. Dittrich, F. Goetz-Neunhoeffler, J. Neubauer, Hydration of Portland cement with high replacement by siliceous fly ash, *Cem. Concr. Res.* 42 (2012) 1389–1400. <https://doi.org/https://doi.org/10.1016/j.cemconres.2012.06.009>.
- [107] J.W. Bullard, A Determination of Hydration Mechanisms for Tricalcium Silicate Using a

-
- Kinetic Cellular Automaton Model, *J. Am. Ceram. Soc.* 91 (2008) 2088–2097. <https://doi.org/10.1111/j.1551-2916.2008.02419.x>.
- [108] D.E. Wurster, H.-L. Weng, D.R. Flanagan, Determination of the Dissolution Rate Controlling Process for Isomeric Amides in Alkane Solvents, *J. Pharm. Sci.* 75 (1986) 1104–1106. <https://doi.org/https://doi.org/10.1002/jps.2600751117>.
- [109] C.A. Utton, R.J. Hand, P.A. Bingham, N.C. Hyatt, S.W. Swanton, S.J. Williams, Dissolution of vitrified wastes in a high-pH calcium-rich solution, *J. Nucl. Mater.* 435 (2013) 112–122. <https://doi.org/https://doi.org/10.1016/j.jnucmat.2012.12.032>.
- [110] M. V Biber, M. dos Santos Afonso, W. Stumm, The coordination chemistry of weathering: IV. Inhibition of the dissolution of oxide minerals, *Geochim. Cosmochim. Acta.* 58 (1994) 1999–2010. [https://doi.org/https://doi.org/10.1016/0016-7037\(94\)90280-1](https://doi.org/https://doi.org/10.1016/0016-7037(94)90280-1).
- [111] D. Damidot, F. Bellmann, B. Möser, T. Sowoidnich, Calculation of the Dissolution Rate of Tricalcium Silicate in Several Electrolyte Compositions, *Cem. Wapno, Bet.* 12/74 (2007) 57–67.
- [112] P. Barret, D. Ménétrier, Filter dissolution of C3S as a function of the lime concentration in a limited amount of lime water, *Cem. Concr. Res.* 10 (1980) 521–534. [https://doi.org/https://doi.org/10.1016/0008-8846\(80\)90096-4](https://doi.org/https://doi.org/10.1016/0008-8846(80)90096-4).
- [113] P. Barret, D. Ménétrier, D. Bertrandie, Mechanism of C3S dissolution and problem of the congruency in the very initial period and later on, *Cem. Concr. Res.* 13 (1983) 728–738. [https://doi.org/https://doi.org/10.1016/0008-8846\(83\)90064-9](https://doi.org/https://doi.org/10.1016/0008-8846(83)90064-9).
- [114] T. Chave, P. Frugier, S. Gin, A. Ayrat, Glass–water interphase reactivity with calcium rich solutions, *Geochim. Cosmochim. Acta.* 75 (2011) 4125–4139. <https://doi.org/https://doi.org/10.1016/j.gca.2011.05.005>.
- [115] L. Armelao, A. Bassan, R. Bertoncello, G. Biscontin, S. Daolio, A. Glisenti, Silica glass interaction with calcium hydroxide: a surface chemistry approach, *J. Cult. Herit.* 1 (2000) 375–384. [https://doi.org/https://doi.org/10.1016/S1296-2074\(00\)01093-1](https://doi.org/https://doi.org/10.1016/S1296-2074(00)01093-1).
- [116] M. Balonis, F.P. Glasser, The Density of Cement Phases - supporting information, (2009) 1–61.
- [117] A.C.A. Muller, K.L. Scrivener, A.M. Gajewicz, P.J. McDonald, Densification of C–S–H Measured by ^1H NMR Relaxometry, *J. Phys. Chem. C.* 117 (2013) 403–412. <https://doi.org/10.1021/jp3102964>.
- [118] S. Sui, F. Georget, K. Scrivener, Developing a generic approach to durability: Factors affecting chloride transport in binary and ternary cementitious materials, *Cem. Concr. Res. Under Revi* (2019) 105783. <https://doi.org/10.1016/j.cemconres.2019.105783>.
- [119] B. Lothenbach, T. Matschei, G. Möschner, F.P. Glasser, Thermodynamic modelling of the effect of temperature on the hydration and porosity of Portland cement, *Cem. Concr. Res.* 38 (2008) 1–18. <https://doi.org/https://doi.org/10.1016/j.cemconres.2007.08.017>.

-
- [120] T. Matschei, B. Lothenbach, F.P. Glasser, Thermodynamic properties of Portland cement hydrates in the system CaO–Al₂O₃–SiO₂–CaSO₄–CaCO₃–H₂O, *Cem. Concr. Res.* 37 (2007) 1379–1410. <https://doi.org/https://doi.org/10.1016/j.cemconres.2007.06.002>.
- [121] C.S. Walker, S. Sutou, C. Oda, M. Mihara, A. Honda, Calcium silicate hydrate (C-S-H) gel solubility data and a discrete solid phase model at 25°C based on two binary non-ideal solid solutions, *Cem. Concr. Res.* 79 (2016) 1–30. <https://doi.org/https://doi.org/10.1016/j.cemconres.2015.07.006>.
- [122] C.S. Walker, D. Savage, M. Tyrer, K.V. Ragnarsdottir, Non-ideal solid solution aqueous solution modeling of synthetic calcium silicate hydrate, *Cem. Concr. Res.* 37 (2007) 502–511. <https://doi.org/https://doi.org/10.1016/j.cemconres.2006.12.002>.
- [123] J. Thomas, H. Jennings, Free-Energy-Based Model of Chemical Equilibria in the CaO–SiO₂–H₂O System, *J. Am. Ceram. Soc.* 81 (2005) 606–612. <https://doi.org/10.1111/j.1151-2916.1998.tb02380.x>.
- [124] N. Holmes, D. Kelliher, M. Tyrer, N. Holmes, D. Kelliher, M. Tyrer, 39 th Cement and Concrete Science Conference Paper Number 012 9-10th, 2019.
- [125] G.M. Moss, B.J. Christensen, T.O. Mason, H.M. Jennings, Microstructural analysis of young cement pastes using impedance spectroscopy during pore solution exchange, *Adv. Cem. Based Mater.* 4 (1996) 68–75. [https://doi.org/https://doi.org/10.1016/S1065-7355\(96\)90053-X](https://doi.org/https://doi.org/10.1016/S1065-7355(96)90053-X).
- [126] C. Labbez, B. Jönsson, I. Pochard, A. Nonat, B. Cabane, Surface charge density and electrokinetic potential of highly charged minerals: Experiments and Monte Carlo simulations on calcium silicate hydrate, *J. Phys. Chem. B.* 110 (2006) 9219–9230. <https://doi.org/10.1021/jp057096+>.
- [127] C. Labbez, I. Pochard, B. Jönsson, A. Nonat, C-S-H/solution interface: Experimental and Monte Carlo studies, *Cem. Concr. Res.* 41 (2011) 161–168. <https://doi.org/10.1016/j.cemconres.2010.10.002>.

Curriculum Vitae

Yosra Briki

yosra.briki@epfl.ch/yosrabriki@live.fr

13/07/1991, TUNISIAN

CHEMIN DE VEILLOUD 34

CH-1024 ECUBLENS/LAUSANNE

+41-793243077

EDUCATION

- 2016 – 2020 **PhD thesis at the Swiss Federal Institute of Technology (EPFL) Switzerland** on the understanding of the limitations of the reactivity of supplementary cementitious materials (SCMs) in blended cements, supported by Heidelbergcement
- 2015 – 2016 **Civil Engineering diploma / Master research degree M2** at the Ecole Centrale and National Institute of applied Science (INSA), Lyon, France
- 2012 – 2015 **Civil Engineering diploma / Master degree M1** at the National School of Engineering of Tunis (ENIT), Tunis, Tunisia
- 2010 – 2012 **Preparatory Institute for Engineering Studies** in Technology and Physics at the National School of Engineering, El Manar, Tunis, Tunisia

PROFESSIONAL QUALIFICATIONS

- 2016 – 2020 **Research assistant Lausanne, Switzerland**
- Established relationships between SCMs properties and their intrinsic reactivity in Limestone Calcined Clay Cements (LC³) and slag blended cements
 - Optimized the formulation of blended cements to improve their performance and reduce their ecological impact and their cost
 - Supervised several master projects on the assessment of SCMs reactivity
 - Launched a course class on concrete mix design for the International Committee of the Red Cross (ICRC). Stressed out the critical parameters for adequate and safe concrete construction
- 2016 **Master thesis Heidelberg, Germany**
- Investigated the influence of grinding aids on cement hydration at Heidelbergcement
 - Found out the enhancement of the performance of blended cements using propylene glycol (PG) and triisopropanolamin (TIPA)
 - Demonstrated through microstructure analysis that this improvement was due to the higher amplitude of dissolution of aluminum ions

-
- 2015 **Research internship Grenoble, France**
- Explored the permeability of soils treated with lime at the Laboratory of Transfers, Hydrology and Environment (LTHE), Joseph Fourier University
 - Quantified the impact of clays on soil permeability
- 2014 **Civil engineering internship Tunis, Tunisia**
- Modelled the construction of a road in the Republic of Benin using Autocad
 - Provided construction schematics to senior officials

PUBLICATIONS

- Sub. 2020 **Journal papers under submission**
- Sub. 2020 Briki Y., Zajac M., Bowen P., Ben Haha M., Scrivener. K. Understanding of the slowing down of metakaolin reaction in LC³ cement at late ages
- Sub. 2020 Briki Y., Ben Haha M., Scrivener K. Strength and phase assemblage of limestone calcined clay cements (LC³) with clinker content from 50% down to 30%
- Sub. 2020 Briki Y., Zajac M., Ben Haha M., Scrivener. K. Factors affecting the reactivity of slag at early and late ages
- Sub. 2020 Briki Y., Zajac M., Ben Haha M., Scrivener. K. Impact of limestone fineness on cement hydration at early age
-
- 2020 **Most relevant conference papers**
- 2020 Briki Y., Ben Haha M., Scrivener K. Interfacial energy of C-S-H and AFm phases in cement paste. Annual International Workshop on Crystallization in Porous Media CRYSPOM. Pau, France.
- 2020 Briki Y., Ben Haha M., Scrivener K. The factors slowing down clinker hydration and SCMs reaction at later ages in low clinker cements. RILEM International Conference on Cementitious Materials and Alternative Binders for Sustainable Concrete Toulouse, France.
- 2019 Briki Y., Ben Haha M., Scrivener K. The factors slowing down clinker hydration and SCMs reaction at later ages in low clinker cements. International conference on Sustainable Materials, Systems and Structures Rovinj, Croatia.
- 2019 Briki Y., Ben Haha M., Scrivener K. Fine limestone addition in Portland cement. 15th International Congress on the Chemistry of Cement Prague, Czech Republic.
- 2017 Briki Y., Ben Haha M., Scrivener K. Fine limestone addition in Portland cement. 37th Cement and Concrete Science (CCS) Conference London, United Kingdom.

INTERESTS

- Hobbies** Violin player in AMATI orchestra in Lausanne
Hiking, running, Nordic skiing